Thesis presented for the Doctor of Philosophy in the Faculty of Science,

Department of Oceanography

August 2023

Synoptic weather systems over Antarctic sea ice: understanding the link between extratropical cyclones and extreme variability in Antarctic sea-ice concentration

By

Ehlke Hepworth

To my family.

Thank you for your never-ending support, encouragement, and love.

Soli Deo gloria.

Supervisor

Prof. Marcello Vichi

Department of Oceanography, University of Cape Town South Africa

Marine and Antarctic Research centre for Innovation and Sustainability (MARIS), University of Cape Town, South Africa

Funding

I am thankful for the funding from the National Research Foundation of South Africa (Grant Numbers: 118598 and 112632), and the Swedish Foundation for International Cooperation in Research and Higher Education (Grant Number: SA2017-7063). Additionally, funding was received from the European Union's Horizon 2020 research and innovation programme under grant agreement no. 101003826 via project CRiceS (Climate Relevant interactions and feedbacks: the key role of sea ice and Snow in the polar and global climate system).

Plagiarism Declaration

I, Ehlke Hepworth, understand the meaning of plagiarism and declare that all the work in the thesis, save for that which is properly acknowledged, is my own. This thesis contains less than 80 000 words including appendices, bibliography, footnotes, tables, equations, and has less than 150 Figures.

I confirm that I have been granted permission by the University of Cape Town's Doctoral Degrees Board to include the following publication in my PhD thesis, and, where co-authorships are involved, my co-authors have agreed that I may include the publication:

Hepworth, E., Messori, G., and Vichi, M. (2022). 'Association Between Extreme Atmospheric Anomalies Over Antarctic Sea Ice, Southern Ocean Polar Cyclones and Atmospheric Rivers', *Journal of Geophysical Research: Atmospheres*, 127(7), pp. 1–15. doi: 10.1029/2021JD036121.

Signature: Date: 28.08.2023

Student Name: Ehlke Hepworth Student Number: DJNEHL001

Abstract

Extratropical cyclones and atmospheric rivers are key drivers in transporting extreme heat and moisture to the poles. Previous studies have shown that extratropical cyclones can promote change in sea-ice concentration at a synoptic scale, however, the extreme variability in synoptic-scale sea-ice concentration and the extent to which it is engendered by cyclones has not yet been studied.

This thesis seeks to quantify extreme variability of Antarctic sea-ice concentration, and assess the role that cyclones and other synoptic features play over the extended Austral winter period (May – September). This is achieved through the use of reanalyses data (based on the European Centre for Medium-Range Weather Forecasts; ERA-Interim and ERA5) and output from a climate model tuned for representing Southern Hemisphere processes, whose atmospheric component is the Conformal Cubic Atmospheric Model (CCAM).

To accomplish this, this study is formulated about three main research aims. The first aim is to test whether circulation patterns associated with cyclones or atmospheric rivers may routinely lead to the presence of unusually warm, moist air masses over ice-covered regions. This thesis points to a strong association between atmospheric rivers and extreme moisture anomalies found over the Antarctic sea-ice environment, while extreme temperature anomalies over Antarctic sea ice are relatively linked with intense cyclones. More specifically, approximately 27% of intense Southern Ocean cyclones and 20% of ARs occur in the vicinity of extreme temperature anomalies, while 12% of intense cyclones and 46% of ARs occur in the vicinity of extreme moisture anomalies. These results, showing that extratropical cyclones play a role in weather circulations over the sea-ice environment, lead to this study's second research aim: to identify extreme variability in Antarctic sea-ice concentration and investigate the extent to which it may be caused by extratropical cyclones. Atmospheric reanalysis and a cyclone-tracking algorithm were used to characterize sea-ice variability and cyclone activity in different Southern Ocean sectors: the King Haakon VII, East Antarctic, Ross/Amundsen, Bellingshausen, and Weddell sectors. The proportion of extreme sea-ice variability engendered by cyclones of different intensities was quantified, and reveals a significant link between variability in winter sea-ice concentration and: (i) all cyclones in the Ross/Amundsen sector; (ii) all but the weakest cyclones in the King Haakon VII, East Antarctic, and Bellingshausen sectors; and (iii) all but the most intense cyclones in the Weddell sector. More generally, roughly 30 – 40% of the extreme sea-ice variability is caused by extratropical cyclones within all regions apart from the Weddell sector, where extreme sea-ice variability is more closely connected to weaker cyclones.

Finally, the third research aim is to explore the relationship between cyclones and synoptic-scale variability in sea-ice concentration in a climate model, CCAM, where simulated sea-ice variability is dynamically driven by the model atmosphere (unlike the second research aim which used the ERA5 reanalysis product). Whilst the use of ERA5 revealed an emphasis on intense cyclones engendering extreme variability, the results derived from the analysis using CCAM showed that extreme variability in sea-ice concentration only

depended on cyclone intensity in the East Antarctic sector. In the other sectors, on average, cyclones of all intensities (apart from the 10% weakest ones) had a significant link to extreme variability in sea-ice concentration at a synoptic scale. Moreover, using CCAM, the total extreme variability in sea-ice concentration linked to cyclones increased to roughly 40 – 60%.

In conclusion, the Antarctic atmosphere-ice interplay over the extended Austral winter period is complex, but the results presented in this thesis shed new light on the relationship between synoptic features over the sea-ice environment, and the role cyclones play in engendering extreme variability in sea-ice concentration. As the atmosphere continues to change with global warming, the results presented in this thesis serve as a foundation for further investigations into how the Antarctic sea-ice environment may also change over time.

Acknowledgements

I would like to express my gratitude to the following people for their contribution to this thesis in various ways:

To Prof. Marcello Vichi., I extend my gratitude to you as my supervisor throughout the past eight years, guiding me from Honours through to PhD. Over this journey, I have experienced significant growth as a scientist. I appreciate the diverse opportunities you provided, contributing to my development in the field.

To Prof. Gabriele Messori for your guidance and encouragement through Chapters 3 and 4.

To Prof. François Engelbrecht for providing information for your guidance around CCAM..

To Dr Kevin Hodges for taking the time to patiently help me implement the cyclone tracking algorithm to the CCAM data.

To the University of Cape Town's ICTS High Performance Computing team who provided the facilities for the computations of this thesis to be performed: hpc.uct.ac.za.

To Prof. Isabelle Ansorge for providing support toward the end.

To James Hepworth. I am deeply grateful to have you directly by my side: through my PhD journey, and through everything in between. Your love and support gave me strength.

To my sister, Janeke Lilford. You have always believed that I can do wonderful things. Your encouragement and love for me is beyond compare. You are my cheerleader: thank you for continuously cheering me on, and for always listening.

To my parents, Antoinette and Johan de Jong. Thank you for the love and support you have always poured out: from when I was a little girl through to my PhD journey. Your love for me, and you being so proud of me, is held close to my heart.

To Kara-Lee Aves. Sharing this PhD journey with you gave comfort during this otherwise lonesome experience.

Finally, to Ann-Maree Tippoo and Mikhail Manuel, for joyfully celebrating every milestone achieved along the way.

Data Availability

i. ERA-Interim and ERA5 reanalyses (used to calculate atmospheric anomalies, atmosphere rivers, and the sea-ice variance indicator) were obtained from the ECMWF website.

ii. CCAM data (used to simulate cyclone tracks and sea-ice variability) was provided by Wits University.

iii. The data for the cyclone tracks identified in Chapter 3 were from the tracking algorithm and methodology of Pinto et al. (2005) (Method 02), and accessed at https://proclim.scnat.ch/de/activities/project_imilast/data_download.

iv. The IPART algorithm for the atmospheric rivers (identified in Chapter 3) was made available by Xu et al. (2020), and accessed at GitHub - ihesp/IPART: Image-Process based Atmospheric River Tracking (IPART) algorithms.

v. The cyclone tracking algorithm used to identify cyclones in Chapters 4 and 5 (Hoskins and Hodges, 2005) may be obtained through contacting Dr Kevin Hodges.

vi. The cyclone track data used in Chapter 4 was provided by Dr Kevin Hodges.

vii. I would like to acknowledge the University of Cape Town's ICTS High Performance Computing team who provided the facilities for the computations of this thesis to be performed: hpc.uct.ac.za.

List of Figures

List of Tables

List of Acronyms

ACW	Antarctic Circumpolar Wave
AR	Atmospheric River
CCAM	Conformal Cubic Atmospheric Model
CMIP	Climate Model Intercomparison Project
ECMWF	European Centre for Medium-Range Weather Forecasts
ENSO	El-Niño Southern Oscillation
ERA	ECMWF Re-Analysis
IFS	Integrated Forecasting System
IPART	Image-Processing based Atmospheric River Tracking
IPCC	Intergovernmental Panel on Climate Change
IVT	Integrated Vapor Transport
MIZ	Marginal Ice Zone
MSLP	Mean Sea Level Pressure
SAM	Southern Annular Mode
SAO	Semiannual Oscillation
SIC	Sea-Ice Concentration
SO	Southern Ocean
SST	Sea Surface Temperature
t2m	temperature 2 m above sea level
tcw	total column water
OSTIA	Operational Sea Surface Temperature and Sea Ice Analysis

Contents

1 CHAPTER ONE

Introduction

1.1. Background to the study

Sea ice is recognized as an important feature in the regional and global climate due to its distinctive characteristics (Meier and Stroeve, 2008). For example, since sea ice creates a barrier over the ocean's surface, it plays a role in the transport of heat and moisture across the ocean-atmosphere interface (Elvidge et al., 2021). This involves insulating the cold atmosphere from the comparatively warmer ocean. The low thermal conductivity of sea ice reduces the conductive heat flux between the ocean and the atmosphere, particularly when a snow layer is present (Batrak and Müller, 2019). Sea ice thus plays an crucial role in air-sea fluxes through dampening the energy transfer between the atmosphere and the ocean. Sea ice additionally has an effect on the ocean's near-surface freshwater flux during formation and melting, impacting the surface energy budget (Perovich et al., 2021).

The high albedo of sea ice (relative to the underlying ocean) results in relatively more solar radiation reflected back into the atmosphere (Pirazzini, 2004). The schematic in Figure 1.1 shows the implications a reduction in sea ice has on the regional and global climate due to its high albedo relative to the underlying ocean. Once there is an increase in atmospheric temperature, the sea ice melts and the darker, underlying ocean surface is exposed. Since the ocean has a lower albedo than sea ice, relatively more solar radiation is absorbed by the ocean, increasing the temperature of the ocean. Subsequently, the sea ice melts, leading to a reduction in albedo, and the ice-albedo positive feedback is established.

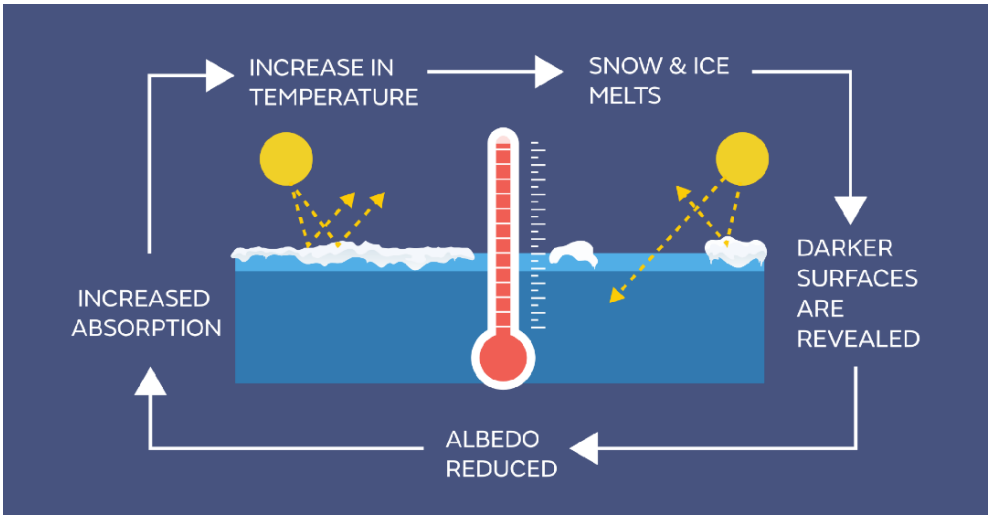

Figure 1.1: Schematic showing the ice-albedo feedback. This figure is courtesy of the United Kingdom Met Office, www.metoffice.gov.uk/research/climate/cryosphere-oceans/sea-ice/index.

There is a plethora of oceanic and atmospheric drivers interlinked with the Antarctic sea-ice environment (e.g., the ocean mixed layer, wind, and solar radiation; Gordon, 1981; Watkins and Simmonds, 1999). This is a result of the Antarctic continent being unbounded by land and thus promoting a high-energy circumpolar Southern Ocean. Indeed, when studying the Southern Ocean polar region, scientific investigations range from extreme weather phenomena (e.g., Raphael, 2007; Matear et al., 2015; Kwok et al., 2017) such as the frequent passage of extratropical cyclones (Uotila et al., 2011; Grieger et al., 2018), to harsh oceanic conditions (Grieger et al., 2018; Smith et al., 2019) such as waves that can break up the sea ice hundreds of kilometres from the ice edge (Kohout et al., 2014; Stopa et al., 2018).

Overall, the Antarctic sea-ice environment is comprised of two parts: the marginal ice zone (MIZ) and pack ice. It is common to analyse these regions using sea-ice concentration (SIC; a measure of the proportion, recorded as a percentage, of open ocean to ice-covered ocean). Conventionally, the MIZ is defined as 15 – 80% SIC (Stroeve et al., 2016), and pack ice as 80 – 100% SIC. The MIZ sits close to the open ocean and is considered as "open pack" conditions, comprised of smaller ice floes that are relatively more responsive to climate variability (Iovino et al., 2022; Vichi, 2022). This region is particularly tightly linked with oceanic and atmospheric phenomena which play a direct role in the MIZ's formation, consolidation, and drift (Weeks and Ackley, 1986; Squire, 2018)

A prominent characteristic of Antarctic sea ice is its large annual seasonality, with minimum sea-ice coverage in February and maximum coverage in September. On an interannual scale, satellite recordings from the year 1979 have revealed an alternation of increase and decrease in sea-ice cover: an annual increase in the mean Antarctic sea-ice coverage observed from 1979 to 2014, following relatively major decreases until 2017, and subsequently an increase to near its long-term average in 2020 (Simmonds and Li, 2021). This is seen in Figure 1.2a, showing the mean interannual sea-ice cover variability for the month of September from 1979 – 2022.

It is important to note that this overall increase in the mean sea-ice coverage has masked large regional variations. For example, there has been an overall increase in the Weddell and Ross seas, with a corresponding decrease in the Bellingshausen and Amundsen seas (Stammerjohn et al., 2008; Eayrs et al., 2020). Figure 1.2b shows the inhomogeneous regional sea-ice cover trends from 1979 – 2010.

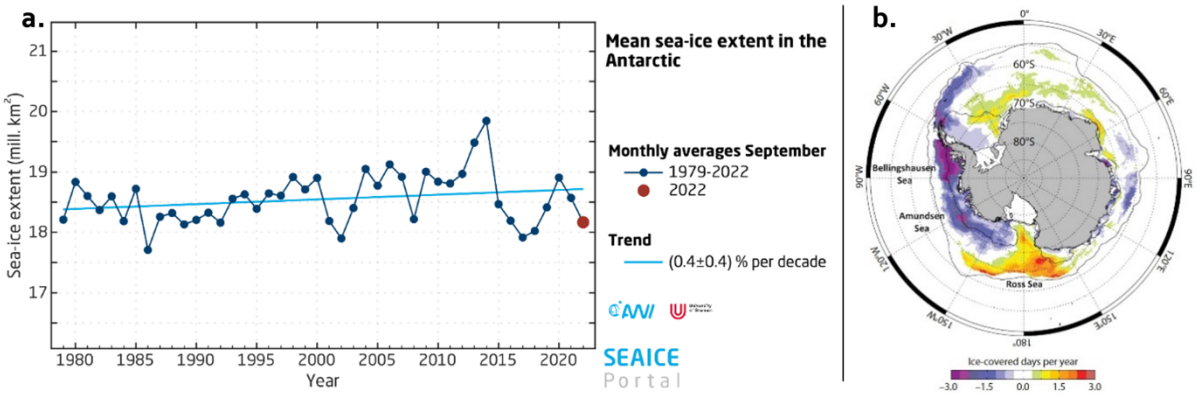

Figure 1.2: Sea-ice trends showing (a) the average interannual sea-ice variability for the month of September from 1979 – 2022 (courtesy of Meeries Portal: Sea ice extent | Data | Meereisportal), and (b) regional sea-ice variability from 1979 – 2010 (from Maksym et al., 2012).

Because of these inhomogeneous trends, studies often analyse the high southern latitudes in separate sectors (e.g., Turner et al., 2015; Hobbs et al., 2016; Turner et al., 2022). Common sectors are described in Parkinson and Cavalieri (2012), and Raphael and Hobbs (2014). Figure 1.3 shows the Southern Ocean divided into the five sectors presented by Raphael and Hobbs (2014) – (i) King Haakon VII, (ii) East Antarctic, (iii) Ross/Amundsen, (iv) Bellingshausen, and the (v) Weddell sectors – as well as highlighting the conventionally defined MIZ.

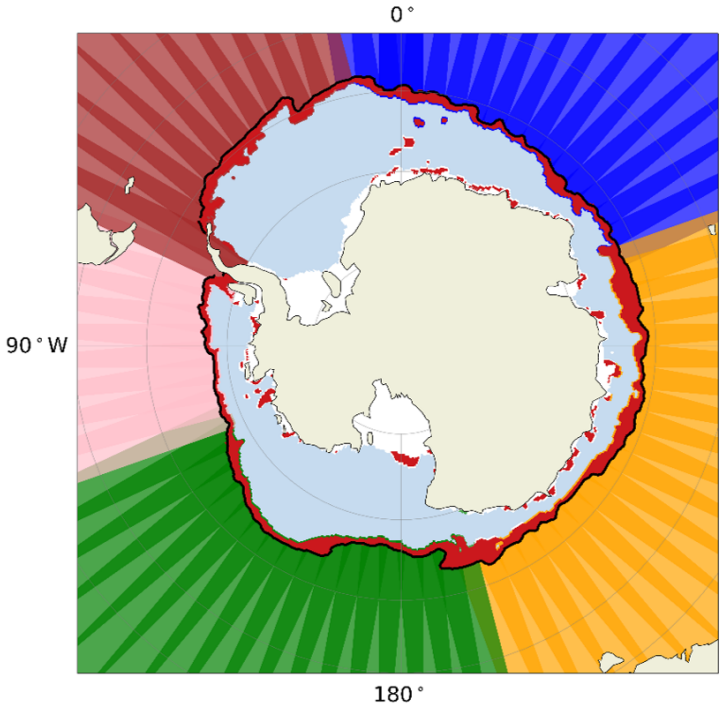

Figure 1.3: Five Southern Ocean sectors are depicted: The King Haakon VII (blue), East Antarctic (orange), Ross/Amundsen (green), Bellingshausen (pink), and the Weddell (brown) sectors. Overlain is the sea ice from 04 July 2017, showing the conventional definition of the marginal ice zone (15 – 80% sea-ice concentration) in red.

1.1.1. Southern Ocean atmosphere and Antarctic sea ice interactions

A general overview

Several atmospheric phenomena cause inhomogeneous sea-ice coverage (Figure 1.3) and large regional variations in the Antarctic sea-ice environment (Figure 1.2b). In general, atmospheric variability in the Southern Hemisphere is dominated by the Southern Annular Mode (SAM) and the El-Niño Southern Oscillation (ENSO) (Stammerjohn et al., 2008). SAM is characterised by the latitudinal position and strength of the midlatitude Southern Hemisphere westerly winds (Thompson and Wallace, 2000; Stewart et al., 2020) expressed by the zonal mean sea level pressure difference between 40°S and 65°S (Stewart et al., 2020). The latitudinal positioning of the SAM may vary monthly while ENSO is a quasi-periodic phenomenon located in the tropical Pacific Ocean and characterised by two phases, each lasting 2 – 7 years: (i) El Niño with relative warming of the surface equatorial Pacific, and (ii) La Niña with a corresponding cooling (Olson et al., 2021)

These atmospheric modes have a direct impact on atmospheric features such as sea surface temperature and cyclones. For example, Figure 1.4 shows how, during a La Niña event, the sub-tropical jet is weakened while the polar front jet is strengthened leading to an increase in the number of cyclones, warmer sea surface temperature conditions, and therefore a decrease in sea-ice cover in the eastern Bellingshausen and western Weddell sectors. Conversely, in the Ross/Amundsen sector, colder conditions with an increase in sea-ice

cover is observed. During an El Niño event (with a relatively warming surface equatorial Pacific), the opposite scenario will apply (Yuan, 2004).

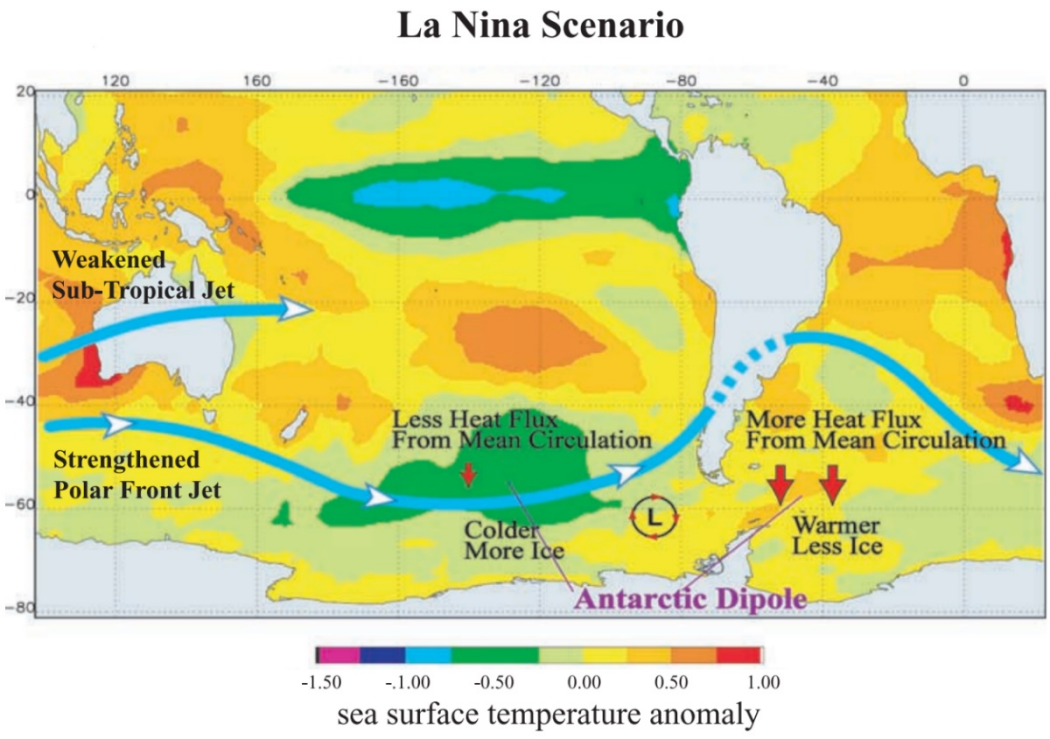

Figure 1.4: Schematic depiction of the high-latitude atmosphere-ice response to La Nina., with the base map showing a La Nina composite of sea surface temperature anomalies. This figure is from Stammerjohn et al. (2008), who adapted it from Yuan (2004).

In general, there is a strong temperature gradient between the mid- and high-latitudes, resulting in baroclinic instability (characterised by strong vertical wind shear in the mid-latitudes) which is intimately linked in complex ways to atmospheric variability and synoptic behaviour (Simmonds and Li, 2021). Cyclones act to reduce the strong temperature gradient through the poleward transport of heat (Walker et al., 2020). The Southern Ocean is, therefore, host to the frequent passage of extratropical cyclones, which can travel thousands of kilometres (more than 5000 km) and last several days (averaging 3 days) (Simmonds and Keay, 2000). These systems vary in intensity (Pinto et al., 2005), and are often (but not always) associated with high winds (Ulbrich et al., 2009; Catto et al., 2015; Walker et al., 2020) and an atmospheric river (Finlon et al., 2020; Francis, K. Mattingly, et al., 2020); as seen in Figure 1.5.

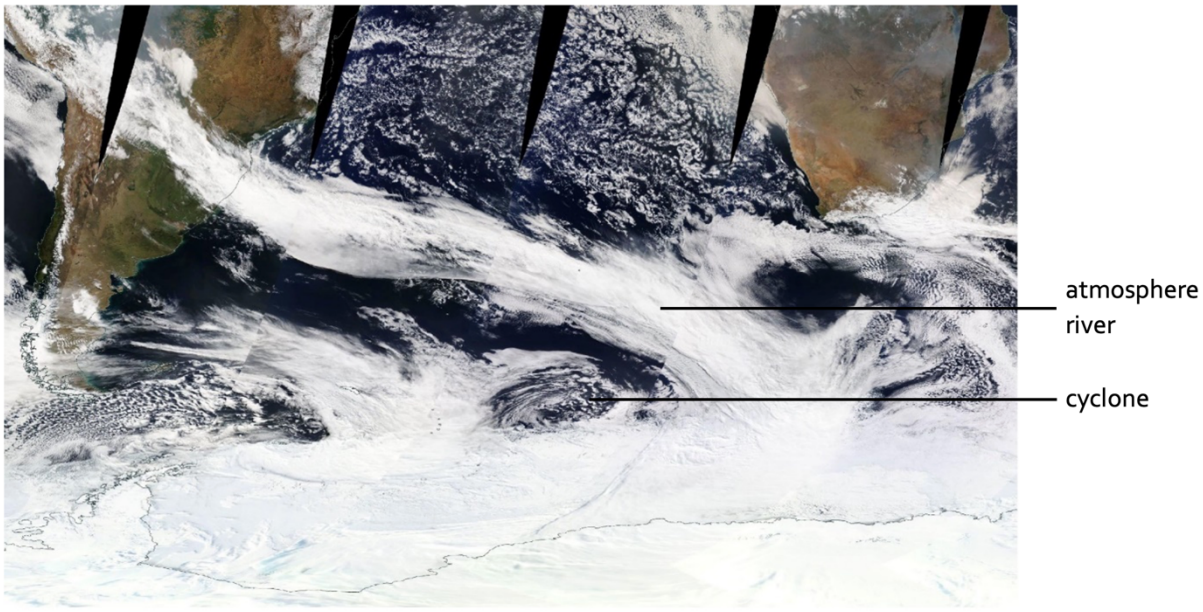

Figure 1.5: A circular cloud formation showing a cyclone, and a band of clouds in an atmospheric river extending from South America to the Antarctic sea-ice zone. This image is courtesy of NASA Worldview (https://doi.org/10.25250/thescbr.brk528), as seen in the case study presented by Francis et al., (2020).

Atmospheric rivers are narrow bands of enhanced horizontal poleward water vapour transport commonly found on the leading side of a cyclone (Figure 1.5), strengthening the cyclone by providing more water vapour for latent heat release (Zhang et al., 2019). These features act as "rivers in the sky": they are believed to account for more than 90% of the annual atmospheric moisture transport from the mid- to high latitudes (Nash et al., 2018; Francis et al., 2020).

Along with large-scale atmospheric phenomena such as SAM and ENSO, both cyclones and atmospheric rivers (which are relatively smaller in scale) play a role in the observed interannual sea-ice variability. For example, the Weddell polynya events (large openings in the winter sea-ice cover) in August 2016 and September 2017 were associated with an intense atmospheric river (Francis et al., 2020) and severe cyclonic activity (Campbell et al., 2019), contributing to the mean annual decrease in sea-ice coverage recorded over these years (see Figure 1.2a). Moreover, as the baroclinicity at the mid-latitudes continues to decrease (as it has been from 1979 – present), the coupled increase in baroclinicity at the higher Antarctic latitudes results in a poleward shift of cyclone tracks (Simmonds and Li, 2021). This shift contributes to altering the sea-ice field both dynamically (e.g., through near surface wind activity) and thermodynamically (Francis et al., 2020; e.g., Hell et al., 2019; Aue et al., 2023). This thermodynamic and dynamic alteration in the sea-ice field is due to the intricate interplay between cyclones, sea ice, and air-sea fluxes. For example, cyclonic activity can give rise to sea-ice regions characterised by increased moisture flux (Grieger et al., 2018) and increased turbulent heat flux, which is typically low during the sea-ice growth period but rises during cyclonic activity (Nilsson et al., 2001). A study by Schreiber and Serreze (2020) demonstrated that in the Arctic, cyclones, through air-sea heat fluxes, cyclones appeared to slow the overall day-today reduction in SIC during warmer months, while amplifying the day-to-day increase in the colder months.

Synoptic-scale interactions between the atmosphere and Antarctic sea ice

Understanding that the Earth's system gains energy in the low-latitudes, and that the excess energy is transported and deposited to the high-latitudes, is central to appreciating the differential effects on the atmosphere and sea ice (Simmonds and Li, 2021). Indeed, atmospheric phenomena play a crucial role in Antarctic sea-ice variability (such as its interannual mean variability, as depicted in Figure 1.2). However, there is also large variability in SIC at a synoptic scale (3 to 5-day timescale of hundreds to thousands of kilometres). Some studies have shown that variability in sea-ice cover over the 3 to 5-day timescale is promoted by cyclones. For example, Jena et al. (2022) presents case studies showing poleward sea-ice advection led by cyclones. de Jager and Vichi (2022) illustrate rotational drift features in the sea ice caused by cyclones, while (Womack et al., 2022) analysed an increase in sea ice meandering and drift speeds during cyclone activity. These studies have shown that ice type plays a more significant role in affecting the relationship between cyclones and sea ice, as opposed to ice thickness. Moreover, Vichi et al. (2019) present a case study showing how an explosive cyclone in the King Haakon VII sector caused an extended region of extreme synoptic-scale variability close to the sea-ice edge; as shown in Figure 1.6.

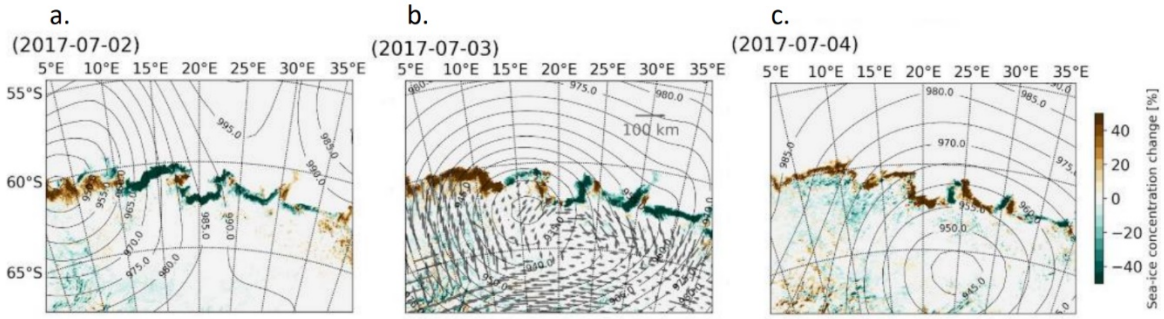

Figure 1.6: The daily changes in sea-ice concentration (mean concentration for the day minus the previous day's value) from AMSR2 ASI data from (a) 02 July 2017, (b) 03 July 2017, and (c) 04 July 2017. For reference, the mean sea level pressure isolines from 00:00 GMT of 03, 04, and 05 July 1017 are overlain in panels a, b, and c, respectively. Panel b also shows the estimated sea-ice displacement (in km) over approximately 48 hours centred on 03 July from OSI-SAF. This Figure adapted from Vichi et al. (2019).

1.1.2. Relevance of the Austral autumn and winter months

As with the inhomogeneous sea-ice coverage between the Antarctic sectors (Figures 1.2b and 1.3), the distribution of extratropical cyclones vary between the sectors too. Figure 1.7 shows the Southern Ocean cyclone density during the four seasons: (a) summer, (b) autumn, (c) winter, and (d) spring.

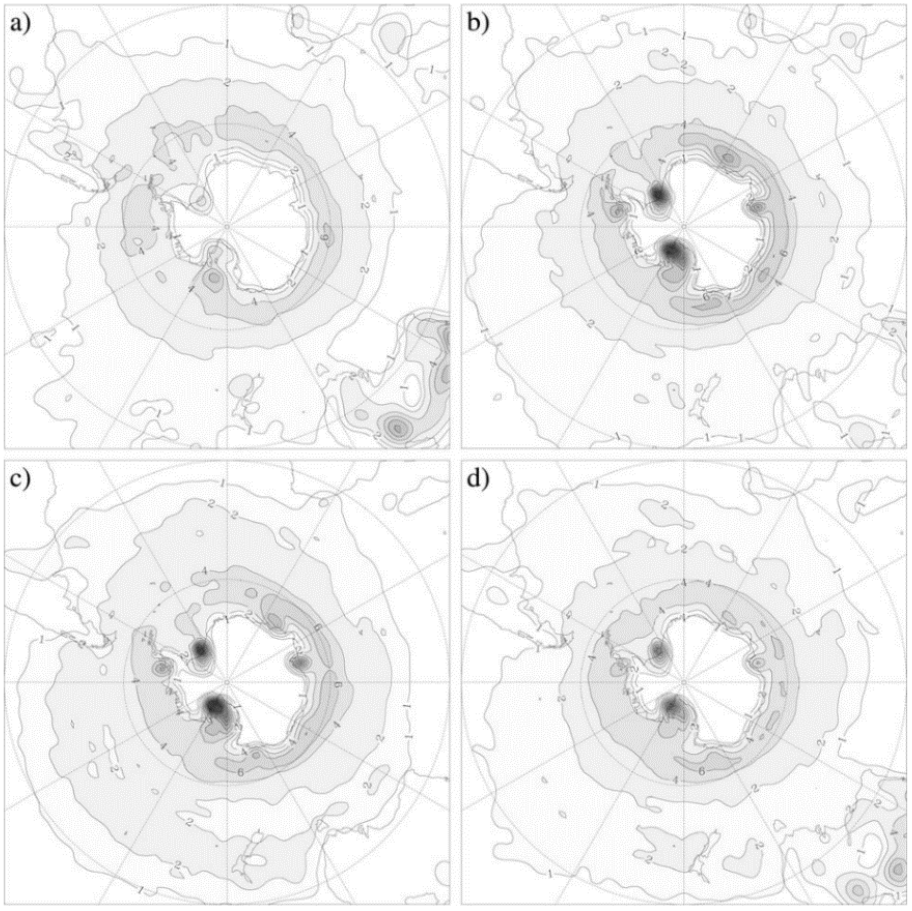

Figure 1.7: Southern Ocean extratropical cyclone density (the mean number found in a 10^3 (degrees latitude)^2 in Austral (a) summer (December – February), (b) autumn (March – May), (c) winter (June – August), and spring (September – November). The contour interval is 2×10^{-3} (degrees latitude)$^{-2}$. An additional isoline at 1×10^{-3} (degrees latitude)$^{-2}$ has been included in the plots. From Simmonds and Keay (2000).

The average number of Southern Ocean extratropical cyclones is highest in Austral autumn and winter (Figures 1.6b and c, respectively): where they are predominantly spread across the King Haakon VII and East Antarctic sectors, with hotspots found in the Ross/Amundsen and Weddell sectors. It is within the extended austral winter period where extratropical cyclones are generally stronger and more frequent (Figure 1.7; Simmonds and Keay, 2000; Grieger et al., 2018), and their role in poleward energy transport is enhanced (Oort and Piexoto, 1983). Moreover, during autumn and winter, the sea-ice coverage expands and is frequently penetrated by extratropical cyclones (Grieger et al., 2018), resulting in a tightly-linked interplay between cyclones and sea ice during this period (e.g., Vichi et al., 2019; Jena et al., 2021).

1.1.1. Studying the multifaceted Antarctic sea-ice environment

Reanalysis data

While satellite data provide baseline direct observations from 1979 to present, reanalyses products allow to expand the record of weather and climate variables. This is because reanalysis data is generated by a

combination of past short-range weather forecasts and meteorological/surface ocean observations through data assimilation into a numerical model of the atmosphere (Dee et al., 2011; Hersbach et al., 2020).

Several studies which have used satellite and/or reanalysis data have been able to show that the sea-ice environment is directly impacted by drivers such as sea surface temperature (e.g., Raphael, 2007; Stammerjohn et al., 2011), precipitation (e.g., Krinner et al., 2007; Papritz et al., 2014), ocean currents (e.g., Armitage, et al., 2018), and the strength of near-surface winds (e.g., Godfred-Spenning and Simmonds, 1996; Turner et al., 2015; Vichi et al., 2019; Matear et al., 2015; Holland and Kwok, 2012; Kwok et al., 2016; Blanchard-Wrigglesworth et al., 2020).

Climate models

Complementary to satellite and reanalysis products are climate models, which are used to simulate the interaction of the atmosphere, ocean, land surface, and cryosphere (Roach et al., 2020). Figure 1.8 is a schematic illustrating the general coupling of physical processes in climate models through the use of discretized grids.

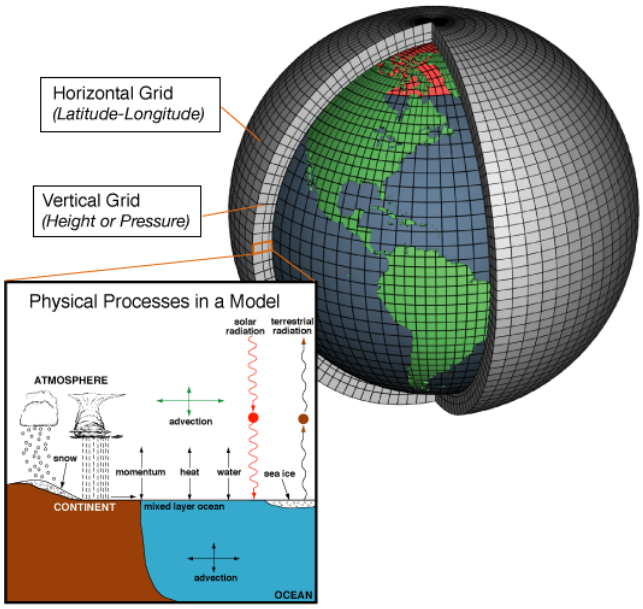

Figure 1.8: Schematic of the concept behind climate models to simulate the interaction of the atmosphere, ocean, land surface, and cryosphere. This figure is courtesy of National Oceanic and Atmospheric Administration (NOAA; celebrating200years.noaa.gov/breakthroughs/climate_model/modeling_schematic.html).

To "run" a model, the Earth is divided into 3-dimensional grid cells (Figure 1.8): mathematical equations that are based on the fundamental laws of physics, fluid motion, and chemistry are resolved for each cell (Gettelman and Rood, 2016). These equations describe the parameterizations and internal dynamics (i.e., the materials in each cell and the way energy moves through the cell). Firstly, climate forcing is specified and the equations in each cell are then solved. Secondly, the results are passed on to the neighbouring grid cells, and the equations are then solved again. This process is repeated through multiple timesteps.

One of the foundational joint initiatives of climate science is the Couple Model Intercomparison Project (CMIP; Eyring et al., 2016), designed to improve knowledge of climate change. The most recent phase, CMIP6, serves as the base intercomparison project for climate research, establishing common practices in producing and analysing large amounts of model output: allowing for models to be shared and compared. As a result, this project reduces duplication of effort, and minimizes operational and computational burdens (Eyring et al., 2016).

Climate models have become a valuable tool for projecting future climate change trends at global and regional scales (Engelbrecht et al., 2011). Yet, climate change projections are inherently uncertain as climate models have different internal dynamics and parameterizations and thus respond differently (to some extent) to the same inputs, producing a range of possible futures (Katzfey, 2015). Even though much of our understanding of Antarctic sea ice and its variability is developed through using ocean-ice models forced by atmospheric data (King et al., 2022), there is currently low confidence in climate model projections for Antarctic sea ice (Roach et al., 2020). Challenges include uncertainties in atmospheric forcing (e.g., Lin et al., 2022) and the non-linear physics of Antarctic sea ice (Carriers et al., 2017; Luo et al., 2023), making it difficult to simulate sea ice.

1.2. Thesis Aims

Since sea ice directly influences the regional and global climate system (Section 1.1; Hobbs et al., 2016), its synoptic-scale variability in concentration may, therefore, act as an indicator in climate change at a regional scale. As mentioned in Section 1.1.1, studies have shown that synoptic-scale variability of sea ice can be promoted by cyclones (e.g., Vichi et al., 2019; Jena et al., 2021; de Jager and Vichi, 2022; Womack et al., 2022). However, the *extreme* variability in sea-ice concentration at the synoptic scale has not yet been studied before. Here, synoptic-scale extreme variability is defined by using the change in sea-ice concentration on a 3-day timescale, and identified as the values above the 95th percentile threshold.

The focus of this thesis is on quantifying the extreme variability of Antarctic sea-ice concentration, and assessing the role that cyclones play through the use of reanalyses data and output from a climate model tuned for representing Southern Hemisphere processes.

To accomplish this, this study is formulated about three main research aims:

i. To test whether circulation patterns associated with cyclones or atmospheric rivers may routinely lead to the presence of unusually warm, moist airmasses over ice-covered regions.
ii. To identify extreme variability in Antarctic sea-ice concentration and investigate the extent to which it may be caused by extratropical cyclones; and
iii. To explore the relationship between cyclones and synoptic-scale variability in sea-ice concentration in a climate model by comparing the results against those generated using the reanalysis products.

1.3. Plan of the Thesis

Throughout this thesis, there is a strong focus on the sea-ice region and its overlying atmosphere. **Chapter 2**, therefore, details how SIC is estimated via the products used throughout this study. Additionally, the data and methodology that are applicable to investigating the three aims (see Section 1.2) are detailed.

Chapter 3 focuses on extreme temperature and moisture anomalies overlying the sea-ice region, and whether they are routinely caused by cyclones (strong or weak cyclones) or atmospheric rivers. Chapter 3 prepares the groundwork for Chapter 4 as understanding the "extremeness" of the overlying atmosphere may assist in understanding extreme variability in SIC and its link with cyclones. This chapter was published as: Hepworth, E., Messori, G., and Vichi, M. (2022). 'Association Between Extreme Atmospheric Anomalies Over Antarctic Sea Ice, Southern Ocean Polar Cyclones and Atmospheric Rivers', Journal of Geophysical Research: Atmospheres, 127(7), pp. 1–15. doi: 10.1029/2021JD036121.

Chapter 4 focusses on the extent to which extreme variability in winter Antarctic SIC may be caused by extratropical cyclones, and how this is related to the cyclone's intensity. This chapter has been submitted as Hepworth, E., Messori, G., and Vichi, M. 'Synoptic-scale extreme variability of winter Antarctic sea-ice concentration and its link to Southern Ocean extratropical cyclone' in the Journal of Geophysical Research: Oceans.

Chapter 5 analyses climate model outputs. The analyses produced in Chapter 4 using atmospheric reanalysis are repeated using a climate model to include the direct coupling of atmosphere-ice interactions. The selected case study model is the Conformal Cubic Atmospheric Model (CCAM), as an Australian model, and adapted by the Commonwealth Scientific and Industrial Research Organisation (CSIRO) for producing daily forecasts for the southern Africa region (Park, 2010).

Chapter 6 summarises the findings by presenting final conclusions and a discussion.

2 CHAPTER TWO

Data Products and Methodology

2.1. Introduction

This chapter is divided into three sections: the first details the gridded products – the reanalyses and climate model – used for this study, with a focus on how these products estimate sea-ice concentration (SIC). The second details the data throughout all aims of this study, namely, Southern Ocean (SO) cyclone tracks, and the third presents the methodology used to investigate the aims of this study (Section 1.2), including the use of cyclone track data to implement a search-radius method for assessing the relationship between cyclones and a variable of interest.

Chapters 3 – 5 that follow are both (i) complementary to one another, and (ii) can be read as self-contained chapters: holding their own introduction, data and methods, results, and discussion sections. Thus, the role of this chapter is simply to highlight the data, methods, and characteristics of the products used that are applicable to those chapters.

2.2. Sea-ice concentration products used in this thesis

2.2.1. Reanalyses: ERA-Interim and ERA5

To meet the first two aims of this study, reanalysis products from the European Centre for Medium-Range Weather Forecasts (ECMWF) Re-Analysis (ERA) data were used: ERA-Interim (Dee et al., 2011; Section 3.2.1), and its successor, ERA5 (Hersbach et al., 2020; Section 4.2.1). The first product was chosen for investigating the first aim, as outlined in Chapter 3, whilst the second product was used to meet the second aim, as detailed in Chapter 4.

It is important to note that the analysis in Chapter 3 makes use of ERA-Interim rather than ERA5, primarily because ERA5 was not publicly available at the time of analysis. Nevertheless, both ERA-Interim and ERA5 are deemed suitable for the analyses of this thesis: King et al. (2022) evaluated their performance against buoy deployments in the Weddell Sea, determining that both reanalyses (with the exception of near-surface air temperature) produced high correlation with *in situ* daily variations in atmospheric conditions (pressure, temperature, humidity, wind, and radiation).

Moreover, since this thesis focuses on sea ice and its overlying atmosphere, understanding how both ERA-Interim and ERA5 estimate SIC was key to evaluating their respective results. Both reanalyses are based on the same Integrated Forecasting System (IFS), which incorporates a forecast model that includes components for the atmosphere, land surface, and ocean waves (Dee, et al., 2011), and benefits from a decade of developments in data assimilation, core dynamics, and model physics (Hersbach et al., 2020). This forecasting system relies on climatological information such as the prescription of sea surface temperature (SST) and sea ice (Herbach et al., 2020). The initially prescribed SIC data is retrieved from the following external providers:

i. **ERA-Interim**: Operational Sea Surface Temperature and Sea Ice Analysis (OSTIA).
ii. **ERA5**: OSI SAF (409a) and the OSI SAF open data sets. The former is used from 1979 August to September 2007, while the latter is used for the remainder of the timeseries (from September 2007 to present).

Overall, the land, atmosphere, and ocean wave domains are coupled in the IFS, while SST and SIC are not available within these coupled domains. Figure 2.1, below, provides a schematic of how these domains are forced between one another.

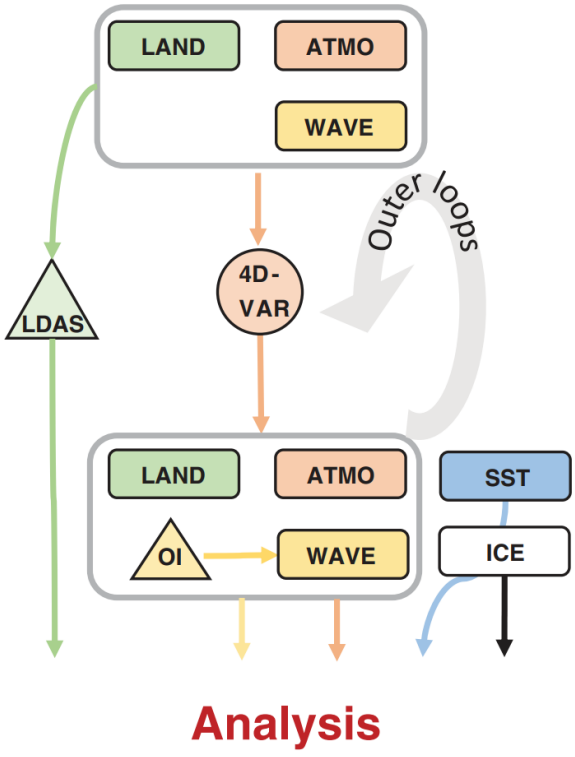

Figure 2.1: Assimilation diagram for ERA-Interim and ERA5 regarding the atmosphere (ATMO), land surface (LAND), ocean waves (WAVE), sea surface temperature (SST), and sea ice (ICE). Large, grey boxes represent outer-loop integrations (trajectories) where the indicated domains are coupled. Triangles represent the land-data assimilation (LDAS) and ocean wave optimal interpolation (OI), while circles correspond to 4D-Variation (4D-Var) inner loops. From Hersbach et al. (2020).

Coupled domains are said to be *forced* between one another if the state of Variable X is influenced by the state of Variable Y, and vice versa. In ERA-Interim and ERA5 (as seen in Figure 2.1), land, atmosphere, and ocean waves are coupled domains and are forced through the implementation of two types of loops: (i) outer-loop integrations (called trajectories) between the coupled domains, and (ii) 4D-variation inner-loops implemented between the coupled domains and between the atmosphere to SST and SIC parameters.

In step (i), the initially prescribed OSTIA and OSI SAF sea-ice data is re-gridded onto their respective ERA model grids and, through outer-loop integrations, forces the coupled domains of land, atmosphere, and ocean waves. Thereafter, the objective of step (ii) is to find the best estimate of the state of the atmosphere within an assimilation time window. This is achieved from meteorological observations falling within a desired time window, and from a given background weather forecast which is valid at the start of the time window. Finally, once the best state of the atmosphere is estimated, SIC is calculated. Moreover, SIC estimates derived from reanalysis products are dependent on shortwave downward radiation. During the austral winter season (the sea-ice growth period), the high-latitude SO experiences relatively low levels of shortwave radiation. This leads to minimal bias, which is attributed to weak shortwave cloud forcing (Schneider and Reusch, 2016; Cerovečki et al., 2022).

2.2.2. Case Study Model: Conformal Cubic Atmospheric Model

In Section 1.1.3, it was briefly explained that, through the fundamental laws of physics, fluid motion, and chemistry, the different spheres in a model (e.g., the atmosphere, ocean, land) interact with each other in a simulation, thus running *coupled* together (Gettelman and Rood, 2016). As a result, based on internal dynamics and coupled integrations, models can freely evolve through each time step (Holland and Hunke, 2022). Gettelman and Rood (2016) illustrates the different parts of a time step in a model (Figure 2.2). Here, I adapt the illustration to show how a model may simulate Antarctic sea ice if the atmospheric temperature and wind speed were to increase (as a result of an extratropical cyclone travelling within the vicinity of sea ice).

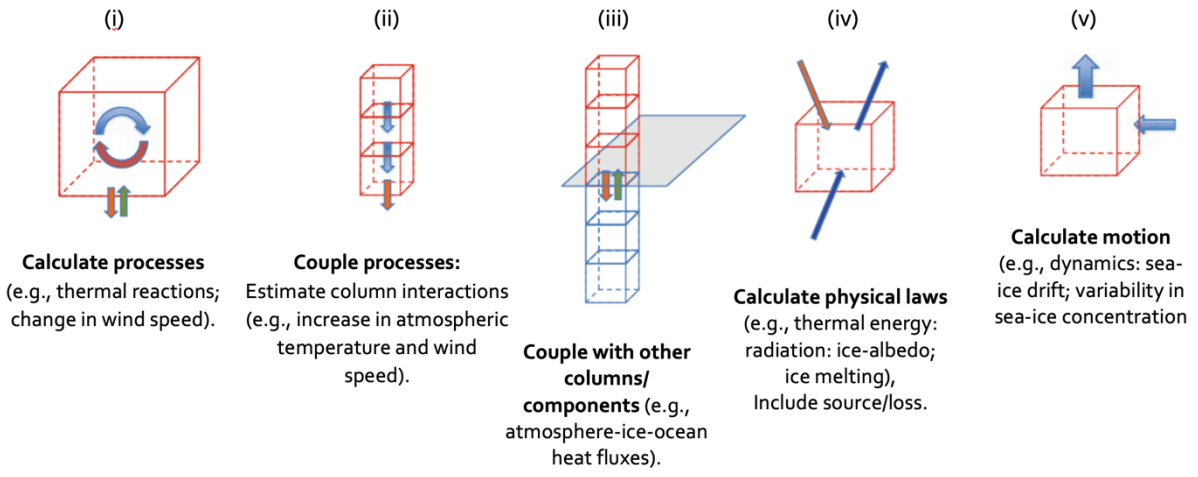

Figure 2.2: Changing the state during one time step. Climate model calculations in a time step that change the state of a mode: (i) calculate processes, (ii) estimate column interactions like change in atmospheric temperature or wind speed, (iii) couple with other columns and components, (iv) calculate physical laws like radiation, (v) estimate motions. Figure is adapted from Gettelman and Rood, (2016).

Much of our understanding of Antarctic sea ice and its variability is developed by using ocean-ice models forced by atmospheric data (King et al., 2022). Simply put, when predicting the state of the sea ice, the basic goal of a climate model is to solve the processes and physical laws that engenders change in sea ice over a given time interval (referred to as a *time step*) to arrive at a new, changed state per grid cell. This is depicted in Figure 2.2, where one box represents a grid cell: (i) there is a change in atmospheric temperature and wind speed, and, as a result, estimated interactions between the boxes take place (ii) in one model column (e.g., a change in atmospheric temperature and wind speed in the neighbouring boxes), and (iii) between component models (e.g., a change in oceanic temperature and wind-induced swells). Subsequently, (iv) physical laws describing internal dynamics are solved (e.g., a rise in atmospheric temperature results in a rise in oceanic temperature and sea-ice melt), and (v) motion is calculated (e.g., wind inducing sea-ice drift: the horizontal movement of sea ice).

The simulation product used to investigate the third and final aim was obtained from CCAM (Conformal Cubic Atmospheric Model; Engelbrecht et al., 2011), a numerical weather prediction model used for forecasting weather events and simulating climate change. This model was developed as an Australian model, and adapted by the Commonwealth Scientific and Industrial Research Organisation (CSIRO) for producing daily forecasts for the southern Africa region (Park, 2010). Overall, CCAM is designed to provide high-resolution climate simulations for specific regions of interest using the Schmidt transformation (Schmidt, 1977; Katzfey, 2015; Thatcher et al., 2016). For example, Engelbrecht et al. (2009) focussed on simulating high-impact weather events in South Africa to project climate change signals in southern Africa, while Mai et al. (2018) simulated temperature and rainfall conditions over Vietnam.

CCAM is a global atmospheric circulation model which, for this study, ran with an inline-coupled dynamic ocean model which has prognostic equations for currents, potential temperature, salinity, and the surface displacement height of the ocean. The ocean model, directly coupled with the atmosphere, solves the hydrostatic equations with a semi-Lagrangian, semi-implicit solution procedure on a reversibly staggered grid, using a terrain-following z-based coordinate system. CCAM includes a cavitating fluid model of sea ice which was formulated on the conformal cubic grid (Thatcher et al., 2016). The sea ice model is relatively new to CCAM, and not discussed in detail in previous papers (e.g., Thatcher et al., 2016). It is used experimentally in this work, due to the strong constraints provided by the nudging techniques.

Simulations are said to be *nudged* in the direction of an input field if their outputs are constrained by that prescribed field. Nudging is a basic assimilation procedure that, in a coupled climate model, ensure to maintain a given set of features. Initially, the atmospheric and oceanic reanalysis model integrates data assimilated from satellites and the observational system administered by the World Meteorological

Organization. The prescribed sea ice data is derived from OSTIA or OSI SAF (see Section 2.2.1). The ocean and sea ice serve as boundary conditions for the atmosphere, with a one-way coupling between the ice and atmosphere. This leads to the atmosphere responding to the state of the sea ice. Subsequently, CCAM atmosphere and ocean are nudged toward the reanalysis fields. This nudging process is detailed in Figure 2.3.

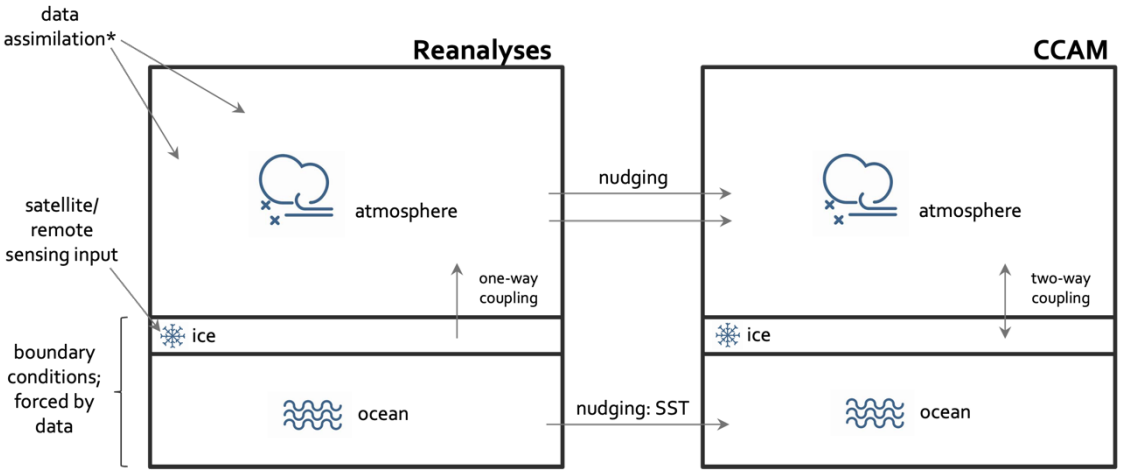

Figure 2.3: A simplified diagram showing the atmosphere-ice-ocean layers, and how CCAM atmospheric and oceanic fields were nudged by the respective reanalysis fields for this study. *data assimilation involves incorporating various sources of data into the atmospheric model, including information from satellites and observational system from the World Meteorological Organisation.

For this experiment, the CCAM forcing data used historical Greenhouse Gas emissions, and its atmosphere simulations ran coupled to its global ocean model. The oceanic and atmospheric simulations underwent three-dimensional spectral nudging at approximately 1000 km towards the reanalysis SST and atmospheric fields, respectively, This approach captured El Niño and La Niña events through weak nudging while preserving large-scale extratropical cyclones. This spectral nudging took place at a frequency of 6 hours using a digital filter following the method of Thatcher and McGregor (2009). Notably, the sea ice was left unconstrained by nudging towards observed sea-ice fields, allowing it to respond freely to both the prescribed reanalysis SST and atmospheric fields.

In summary, CCAM ran coupled with its global ocean model, and the sea-ice variability simulated in Chapter 5 was dynamically driven by the model atmosphere and ocean. Consequently, the sea ice maintains physical consistency with the atmosphere and ocean, responding freely to the respective atmospheric and oceanic dynamics.

2.2.3. Comparing ERA-Interim and ERA5 with CCAM

The products detailed in this thesis (namely, ERA Reanalyses and CCAM) possess different characteristics, such as initially prescribed fields and how the variables are constrained. These characteristics play a role in the final given sea-ice field. Table 2.1 shows the primary differences between these products.

Table 2.1: Summary of the characteristics of the products used in this thesis.

Type	Product Used	Prescribed Fields	Constrained through:	Output
Reanalyses	ERA-Interim; ERA5	SST; SIC (from external providers)	Coupled domains (of land, ocean waves, and atmosphere) forced between one another	ERA-Interim SIC; ERA5 SIC
Atmospheric model	CCAM	SST and atmospheric fields (from ERA-Interim)	Nudging towards ERA-Interim atmospheric fields and sea surface temperature	CCAM SIC

In summary, (i) with regards to the ERA products, atmospheric and oceanic conditions determine the forcing on sea ice, and (ii) with CCAM, the simulated sea-ice field is nudged towards ERA-Interim atmospheric and SST fields. As a result, the sea-ice field for the ERA products and CCAM are contingent to atmospheric forcing.

2.3. Southern Ocean cyclone track data

The identification and tracking of Southern Ocean extratropical cyclones were employed in the analyses presented in Chapters 3 – 5. This section introduces the main features of cyclone tracking algorithms and how they have been used throughout this thesis.

Extratropical cyclones are three-dimensional features of the atmosphere (Pinto et al., 2005), possessing defining characteristics of atmospheric fields such as (i) a minimum mean sea level pressure (MSLP) at its core, (ii) a temperature gradient of cold and warm air, triggering a vorticity of strong winds (clockwise in the Southern Hemisphere and anticlockwise in the Northern Hemisphere), (iii) a cold and warm front extending from the cyclone's core, and (iv) relatively high precipitation. These cyclone features are illustrated in Figure 2.4.

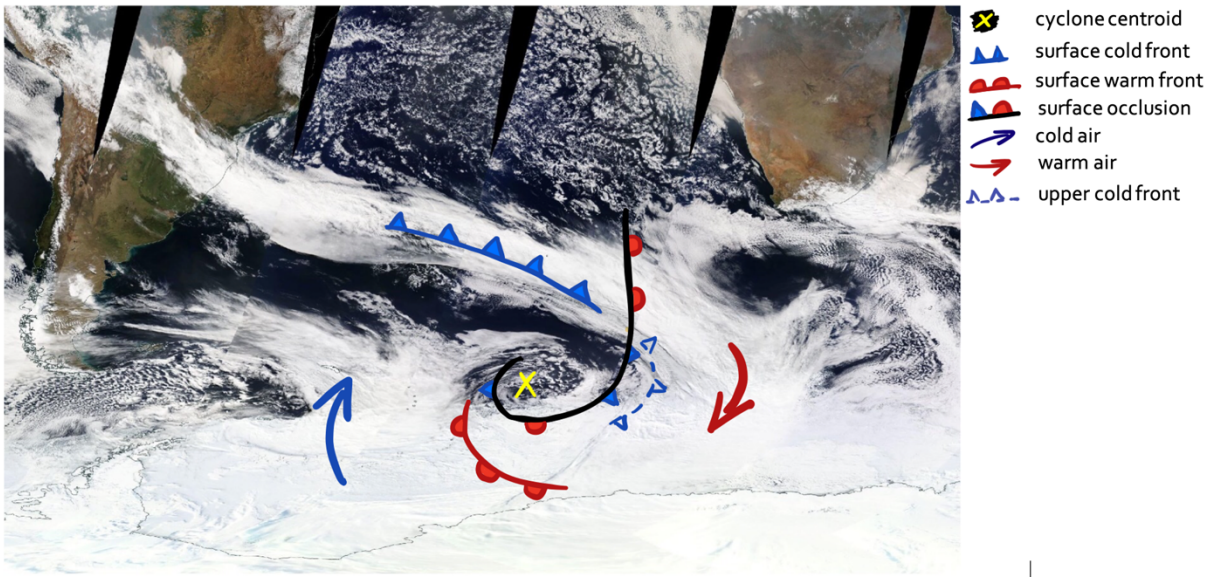

Figure 2.4: Schematic showing features of a Southern Ocean extratropical cyclone: such as cold and warm air (blue and red arrows, respectively), MSLP grid point minimum at the cyclones core (labelled "X"), a cold front (blue triangles) and warm front (red semicircles), and the cyclonic rotation (emphasized by the arrows). This image is adapted from NASA Worldview (https://doi.org/10.25250/thescbr.brk528).

Due to the fact that there are several defining characteristics of a cyclone, there are multiple methods to identify and track it. For example, cyclone cores are defined in terms of minima at sea level or at 1000 hPa geopotential heights (Pinto et al., 2005), or maxima in low level vorticity (e.g., Hodges, 1994), or a combination of both (e.g., Konig et al., 1993). The simplest methods are based on defining the cyclone's local MSLP grid point minimum (e.g., Lambert, 1998), and eliminating non-significant "systems" at a later stage (Pinto et al., 2005). Using a wide range of atmospheric fields helps identify cyclonic features of different scales. For example, vorticity focusses on the relatively small-scale end of the synoptic range (in a geostrophic sense), while MSLP and geopotential focusses on the relatively large-scale end of the range (Hoskins and Hodges, 2005).

Two different cyclone-tracking algorithms were used in this thesis. Table 2.2 summarises the attributes of these algorithms.

Table 2.2: Cyclone-tracking algorithms used in this thesis.

Chapter	Main reference for method description	Product used to obtain atmospheric variables	Atmospheric variable used to identify cyclones
Chapter 3	Pinto et al. (2005)	ERA-Interim	MSLP, vorticity
Chapter 4	Hoskins and Hodges (2005)	ERA5	MSLP, vorticity
Chapter 5	Hoskins and Hodges (2005)	CCAM	MSLP

The first algorithm was one by Pinto et al. (2005) (see Section 3.2.3 for more details), and the second was developed by Hoskins and Hodges (2005) (see Section 4.2.2 for more details). In the first two analyses using ERA-Interim and ERA5, MSLP and vorticity were utilised to identify cyclones, while the third analysis, employing CCAM, exclusively relied on MSLP. The reason only MSLP was used in the latter case was due to the unavailability of wind velocity fields at the same output frequency at the time of analysis.

The consequence of using (i) different tracking algorithms, (ii) different atmospheric variables to identify the cyclones, and (iii) different products is discussed in Chapter 6. Yet, it is important to note that, by using the same database for the sea ice, atmosphere, and cyclone tracks, consistency was provided throughout each chapter.

2.4. A cyclone's area of impact

In addition to cyclones being associated with extreme temperature differences, high winds, vorticity, and high precipitation (Figure 2.4), each cyclone can range in (i) size and (ii) intensity. Depending on the phase of the cyclone's lifecycle (Simonds, 2000) and geographical location (Lim and Simmonds, 2007), these systems can have radii ranging from 500 km to 2000 km (Hoskins and Hodges, 2005; Yuan et al., 2009; Uotila et al., 2011). Moreover, it is common for the more intense cyclones to have a relatively smaller radius, measuring approximately 330 – 665 km (4 – 6° latitude; Uotila et al., 2011). However, large case-to-case variability has been observed in the literature: for example, an intense cyclone described by Vichi et al. (2019) during July 2017 displayed a radius exceeding 1000 km. Additionally, the stage of a cyclone's lifecycle influences its strength. For example, (as cyclones act to reduce the strong temperature gradient between the mid- and high-latitudes), cyclogenesis takes place in the mid-latitudes. These cyclones are relatively weaker, and, while propagating over the ocean surface, become relatively more intense before reaching cyclolysis closer to the Antarctic continent (Simmonds and Keay, 2000).

Depending on the cyclone's size and strength, each system has an "area of impact" on the ocean surface, contributing to altering its surrounding environment both dynamically (e.g., through near surface wind activity) and thermodynamically. For example, as a cyclone passes over the open-ocean's surface, near surface wind stress can cause a domino effect of upper-ocean mixing, intensified heat fluxes, and the generation of waves (Hell et al., 2019). The schematic detailed in Figure 2.5 shows the potential effects a cyclone can have on its area of impact that includes the open and ice-covered ocean.

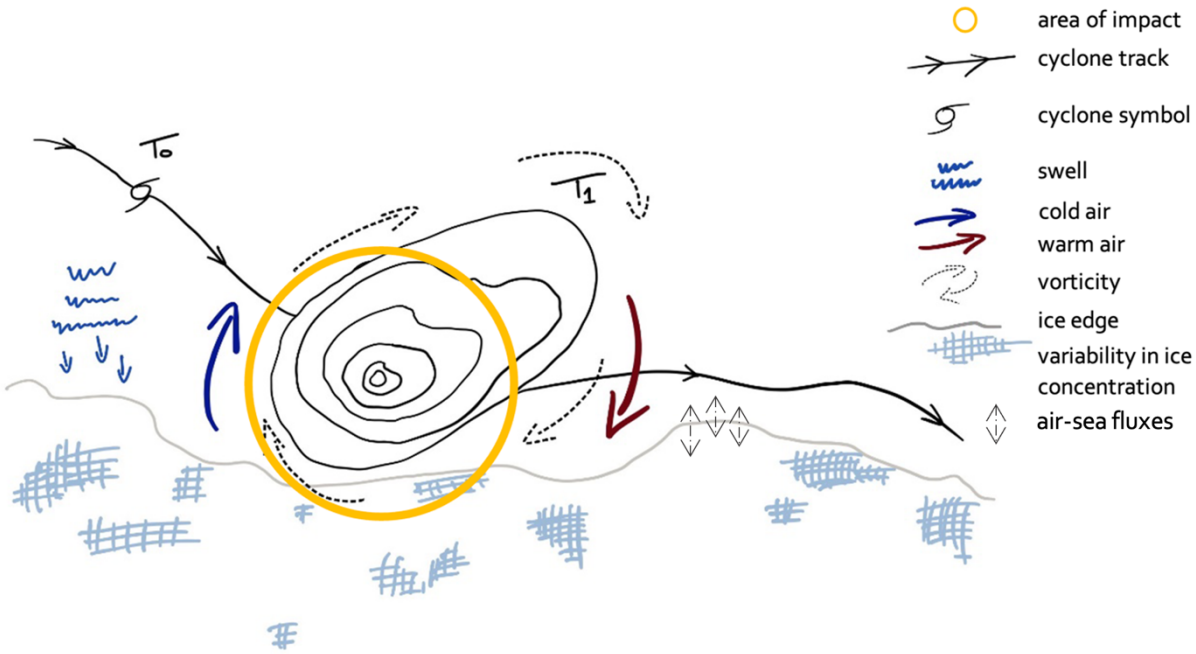

Figure 2.5: Schematic showing the track of a Southern Ocean extratropical cyclone (black line with black arrows) moving over the open ocean in a south westward direction over two days ($T_0 - T_1$). The position of the cyclone at the location of the first timestep (T_0) is shown using a cyclone symbol, while the cyclone at the second timestep (T_1) is depicted using isolines, along with defining features: the direct area of impact relative to the cyclone's centroid (yellow circle), the southward ocean swell (blue squiggles), cold air (blue arrow) and warm air (red arrow), and clockwise vorticity (dashed, black arrows). The cyclone is moving over the open ocean, slightly north from the Antarctic sea-ice edge (grey line). Change in sea-ice concentration (blue-grey hatchings) is depicted across the sea-ice region, and air-sea fluxes are depicted using two-way dotted arrows.

Figure 2.5 shows that, as a Southern Ocean extratropical cyclone travels south-westward, concurring as well as lagged effects take place. Lagged effects include swells penetrating the ice (e.g., Squire, 2018), and sea-ice break-up promoting air-sea interactions which consequently regulate sea-ice growth and melt (Kousal et al., 2022). Concurring effects include inducing change in SIC through ice drift causing sea ice to be "pushed" south on the leading side of the cyclone, while concurrently being "pulled" north on its lagging side (as shown by Vichi et al. (2019); Figure 1.6).

This thesis focussed on the immediate impacts a cyclone has within a given impact area defined through an arbitrary search-radius. In Chapters 3 and 4, the search-radius method was applied between cyclones or

atmosphere rivers (ARs) and the location of a feature of interest, such as atmospheric moisture or extreme change in SIC. This method is detailed in Sections 3.2.4 and 4.3.2, and summarised as follows:

i. The location of each cyclone track centroid was extracted as the key indicator for cyclone detection.
ii. To test the relationship between cyclones and a feature of interest, the location of the feature of interest was also extracted (see Sections 3.2.2, and 4.3.1).
iii. The geodetic distance was considered, and the feature was considered associated with a cyclone if it was within the search-radius.
iv. Given the large variability of cyclone-radii, the sensitivity of the results to the arbitrary length was tested by repeating the method using search-radii of 400 km, 600 km, or 1000 km.

Indeed, studies have shown that cyclones can impact the sea-ice environment when directly overlying the sea-ice region (e.g., de Jager and Vichi, 2022), or located slightly north of the sea-ice edge (e.g., Jena et al., 2022). Therefore, since this thesis primarily focuses on the sea-ice environment and its overlying atmosphere, the area of interest for this study was over Antarctic sea ice and 600 km north of the ice edge. The search-radius method was then performed within this area of interest.

3 CHAPTER THREE

Association between extreme atmospheric anomalies over Antarctic sea ice, Southern Ocean extratropical cyclones and atmospheric rivers

This Chapter was published as:

Hepworth, E., Messori, G., and Vichi, M. (2022). 'Association Between Extreme Atmospheric Anomalies Over Antarctic Sea Ice, Southern Ocean Polar Cyclones and Atmospheric Rivers', Journal of Geophysical Research: Atmospheres, 127(7), pp. 1–15. doi: 10.1029/2021JD036121.

3.1. Chapter Overview

Understanding that the Earth's system gains energy in the low-latitudes, and the excess energy is transported and deposited to the high-latitudes, is central to appreciating the differential effects on the atmosphere and sea ice (Simmonds and Li, 2021). In this chapter, I first focus on the atmosphere overlying the Antarctic sea-ice region before shifting our attention to an atmosphere-ice relationship in Chapter 4.

Abstract

This study analyses the association of Southern Ocean extratropical cyclones and atmospheric rivers (ARs) with extreme temperature and/or moisture atmospheric anomalies over Antarctic sea ice. The hypothesis we test is whether the circulations associated with cyclones and ARs may routinely lead to the presence of unusually warm, moist airmasses over ice-covered regions. The analysis is conducted over the extended Austral winter seasons (May – September) between May 1979 and September 2012, based on the European Centre for Medium-Range Weather Forecasts Interim reanalysis data. Approximately 27% of intense Southern Ocean cyclones and 20% of ARs occur in the vicinity of extreme temperature anomalies, while 12% of intense cyclones and 46% of ARs occur in the vicinity of extreme moisture anomalies. We summarize our results as follows: (1) extreme atmospheric anomalies over sea ice often occur in the absence of cyclones or ARs; (2) intense cyclones have a stronger association with extreme temperature anomalies than ARs; (3) approximately half of the ARs are in the vicinity of extreme moisture anomalies, while the latter's link with cyclones is weak; (4) if an AR is in the vicinity of an extreme temperature anomaly, there will likely be a concurrent extreme moisture anomaly. This points to a strong association between ARs and moisture extremes, and a nuanced link between Southern Ocean extratropical cyclones and atmospheric anomalies over Antarctic sea ice.

3.2. Introduction

The ocean-ice-atmosphere dynamics of the Antarctic and sub-Antarctic regions continue to test our understanding both at synoptic and climate timescales. Specific scientific challenges include reducing biases in ocean-ice models forced by atmospheric reanalyses (e.g. in ice motion; Massonnet et al., 2011; Uotila et al., 2014; Lecomte et al., 2016), and accurately representing Antarctic features (such as sea ice) in climate models (e.g. Barthélemy et al., 2018). Notwithstanding recent work in advancing our understanding of ocean-ice-atmosphere dynamics (e.g., Bromwich et al., 2020), progress is hampered by the intrinsic difficulty of acquiring accurate measurements in the high southern latitudes, especially in winter. Obstacles range from hostile environmental conditions (Grieger et al., 2018; Smith et al., 2019), to extreme weather phenomena (e.g., Raphael, 2007; Matear et al., 2015; Kwok et al., 2017), to the need to account (from an observational viewpoint) for the complex matrix of synoptic interactions between ocean, sea ice, and atmosphere (e.g., Vichi et al., 2019). These interactions are largely specific to the southern polar region.

In contrast with the Arctic Ocean, the Southern Ocean (SO) is host to frequent intense extratropical (polar) cyclones, and strong baroclinicity (Simmonds et al., 2003). The SO cyclones are some of the most severe storms on Earth and play a potentially large – but scarcely understood – role in modulating the ocean-ice-atmosphere interplay (Godfred-spenning and Simmonds, 1996; Simmonds, 2015; Vichi et al., 2019), and, more broadly, the regional atmospheric circulation (Simmonds, 2003; Uotila et al., 2011). Over the satellite period, the baroclinicity at the poles has increased (coupled with a decrease in baroclinicity at the midlatitudes) resulting in a poleward shift of the cyclone tracks (Simmonds and Li, 2021). The total number of SO cyclones calculated within a given area varies depending on the cyclone-tracking algorithm used (e.g. Grieger et al., 2018; Messmer and Simmonds, 2021). However, irrespective of the tracking algorithm, there is robust agreement on the cyclones' climatological lifecycle. Cyclogenesis primarily takes place in the mid-latitude Atlantic and Pacific Ocean sectors. The SO synoptic cyclones then typically follow a southeastward trajectory, and undergo cyclolysis closer to the Antarctic continent (Keable et al., 2002; Simmonds et al., 2003; Yuan et al., 2009), with maximum cyclone density found in the higher-latitude Atlantic and Indian Ocean sectors (Simmonds and Keay, 2000a; Simmonds and Keay, 2000b; Grieger et al., 2018; Hoskins and Hodges, 2005; Yuan et al., 2009). The cyclones' radii commonly range between 500 km and 2000 km (Hoskins and Hodges, 2005; Yuan et al., 2009; Uotila et al., 2011), with the more intense systems typically measuring approximately 4 – 6° latitude (~330 – 665 km) (Uotila et al., 2011). The radius of a cyclone does, however, depend on the phase of the cyclone's life cycle (Simmonds, 2000), as well as its geographical location (Lim and Simmonds, 2007). There is large case-to-case variability observed in the literature: for example, an explosive cyclone described by Vichi et al. (2019) during the austral winter of 2017 displayed a radius in excess of 1000 km.

A related, yet distinct atmospheric feature that can affect the ocean-ice-atmosphere dynamics are atmospheric rivers (ARs). ARs are synoptic-scale long and narrow corridors of water vapor, often originating from tropical moisture sources (Nieman et al., 2009). They account globally for ~90% of the

meridional water vapor transport towards the mid and high-latitudes (Nash et al., 2018; Wille et al., 2021), acting as key contributors to the interannual variability of precipitation across sea ice (Wille et al., 2021). In the Southern Hemisphere, ARs are predominantly located between 40°S and 60°S and can extend poleward achieving lengths in excess of 2000 km (Simmonds et al., 2012). ARs are typically identified ahead of the cyclone's cold front (Zhu and Newell, 1998; Nash et al., 2018; Francis, K. S. Mattingly, et al., 2020), which is a region of enhanced water vapor content (Nieman et al., 2009). Intense ARs can in turn aid in the strengthening of cyclones by providing more water vapor for latent heat release (Zhang et al., 2019). Although it is common for ARs to be associated with cyclones, it is relatively not as common for cyclones to be paired with an AR (Zhang et al., 2019).

A key role of both SO cyclones and ARs is their contribution to the poleward energy transport (Patoux et al., 2009), which can be associated with large moisture and temperature anomalies in the high latitudes (Grieger et al., 2018; Francis et al., 2020). For example, Krinner et al. (2007) presented observations indicating that frequent, strong cyclones off the Antarctic coast bring the bulk of the annual total precipitation. A high match between cyclones and precipitation is shown by Papritz et al. (2014), demonstrating that, over the Southern Ocean, between 60% and 90% of strong precipitation (>75th percentile) events are a result of cyclones and fronts.

However, an analysis of the concurrent relationship of extratropical cyclones and ARs with ice-covered Antarctic regions has not been attempted before in the literature. Warm-core anomalies have been identified in five cyclones crossing the winter South Atlantic marginal ice zone (MIZ), supported by in-situ measurements on sea ice (Vichi et al., 2019). ARs have further proven to play a key role for understanding the Antarctic surface mass balance (e.g., Gorodetskaya et al., 2014; Francis et al., 2020). For example, the anomalously high amounts of total precipitable water and cloud liquid water content (as a result of ARs) were a key contribution to the sea ice melt in the observed Weddell Polynyas in November 1973 and September 2017 (Francis et al., 2020). These findings are in agreement with Wille et al. (2019) who indicated that surface melt events in the West Antarctic are linked with ARs and the related anomalous poleward moisture transport. These results support the hypothesis that it is common for ARs and intense cyclones to engender large temperature and/or moisture anomalies over the southern high latitudes, and that these in turn can affect sea ice.

Previous studies have also highlighted the role of other dynamical processes in modulating extreme atmospheric anomalies over the SO. These include the El-Nino-Southern Oscillation (ENSO) and the related Southern Annular Mode (SAM) (Hobbs et al., 2016; Stueker et al., 2017), atmospheric Rossby waves propagating to the high-latitude southeast Pacific (Turner, 2004; Ding and Steig, 2013), and the semiannual oscillation (SAO) and Antarctic circumpolar wave (ACW) (e.g., Simmonds, 2003). Similar to the synoptic-scale features, analyses specifically dedicated to sea-ice covered regions are largely lacking. As a first step to address this broad knowledge gap, and to keep our analysis focused, we test the hypothesis that the circulations associated with cyclones and ARs may routinely lead to the presence of unusually warm, moist

airmasses over sea-ice covered regions of the SO. Specifically, we track cyclones and ARs located over or in the vicinity of sea ice throughout their life-cycle, and analyse extreme atmospheric anomalies over the sea ice and their association with the presence of cyclones and ARs.

In Section 2, the data and methods used to assess the link between the two synoptic systems (cyclones and ARs) and extreme atmospheric anomalies are outlined. We consider sensitivity to the distance between the synoptic systems and extreme atmospheric anomalies, and to the intensity of cyclones. This enables a comprehensive characterization of the relationship that both cyclones and ARs have with extreme temperature and moisture anomalies over Antarctic sea ice (Section 3), which is not yet quantified in the literature. Concluding remarks are presented in Section 4.

3.3. Data and Methods

3.3.1. Data

We based our analysis on the European Centre for Medium-Range Weather Forecasts (ECMWF) Interim Re-Analysis (ERA-Interim; Dee et al., 2011) over all extended Austral winter seasons (May – September; MJJAS) between May 1979 and September 2012. ERA-Interim provides 6-hourly data at a horizontal resolution of 0.75 degrees.

ERA-Interim was used because the cyclone tracking method used for our analysis (see Section 2.3) was developed using the ERA-Interim mean sea level pressure (MSLP). Consistency was thus provided throughout this study by using the same database for the sea ice and atmospheric variables (Section 2.2). In addition, recent work has shown that ERA-Interim and its successor, ERA5, have similar skill in reproducing the observed atmospheric conditions associated with intense cyclones over the Antarctic MIZ (Vichi et al., 2019). Similarly, McDonald and Cairns, (2020) compared the consistency in surface winds in eight reanalysis products and found that very similar patterns resulted from the ERA-Interim output and other reanalyses (including ERA5). McDonald et al. (2019) continued to recommend using either ERA-Interim or ERA5 over their region of interest, the Ross Sea.

3.3.2. Atmospheric anomalies

Our analysis of extreme atmospheric temperature and moisture anomalies focuses on the Antarctic sea ice region, defined here as the region where the sea ice concentration (SIC) is above 15% (Meier and Stroeve, 2008). Temperature 2 m above sea level (t2m) and total column water (tcw) were used to locate positive temperature and moisture anomalies. These atmospheric anomalies were computed as deviations from their respective climatologies, which were calculated as grid-cell averages over 1979 – 2012, with a 6-hourly temporal resolution.

From these results, the 95th percentile of the anomalies was calculated and the values above this threshold were defined as extreme atmospheric anomalies (which we, hereafter, refer to as "extremes"). Figure 1

shows an example of temperature and moisture extremes identified over sea ice for 30 July 1990 at 06h00 UTC.

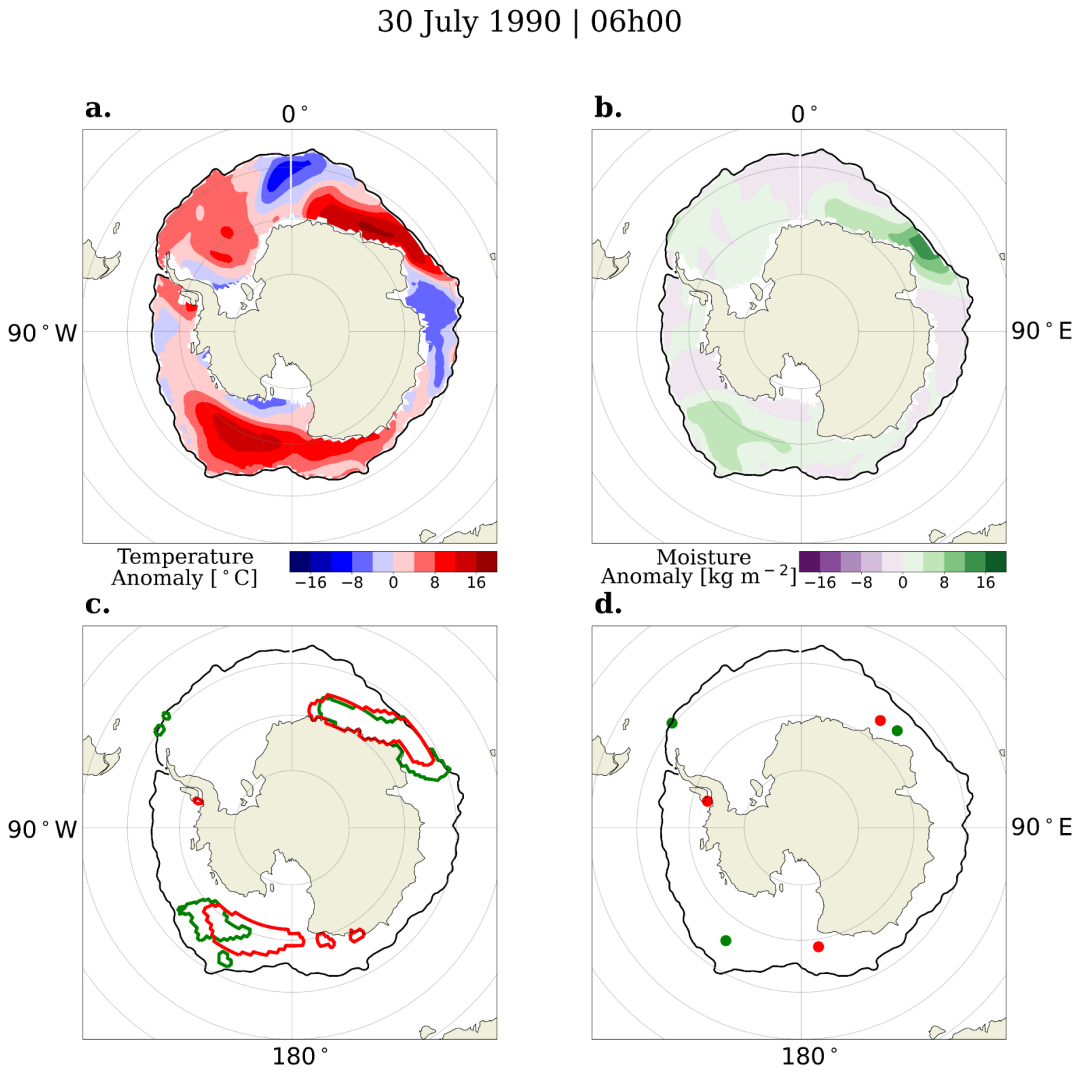

Figure 3.1: Atmospheric (a) temperature and (b) moisture anomalies (over Antarctic sea ice), from the ERA-Interim data set on 30 July 1990 at 06h00 UTC, from which (c) temperature extremes (red contours) and moisture extremes (green contours) were extracted, and (d) the location of each anomaly's centroid was calculated. The sea-ice edge is denoted by the black contour lines.

Atmospheric extremes are typically detected in clusters of contiguous grid cells (Figure 3.1c). Each cluster is identified, and the longitude and latitude of its centroid are used to define the location of the extremes (Figure 3.1d). If the distance between two or more extreme anomaly centroids is below a given threshold, the extremes are grouped together, and their location is defined as the average of the centroids. We tested threshold distances of 400 km, 600 km, and 1000 km, depending on the size of the search-radius between a cyclone and an atmospheric anomaly (as explained in Section 2.3).

Separate 95% thresholds to define the atmospheric extremes were initially tested for the outer and inner sea-ice regions (which were defined as the regions of relatively higher or lower sea-ice variability, respectively). However, we observed that separating these regions provided a discontinuous distribution (not shown) and, thus, a single threshold for the entire Antarctic sea ice region was used to produce a more spatially coherent distribution of atmospheric extremes.

3.3.3. Detection of cyclone and atmospheric river tracks

The present study uses the tracking algorithm developed by Pinto et al. (2005) which identifies cyclone core tracks using vorticity calculated from the Laplacian of the MSLP. The tracks have been computed from ERA-Interim reanalysis at 6-hourly temporal resolution, as provided in the intercomparison by Neu et al. (2013) and analysed by Grieger et al. (2018). Since consistency across different cyclone-tracking methods is generally higher for intense cyclones than for shallow ones (Neu et al., 2013), we expect our analysis not to be overly sensitive to the choice of the tracking algorithm. We discuss this aspect further in Section 4.

To identify atmospheric rivers, the Image-Processing based Atmospheric River Tracking (IPART) algorithm, made available by Xu et al. (2020), was used. This algorithm was used to detect and track ARs from gridded Integrated Vapor Transport (IVT) data from ERA-Interim reanalysis at 6-hourly temporal resolution. In contrast with cyclones, ARs are not identified by an unambiguous core. Since we are interested in anomalies over sea ice, the southernmost point of each AR was used as its location. The intensity of ARs was not considered in this analysis.

3.3.4. Search-Radius method and random association

The location of each atmospheric extreme's centroid was extracted (see Section 2.2), and the number of cyclones and ARs within a given radius of the centroid was calculated (which we term search-radius method). We then considered: (i) the distance that a cyclone or AR was from an atmospheric extreme; and (ii) the definition of cyclone intensity.

i. When considering distance, the search-radius method was repeated using a radius (considered as the impacting area of individual cyclones or ARs) of 400 km, 600 km, or 1000 km. Therefore, the cyclones and ARs included in this analysis were those within a given radius of an atmospheric extreme centroid on sea ice. The percentage of cyclones or ARs within a given radius from an extreme, relative to the total number of cyclones or ARs tracked, was calculated. The total number of cyclones or ARs tracked was defined as their respective total numbers over the sea ice or north of the sea ice but within one search radius from the sea ice edge.
ii. When considering cyclone intensity, the search-radius method was applied separately for intense cyclones as well as non-intense cyclones. There are numerous ways to define intense cyclones. For example, considering the MSLP climatological field, and defining intensity in

terms of 'relative' central pressure (e.g., Simmonds and Wu, 1993; Lim and Simmonds, 2002), or in terms of percentile thresholds (Grieger et al., 2014). This study classified intense cyclones as tracked cyclones (see point (i) above) with minimum central pressure threshold below the 1st, 5th, or 10th percentiles of the distribution of all tracked cyclones over MJJAS. Conversely, non-intense cyclones were identified as those with minimum pressure levels greater than the chosen threshold. These thresholds were computed separately for each month (from May to September), with an average minimum central pressure threshold of around 941 hPa, 952 hPa, and 957 hPa below the 1st, 5th, and 10th percentiles, respectively.

The results for these different thresholds were compared. In Section 3.1, an atmospheric extreme is considered to be associated with a cyclone or with an AR if its centroid is within a search-radius (400 km, 600 km, or 1000 km) from the cyclone or AR's location. In Section 3.2 we focus on the results using the 600 km radius and the 5th percentile threshold. This is because very large cyclones (with a radius larger than approximately 6° latitude (~665 km)) are typically not very intense (Uotila et al., 2011), and the 5th percentile provides a good balance between extremeness of the cyclones and sample size. We nonetheless show the results for the two additional search radii (400 km and 1000 km) and intensity thresholds (1st and 10th percentiles) to verify the robustness of our conclusions to the chosen parameters.

Additionally, to validate the strength of the relationship between the extremes and synoptic systems, we implemented a random sampling procedure. This was done by randomly drawing the same number of grid cells as the number of tracked ARs or intense cyclones (within the 5th percentile threshold). This was repeated 2000 times, and the 95th percentile of the number of grid cells that were within 600 km from the extremes in each one of the 2000 random draws was calculated. These results provide an indicative upper confidence interval for a statistically significant link between the synoptic features and on-ice extremes.

3.4. Results

3.4.1. Multifarious links between cyclones, ARs, and extreme atmospheric anomalies

To make an initial evaluation of the link between SO cyclones, ARs, and extreme atmospheric temperature and moisture anomalies, some illustrative case studies are presented.

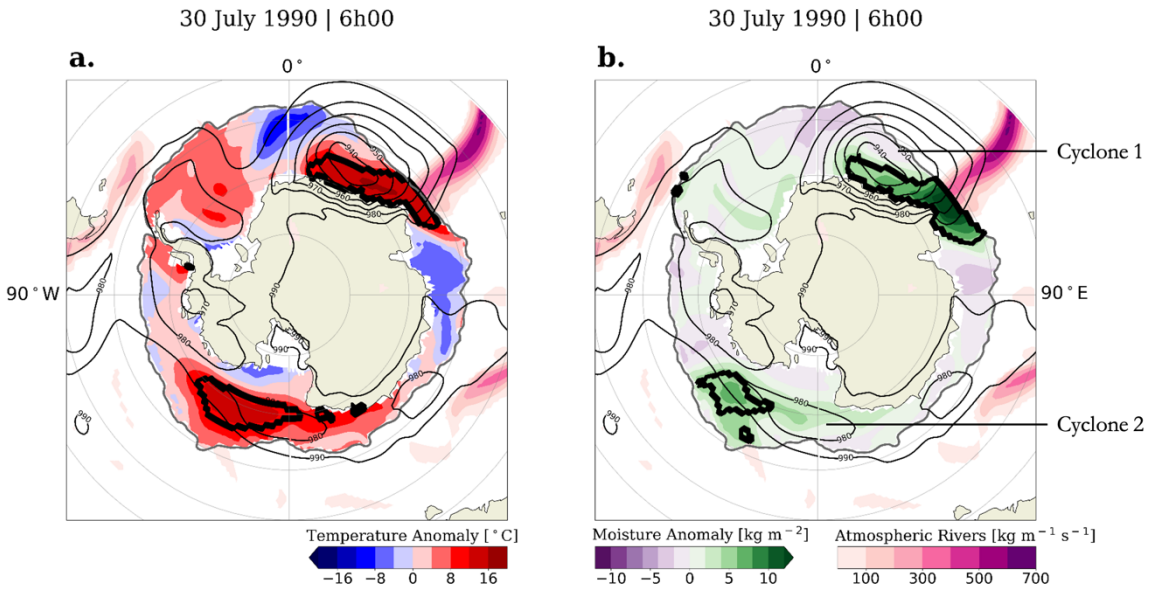

Figure 3.2: Atmospheric (a) temperature, and (b) moisture anomalies shown over Antarctic sea ice (intermediate grey contour lines) on 30 July 1990 at 06h00 UTC (case study 1). The extreme atmospheric (a) temperature and (b) moisture anomalies are denoted with thick black contour lines. The mean sea level pressure isolines are overlain (thin black contour lines), and the atmospheric rivers are denoted by the elongated pink and purple features. All data are from the ERA-Interim data set.

Case study 1 (30 July 1990 at 06h00 UTC, Figure 2) shows that atmospheric extremes can be induced by intense as well as non-intense cyclones, and that ARs are found on the leading side of a cyclone. The chosen timestep displays both an intense cyclone (labelled "Cyclone 1" in Figure 2b) with a minimum pressure of 933 hPa and a non-intense cyclone (labelled "Cyclone 2") with a minimum pressure of 972 hPa. There are temperature and moisture extremes on the eastward and poleward flank of Cyclone 1 in the East Atlantic Ocean as well as in the Ross Sea in the vicinity of Cyclone 2. Additionally, on the leading side of Cyclone 1, there is an AR extending poleward, while no AR is observed in Cyclone 2. After a visual inspection of several cases reveals that the extremes are often located on the south-eastern flank, downstream of the cyclone's direction, with the temperature anomaly extending over the core of the cyclones.

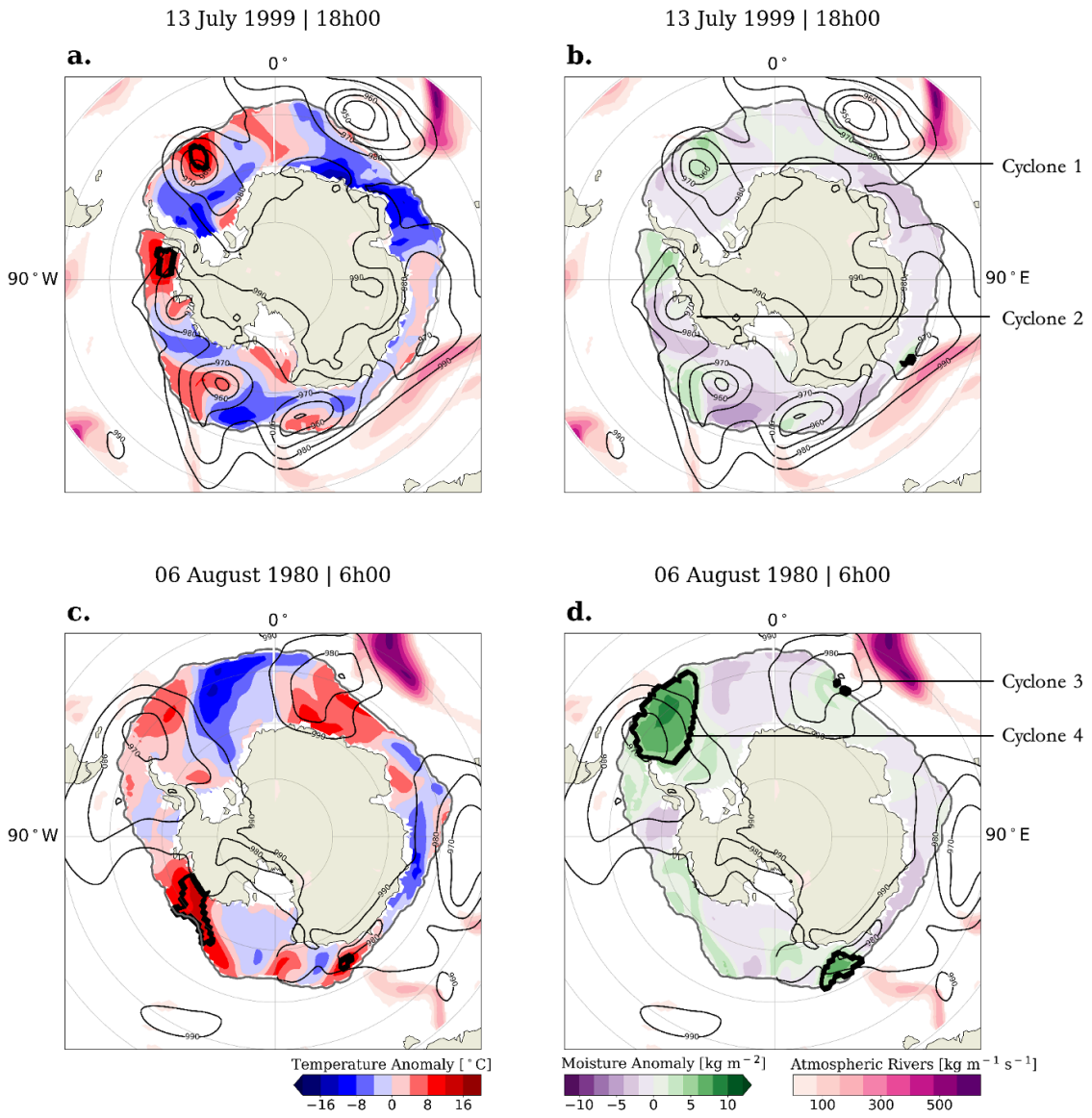

Figure 3.3: As Figure 2, but for (a,b) 13 July 1999 at 18hoo UCT (case study 2), and (c,d) 6 August 198o at o6hoo UTC (case study 3).

Case studies 2 (13 July 1999 at 18h00 UTC, Figure 3a,b) and 3 (6 August 1980 at 06h00 UTC, Figure 3c,d) suggest that temperature and moisture extremes need not occur concurrently, that intense cyclones or ARs do not necessarily engender on-ice extremes, and that such extremes can occur in the absence of cyclones or ARs. In case study 2, in the Weddell and Bellingshausen sectors, two cyclones (labelled "Cyclone 1" and "Cyclone 2" in Figure 3b) are associated with temperature extremes, while the co-located moisture anomalies are positive but not extreme. Conversely, in case study 3, two cyclones are associated with moisture extremes in the eastern Atlantic and Weddell sectors (labelled "Cyclone 3" and "Cyclone 4" in Figure 3d) but the temperature anomalies in these sectors are not extreme. There is an AR on the leading side of an intense cyclone (in the 5th percentile range) in the East Atlantic sector, but neither the cyclone nor the AR are associated with extreme on-ice anomalies (case study 2; Figure 3a,b). There are also ARs on

the leading edges of non-intense cyclones in the Indian Ocean (case study 2) and East Atlantic (case study 3) sectors (Figures 3a,b and c,d, respectively). In both cases, the non-intense cyclones and ARs are associated with small-scale moisture extremes but not temperature extremes. Although Cyclones 1 and 4 are associated with a temperature and moisture extreme, respectively, there is no AR present on the leading side of these cyclones (Figures 3a and 3d, respectively). Finally, case study 3 also shows that one may have extensive regions of temperature extremes without any cyclone or atmospheric river in the vicinity (Figure 3c).

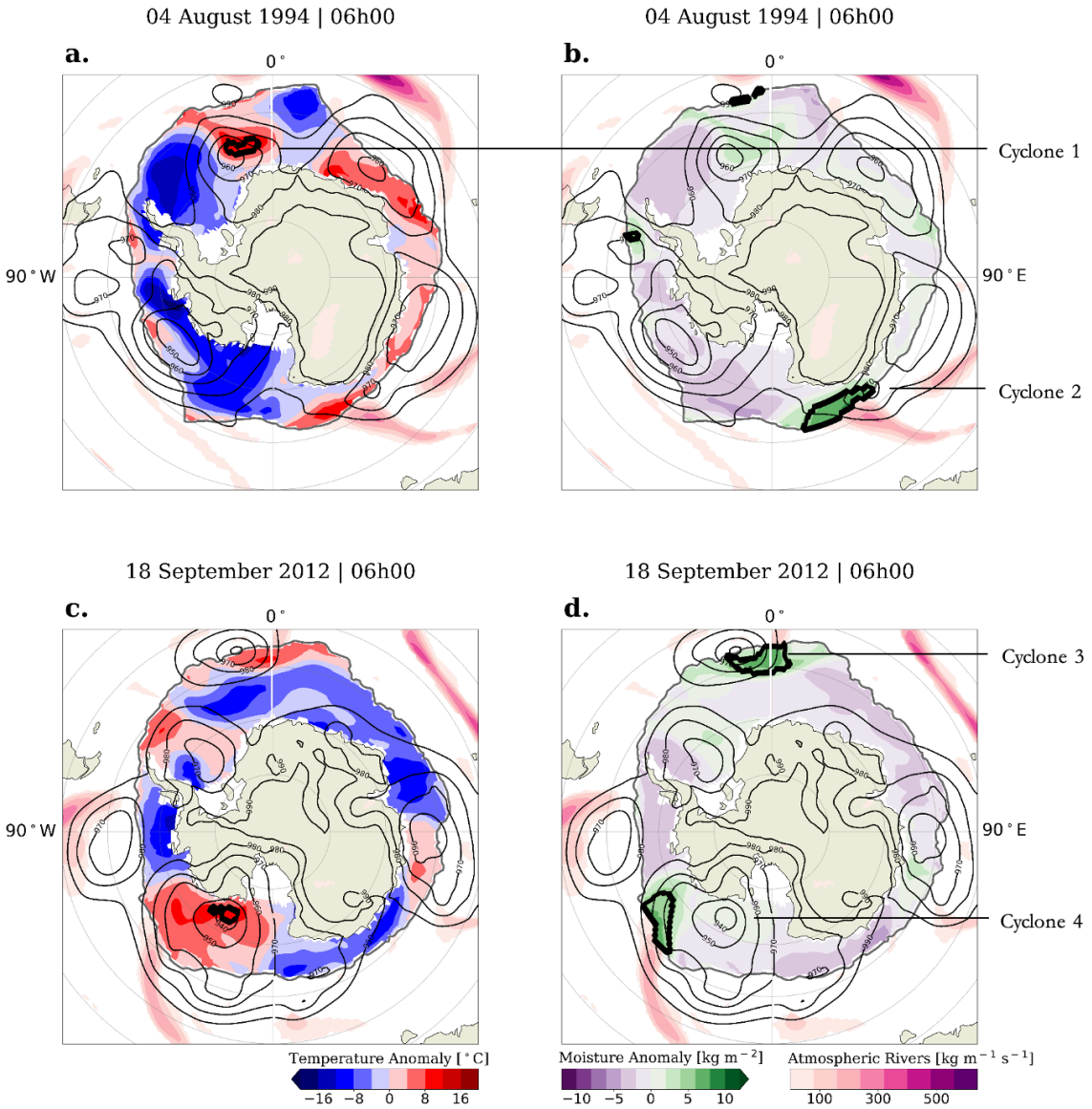

Figure 3.4: As Figure 2, but for (a,b) 4 August 1994 at 06h00 UTC (case study 4) and (c,d) 18 September 2012 at 06h00 UCT (case study 5).

Case studies 4 (4 August 1994 at 06h00 UTC, Figure 4a,b) and 5 (18 September 2012 at 06h00 UTC, Figure 4c,d) highlight the fact that temperature and moisture extremes can be induced by cyclones both close to

the ice edge as well as deep into the ice. For example, moisture extremes are associated with Cyclones 2 and 3 (labelled in Figures 4b and 4d, respectively) which are close to the ice edge (155 km and 120 km from the edge, respectively). On the opposite, a temperature extreme is associated with Cyclone 1 (labelled in Figure 4a) which is deep into the ice (1095 km from the ice edge), and concurrent temperature and moisture extremes are associated with Cyclone 4 (1200 km deep into the sea ice; labelled in Figure 4d). Furthermore, in relation to Cyclone 4, which affects the extended Ross Sea ice surface, the warm-core extreme penetrates deep into the ice, while the moisture extreme is confined to the ice edge. A contrasting location of the temperature and moisture extremes relative to the cyclone's core is thus observed. There are ARs on the leading sides of Cyclones 2 and 4 which in both cases may be visually associated with the presence of moisture extremes (Figure 4b,d).

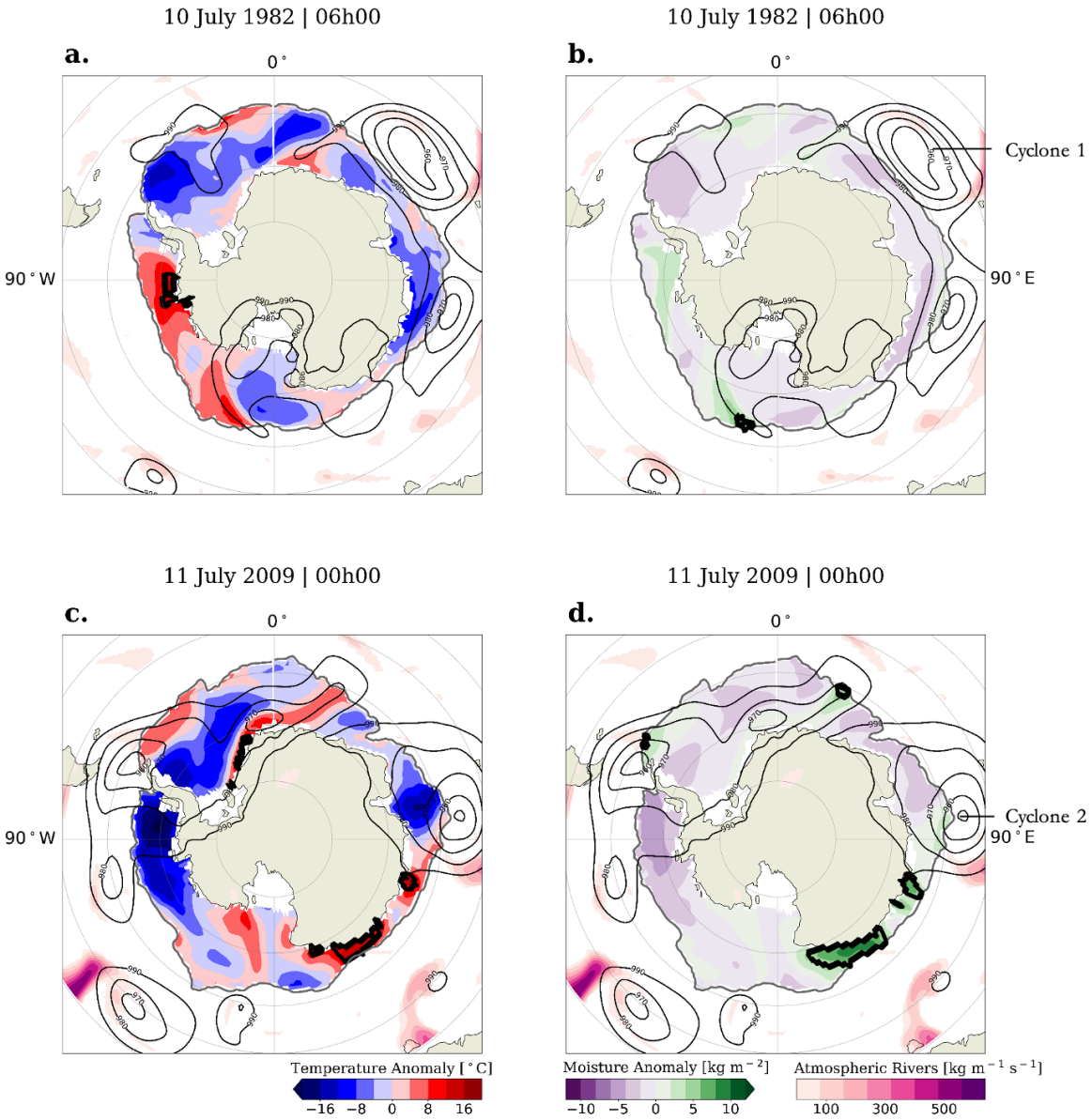

Figure 3.5: As Figure 2, but for (a,b) 10 July 1982 at 06h00 UTC (case study 6), and (c,d) 11 July 2009 at 00h00 UTC (case study 7).

To conclude our qualitative review, case studies 6 (10 July 1982 at 06h00 UTC, Figure 5a,b) and 7 (11 July 2009 at 00h00 UTC, Figure 5c,d) expand on case studies 2 and 3 in showing that extremes are not always found in correspondence with cyclones or ARs, and that even cyclones belonging to the high intensity categories can engender little or no atmospheric extremes. For example, in case study 6, a temperature extreme in the Amundsen/Bellingshausen sector is observed with no cyclone or AR in the vicinity, and an intense cyclone (in the 5th percentile range; labelled "Cyclone 1" in Figure 5b), with a relatively small AR on its leading side in the East Atlantic Ocean, engenders no extremes. Similarly, in case study 7, there is an intense cyclone (in the 1st percentile range; labelled "Cyclone 2" in Figure 5d) in the Indian Ocean sector, with an AR, leading to only limited atmospheric extremes, while the more extensive extremes in the East Pacific sector are not located in the vicinity of a cyclone nor of an AR.

3.4.2. Distribution of synoptic features and extreme atmospheric anomalies

The case studies presented above indicate that the association that cyclones and ARs have with atmospheric extremes is complex. To gain a more systematic understanding, we next analyse the full data set used in this study.

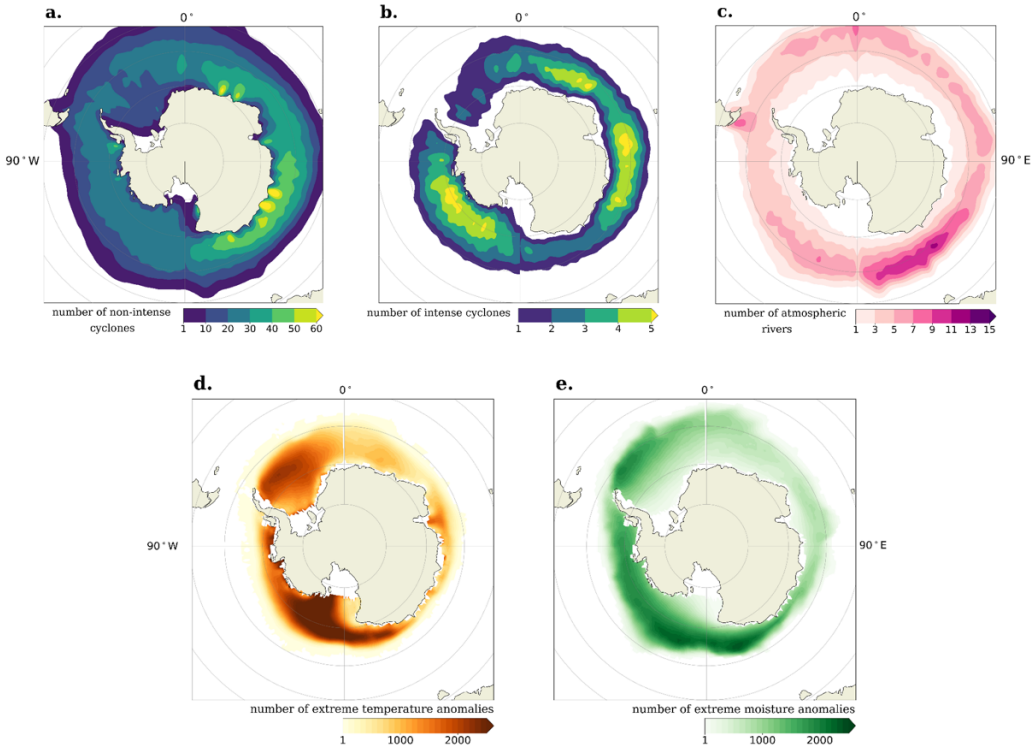

Figure 3.6: The total number of (a) non-intense cyclones, (b) intense cyclones, and (c) atmospheric rivers over Antarctic sea ice and 600 km north of the ice edge, and (d) temperature and (e) moisture extremes over Antarctic sea ice from 1979 – 2012 over the extended Austral winter period of May – September. The cyclone data are from the cyclone-tracking method developed by Pinto et al. (2005), the AR data are from the IPART algorithm, made available by Xu et al. (2020), and the extreme atmospheric data is from the ERA-Interim data set. The total number of cyclones and ARs is computed per grid cell on the ERA-Interim grid and smoothed using a Gaussian Filter (with σ=2).

As documented by e.g., Simmonds and Keay, (2000a, 2000b), Hoskins and Hodges, (2005) Yuan, Patoux and Li, (2009), and Grieger et al., (2018), the highest numbers of SO cyclones are found in the Atlantic and Indian Ocean sectors. Non-intense cyclones and ARs, which are largely grouped in the Atlantic and eastern Antarctic sectors, follow this geographical distribution. Moreover, there is a hotspot of both non-intense cyclones and ARs in the eastern Pacific sector (Figure 6a and 6c, respectively). The intense cyclones instead cluster in three hotspot areas, namely the eastern Atlantic sector, western Pacific sector, and the Ross/Amundsen sector (Figure 6b). The atmospheric extremes, detected as described in Section 2.2, present yet a different distribution. Overall, the extremes are mostly located in the western Antarctic region with the Ross/Amundsen sector emerging as a hotspot, especially for temperature extremes (Figure 6d,e). Temperature extremes and cyclones are predominantly found closer to the Antarctic continent (Figure 6a,b,d) while moisture extremes and ARs are predominantly located further away from the continent and closer to the sea-ice edge (Figure 6c,e).

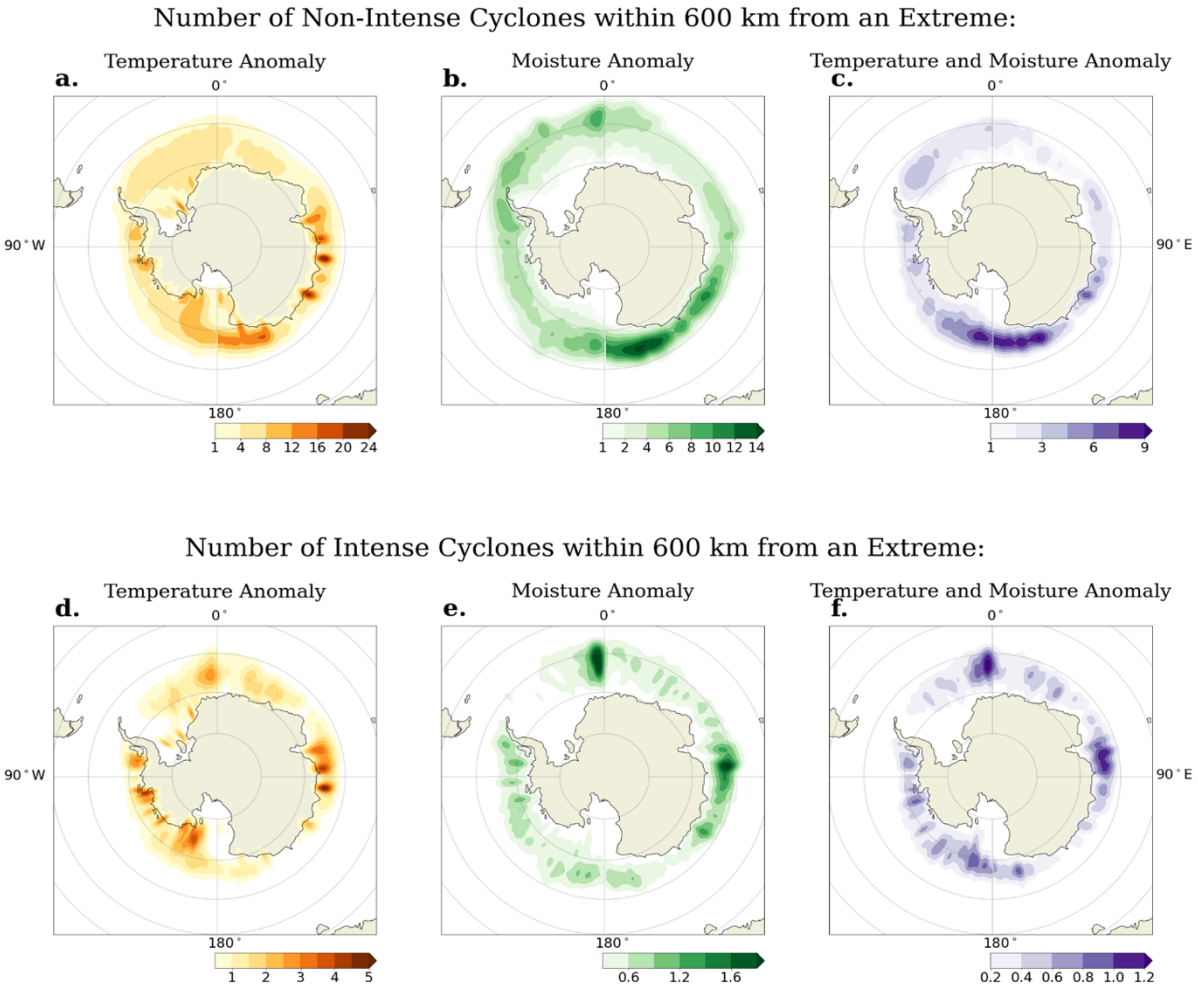

Figure 3.7: The total number of Southern Ocean (a-c) non-intense and (d-f) intense cyclones within a 600 km radius of extreme atmospheric anomalies: (a,d) temperature, (b,e) moisture, and (c,f) concurring temperature and moisture. The total number of cyclones is computed per grid cell on the ERA-Interim grid and smoothed using a Gaussian Filter (with σ=2).

To gain a more in-depth understanding of the difference between intense and non-intense cyclone distributions, we now turn our attention to the identification of cyclones found within a given search-radius from the extremes' centroids (see Section 2.4). Temperature extremes are frequently associated with both intense and non-intense cyclones close to the Antarctic continent (Figure 7a,d), whereas moisture extremes are primarily associated with those close to the sea-ice edge (Figure 7b,e). Temperature extremes appear less sensitive to the intensity of cyclones than moisture extremes (see also Figure 8), and thus are found in the regions where cyclones are modally located: the high number of non-intense cyclones in the eastern Antarctic sector (Figure 6a) and the three hotspot regions of the intense cyclones (Figure 6b) emerge clearly in Figures 7a and 7d, respectively. Moisture extremes show a frequent association with non-intense cyclones in the eastern Pacific sector (Figure 7b), whereas the moisture extremes associated with intense cyclones are observed chiefly in the mid- Atlantic and Indian Ocean sectors (specifically located around 0° and 90°E, respectively; Figure 7e).

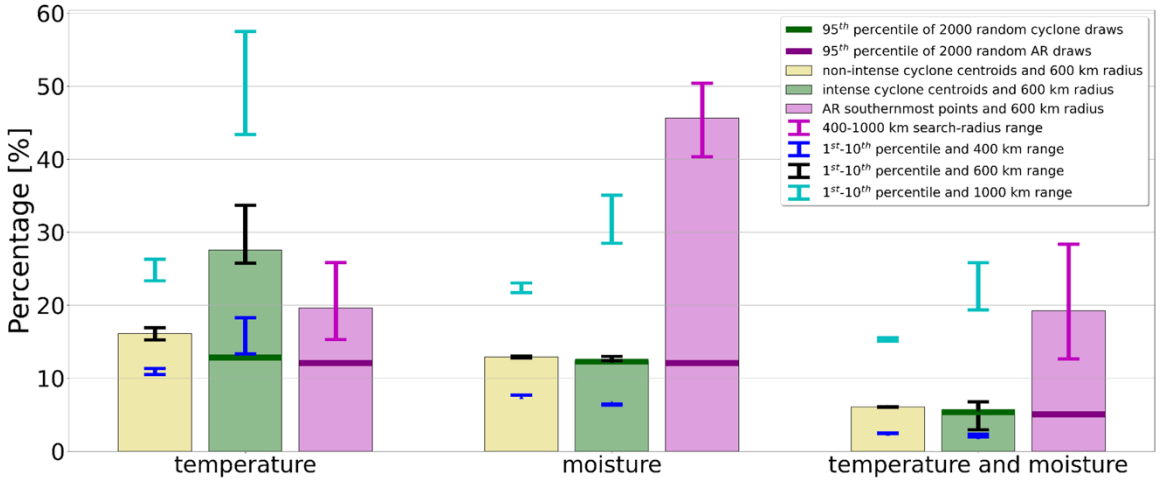

Figure 3.8: Percentage of the non-intense cyclones (yellow bars), intense cyclones (green bars), and ARs (purple bars) within 600 km of extreme atmospheric temperature anomalies, moisture anomalies, and concurrent temperature and moisture anomalies. The results for the extreme cyclones defined using the 1st and 10th percentile thresholds are denoted by the upper and lower limits of each range bar, respectively, for the 400 km (dark blue range bars), 600 km (black range bars), and 1000 km (light blue range bars) search radii. The AR 1000 km and 400 km search radii are denoted by the upper and lower pink range bars. The horizonal bars denote an indicative upper confidence interval for our random sampling.

To quantify the frequency with which (non-intense or intense) cyclones and ARs are associated with temperature and moisture extremes, we computed the percentage of cyclones and ARs within selected radii from the atmospheric extremes (Figure 8). The histogram bars highlight the results specific to the 600 km search-radius and the non-intense cyclones (greater than the 5th percentile threshold), the intense cyclones (within the 5th percentile range), and the ARs. Additional search radii and percentile ranges are shown by the thin range bars and illustrate the sensitivity of the relationship that cyclones and ARs have with atmospheric extremes to the chosen parameters.

The results for the 600 km radius (Figure 8, Section 2.4) show that approximately 16% of the non-intense SO cyclones, 27% of the intense cyclones, and 20% of the ARs are in the vicinity of temperature extremes. Similar percentages of both intense and non-intense cyclones (12-13%) are within 600 km of moisture extremes, while 46% of ARs are within 600 km of moisture extremes. Only 6% of either non-intense or intense cyclones, and 19% of ARs are in the vicinity of both a temperature and moisture extreme. The highest percentage of cyclone cores in the vicinity of atmospheric extremes expectedly occurs when the search-radius is the greatest (1000 km) and the intense cyclones are below the lowest percentile threshold (1st percentile). For this combination of parameters, approximately 57% of intense cyclones can be associated with temperature extremes, 35% with moisture extremes, and 26% with concurrent temperature and moisture extremes. Moreover, approximately 26% of ARs are 1000 km from temperature extremes whereas 28% are 1000 km from concurrent temperature and moisture extremes. This slight increase shows that, when increasing the search radius to 1000 km, an AR can concurrently be in the vicinity of a temperature extreme and more than one moisture extreme.

The 95th percentile of our random sampling (see Section 2.4) suggests that there is approximately a 12-13% chance that an intense cyclone or an AR will be 600 km from an extreme temperature or moisture anomaly. This decreases to approximately a 5% for concurrent temperature and moisture extremes.

3.5. Discussion and Conclusions

Vichi et al. (2019) presented an observational case study where an explosive cyclone crossing the East Antarctic MIZ in July 2017 engendered large atmospheric temperature anomalies over the sea ice that propagated towards the Antarctic continent. This observation resonates with previous work that highlighted the role of SO cyclones in contributing to the average poleward transport of energy and moisture (Patoux et al., 2009), and in driving large temperature and moisture anomalies (e.g. Lynch, Uotila and Cassano, 2006; Krinner et al., 2007; Uotila et al., 2011; Papritz et al., 2014). However, a systematic classification of this relationship has not been attempted before. Additionally, it is known that ARs (which are typically found on the leading side of cyclones) play a large role in transporting heat and moisture poleward over sea ice (Francis et al., 2020). Recent studies have shown the regional-scale impact that ARs and large moisture influxes have within the SO and in the Antarctic region (e.g., Francis et al., 2020; Wille et al., 2019; and Gorodetskaya et al., 2014). We therefore adopted the working hypothesis that it is common for ARs and intense cyclones to engender extreme temperature and/or moisture anomalies over the ice-covered regions of the SO, and have tested this using reanalysis data and algorithms which track cyclones and ARs. In our methodology, an extreme atmospheric anomaly was associated with a cyclone or an AR if it was within a 600 km radius of the synoptic system's location. The percentage of association changed with the choice of the search radius, but the conclusions are robust to reasonable alterations of this threshold. We evaluate the strength or weakness of the associations relative to a random sampling procedure which

indicates that, given our methodology and parameter choices, one may take a 12-13% chance of an AR or intense cyclone being in the vicinity of an extreme as a reasonable confidence bound.

The association of intense cyclones or ARs with temperature extremes over sea ice are, respectively, relatively low and moderate, and there is a weak link between cyclones and moisture extremes. This is seen in Figure 8 where approximately one sixth (16%) of non-intense cyclones, a quarter (27%) of intense SO cyclones, and a fifth (20%) of ARs are in the vicinity of extreme temperature anomalies. This is in line with results presented by Sinclair and Dacre, (2019) who showed that moisture transport to Antarctica was less dependent on cyclone intensity and more dependent on the translation speed of the cyclone. We also note that when considering the most intense cyclones and an expanded search radius around them, over half of them (57%) match a temperature extreme, and about one third (35%) match a moisture extreme, and about a quarter (26%) match concurrent temperature and moisture extremes. Additionally, our results show a strong link between ARs and moisture extremes, as approximately half of the ARs (47%) are in the vicinity of a moisture extreme. It is interesting to observe that 20% of ARs are 600 km from temperature extremes, and 19% are 600 km from concurrent temperature and moisture extremes. This indicates that if an AR is in the vicinity of a temperature extreme, there will likely be a concurrent moisture extreme Our main conclusions can be summarised as follows: (1) extreme atmospheric anomalies over sea ice often occur in the absence of cyclones and ARs; (2) intense cyclones have a stronger association with temperature extremes than ARs; (3) approximately half of the ARs are in the vicinity of moisture extremes, while the latter's link with cyclones is weak; (4) if an AR is in the vicinity of a temperature extreme, there will likely be a concurrent moisture extreme. In other words, we find a moderate but significant association between intense cyclones and temperature extremes, a strong association between ARs and moisture extremes, little to no association between cyclones and moisture extremes, and that, relative to ARs, intense cyclones have a higher association with temperature extremes.

Our working hypothesis was that it is common for intense cyclones and ARs to engender temperature and/ or moisture extremes over the SO, including over Antarctic sea ice. There indeed is a strong association between ARs and moisture extremes over sea ice. However, although cyclones are considered to be a primary transport mechanism of heat and moisture into the polar regions (particularly in winter; Grieger et al., 2018), the link between intense cyclones and temperature and moisture extremes over Antarctic sea ice proves to be more complex than originally hypothesized. Our results do show that, relative to non-intense cyclones, intense cyclones are more likely to induce extreme atmospheric anomalies (Figure 8). Nonetheless, the case study by Vichi et al. (2019) is only representative of 57% of intense cyclones below the 1st percentile threshold, which is the most restrictive definition we considered here. Our results further highlight important differences between temperature and moisture extremes. The geographical composites presented in Figure 7 show that temperature extremes are less dependent on cyclone intensity than moisture extremes, as the former are found in regions where non-intense and intense cyclones are modally located (Figures 7a and 7d, respectively). The moisture extremes associated with intense cyclones are predominantly located in the mid- Atlantic and Indian Ocean sectors (Figure 7e), in agreement with Grieger et al. (2018). Additionally,

in the Ross/Amundsen sector, there is a relatively high number of intense cyclones as well as extreme atmospheric anomalies (Figures 6b,c,d). Our methodology cannot determine whether atmospheric extremes in this region are due to the relatively higher number of intense cyclones, or, vice versa, whether the extremes provide favourable conditions for intense cyclones surviving over the sea ice. Based on the literature, the former may seem more plausible (e.g., Lynch, Uotila and Cassano, 2006; Krinner et al., 2007; Papritz et al., 2014). Our results highlight the need to focus future work on regional scales, to verify whether, and through which physical mechanisms, intense cyclones are more or less likely to engender atmospheric extremes in specific sectors of the SO. This includes clarifying whether the explosive nature of cyclones or details of their tracks and translation speed may affect their ability to generate on-ice atmospheric extremes.

We can also leverage our analysis to make hypotheses about the role of sea ice in modulating these extremes. We find that extreme temperature anomalies over sea ice are mostly located closer to the Antarctic continent (where sea ice is more consolidated with lower variability), and moisture extremes are largely observed closer to the sea-ice edge (where sea-ice variability is higher) (Figures 6 and 7d,e). We therefore speculate that there is an interactive role between the atmospheric extremes and sea-ice variability. Krinner et al. (2007) provides specific regional-scale examples of how changes in SIC influence the number of cyclones which, in turn, leads to changes in precipitation. Additionally, Francis et al (2020) and Wille et al. (2019) indicate the impact ARs (bringing in moisture) can have on the sea ice region. Our results support the hypothesis that extreme atmospheric anomalies are, in turn, likely to contribute to sea ice conditions. Although this is an aspect which we did not address explicitly here, we identify it is a key area for future research activity. It is interesting to note that, although temperature increases tend to lead to increased moisture transport due to the higher moisture holding capacity of warmer air, an extreme temperature anomaly rarely occurs within the same cyclone as an extreme moisture anomaly. Additionally, only 19% of ARs are in the vicinity of both a temperature and a moisture extreme. It is, therefore, possible that many of the analysed cases may lead to intense solid precipitation without extreme warming. This would preserve the snow on the sea ice, and by serving as insulation and reducing the conductive heat-flux (Batrak and Müller, 2019), potentially extending the persistence of underlying ice. These factors may contribute to the large sea-ice variability observed closer to the Antarctic sea-ice edge. Therefore, a stimulating analysis would be to repeat the present study over regions of high and low sea-ice variability.

It is important to note that our analysis needs to be repeated using other atmospheric data sets and cyclone tracking methods in order to investigate its robustness. For example, results presented by Grieger et al. (2018) and Messmer and Simmonds (2021) show that the total number of SO cyclones vary depending on the cyclone tracking algorithm used. The cyclone tracking algorithm by Pinto et al. (2005) that was used here, identifies a larger number of tracks in the SO than other algorithms (Neu et al., 2013). While we do not expect this to have a large impact for intense cyclones – where different algorithms generally show a good level of agreement (Neu et al., 2013; Grieger et al., 2018) – it is likely to lower the percent association between non-intense cyclones and extreme atmospheric anomalies. Indeed, given a fixed number of atmospheric extremes, an algorithm identifying more cyclone tracks may intuitively lead to fewer of these

being associated with the extremes. At the same time, the Pinto et al. (2005) algorithm identifies roughly 20% more cyclones in the SO than the average of all algorithms considered in Neu et al (2013). As such, we deem that our qualitative conclusions concerning the fact that only a modest fraction of non-intense cyclones engender extreme atmospheric anomalies would hold even if using algorithms identifying a lower number of tracks. Additionally, it will be fruitful to repeat this analysis using a relative central pressure method to identify intense cyclones (rather than the percentile threshold method we adopted). This is motivated by previous studies that have shown how the dynamic meaning of the cyclone's central pressure can be better understood relative to the background climatological MSLP (Lim and Simmonds, 2002). For example, Simmonds and Wu (1993) have shown that cyclones become weaker (relative to the climatological MSLP) over most of the Antarctic sea ice region. Moreover, using the centroid of the extreme temperature and atmospheric anomalies will change the results of the search-radius analysis compared to using the nearest point to the cyclone. Nevertheless, this approach proved highly effective in our analysis for identifying extreme-cores within the vicinity of a cyclone-core. It is worth considering the possibility of replicating this methodology by utilizing the nearest point of the extreme anomaly to the cyclone, as was implemented for the atmospheric rivers. Lastly, the algorithm used to identify ARs is primarily designed for global detection (Xu et al., 2020). It is worth noting that this may exhibit weaker detection capabilities in the Antarctic region. In contrast, Liang et al. (2022) utilized a polar-specific AR detection algorithm, demonstrating capability in detecting high-impact ARs over the Antarctic sea-ice region.

As alluded to in Section 1, previous studies have assisted in improving our understanding of ocean-ice-atmosphere dynamics in the Antarctic and subantarctic regions (e.g., Bromwich et al., 2020). Our results contribute to this effort by providing a quantitative evaluation of the link between SO cyclones, ARs, and extreme temperature and moisture over sea ice.

4

CHAPTER FOUR

Synoptic-scale extreme variability of winter Antarctic sea-ice concentration and its link to Southern Ocean extratropical cyclones

This chapter is under review as:

Hepworth, E., Messori, G., and Vichi, M. 'Synoptic-scale extreme variability of winter Antarctic sea-ice concentration and its link to Southern Ocean extratropical cyclones' in the Journal of Geophysical Research: Oceans.

4.1. Chapter Overview

In Chapter 1, the importance of sea ice (in the global climate) and studying it at both an interannual scale and at a regional scale was introduced. Thereafter, it was shown that (i) previous studies have identified a link between cyclones and sea-ice variability (Section 1.1.1), (ii) that the average number of Southern Ocean extratropical cyclones is the highest in Austral autumn and winter (Section 1.1.2), and that (iii) extreme temperature anomalies over Antarctic sea ice are relatively closely linked with intense cyclones (Chapter 3). Therefore, since extratropical cyclones play a role in the variability of Antarctic sea ice and weather circulations over the sea-ice environment, it is hypothesized that Southern Ocean extratropical cyclones play a key role in engendering extreme variability in Antarctic sea-ice concentration over the extended Austal winter period.

Here, this hypothesis is tested by identifying extreme variability in Antarctic sea-ice concentration at a synoptic scale, and by investigating the extent to which it may be engendered by extratropical cyclones.

Abstract

This study provides a systematic analysis of the extent to which extreme variability in winter Antarctic sea-ice concentration may be caused by extratropical cyclones. We characterise sea-ice variability and cyclone activity in different Southern Ocean sectors using atmospheric reanalyses and a cyclone-tracking algorithm, and then quantify the proportion of extreme sea-ice variability engendered by cyclones of different intensities. The regions with relatively lower sea-ice area (the King Haakon VII, East Antarctic, and Bellingshausen sectors) have an even distribution of cyclones within all intensity ranges, while, in the sectors with higher sea-ice area, the Ross/Amundsen displays a higher number of intense and weak cyclones, and the Weddell sector has the majority of weak cyclones. Our systematic analysis reveals a significant link between extreme variability in winter sea-ice concentration and: (1) all cyclones in the Ross/Amundsen sector; (2) all but the weakest cyclones in the King Haakon VII, East Antarctic, and Bellingshausen sectors; and (3) all but the most intense cyclones in the Weddell sector. The latter result is explained by the fact that the Weddell sector experiences more frequent, weaker cyclones that the other sectors. Cumulatively, approximately 30 – 40% of the extreme sea-ice variability is caused by extratropical cyclones within all regions.

Plain Language Summary

The Antarctic is surrounded by a vast region of ice-covered ocean (sea-ice). This ice is not a solid lid over the ocean, but rather an ever-changing mosaic of ice, water, and air. The ice is affected and moved around by both the ocean and the atmosphere. A phenomenon which can have a particularly large impact on the sea-ice is extratropcial cyclones. Here, we analyse how cyclones can cause the amount of sea-ice to change within a few days, and whether this depends on the strength of the cyclone. We looked separately at different regions of Antarctica and the surrounding ocean. Our results show that 30 – 40% of the extreme change in sea-ice cover is associated to cyclones, with the most intense cyclones contributing to 6%. In the Weddell sector, extreme sea-ice changes are more closely connected to frequent weaker cyclones.

4.2. Introduction

In contrast to the Arctic, the growth of the Antarctic sea-ice region is unbounded by land: promoting an environment for waves from the open ocean to break up the ice hundreds of kilometers from the ice edge (Kohout et al., 2014; Stopa et al., 2018; Kohout et al., 2020), and for the frequent passage of extratropical cyclones (Uotila et al., 2011; Hepworth et al., 2022). The Antarctic sea-ice region is, therefore, home to a complex web of ocean-ice-atmosphere interactions (Godfred-Spenning and Simmonds, 1996; Eayrs et al., 2019), and continuously influenced by both oceanic and atmospheric drivers. These include the strength of near-surface winds (e.g., Godfred-Spenning and Simmonds, 1996; Turner et al., 2015; Vichi et al., 2019; Matear et al., 2015; Holland and Kwok, 2012; Kwok et al., 2016; Blanchard-Wrigglesworth et al., 2021a; Blanchard-Wrigglesworth et al., 2021b), sea surface temperature (e.g., Raphael, 2007; Stammerjohn et al., 2011), and ocean currents (e.g., Armitage, et al., 2018). In parallel with the annual advance and retreat in sea-ice extent, there is a large variability in sea-ice concentration (SIC) at a synoptic scale (e.g., Vichi et al., 2019; de Jager and Vichi, 2022; Jena et al., 2021). However, there is currently no consensus on the primary mechanisms modulating synoptic-scale change in SIC (Eayrs et al., 2019; Blanchard-Wrigglesworth et al., 2021a). Reasons for the lack of consensus include the scarcity of Southern Ocean (SO) in-situ data (Smith et al., 2019), and the complexity of the ocean-ice-atmosphere system in the Southern Hemisphere (e.g., Eayrs et al., 2019).

A strong link between the variability of SIC (hereafter referred to as SIV) and surface wind has been highlighted in several studies (e.g., Godfred-spenning and Simmonds, 1996; Holland and Kwok, 2012; Matear et al., 2015; Turner et al., 2015; Kwok, Pang and Kacimi, 2017; Vichi et al., 2019; Blanchard-Wrigglesworth et al., 2021a). The surface winds (influencing Antarctic SIV) are associated with weather systems such as SO extratropical cyclones (Matear et al., 2015) which are some of the most severe storms on Earth. There is growing evidence that synoptic-scale SIV is potentially caused by SO extratropical cyclones. Over Austral autumn and winter, intense cyclones have been shown to reshape the Antarctic sea-ice cover (Vichi et al., 2019; Jena et al., 2022), and the change in storm-track activity and location linked to the trends in the Antarctic Oscillation (Fogt and Marshall, 2020) is thought to be a significant forcing factor in observed sea-ice trends (Simmonds et al., 2003; Eayrs et al., 2019). The effect cyclones have on sea-ice cover has been mostly investigated in the Arctic; on a first order, it depends on the characteristics of the cyclone and of the affected ice (Clancy et al., 2021; Schreiber and Serreze, 2020). As a cyclone passes over the open-ocean's surface, near surface wind stress can cause upper-ocean mixing, intensified heat fluxes, and the generation of waves (Hell et al., 2019). In turn, this can lead to concurring effects on the sea ice (e.g., Vichi et al., 2019; Jena et al., 2022) as well as lagged effects which can include swells penetrating the ice (e.g., Squire, 2018), and sea-ice break-up promoting air-sea interactions which consequently regulate sea-ice growth and melt (Kousal et al., 2022). In the Arctic, some cyclones may bolster the ice while others may weaken and diminish it (Morello, 2013; Schreiber and Serreze, 2020). For example, cyclones causing divergence expose the low-albedo open water, which may promote greater melt through increasing absorption of solar radiation (Lei et al., 2020). Conversely, if the atmosphere is sufficiently cold, divergence

may promote regions of new ice growth (Kriegsmann and Brümmer, 2014). Moreover, in the Arctic, as a cyclone propagates over the sea ice, sea-ice convergence on the west of the cyclone, promoting increased sea-ice thickness (Clancy et al., 2022). It is currently unknown whether the variability in Antarctic sea-ice concentration would respond to extratropical cyclones similarly as in the Arctic.

Since SIV can directly influence regional climate (such as through modulating surface albedo, and the exchange of heat, freshwater, and carbon between the ocean and atmosphere), understanding the impact cyclones have on synoptic-scale SIV may contribute to better project future climate change in the Antarctic region (Matear et al., 2015b; Iovino et al., 2022). Indeed, the number of cyclone tracks observed in the SO vary depending on the cyclone-tracking algorithm used (e.g. Grieger et al., 2018; Messmer and Simmonds, 2021; Simmonds and Li, 2021). Results presented by Grieger et al. (2018) do, however, show that cyclone tracking algorithms present similar results when observing the stronger cyclones (with lower central pressures), while the consensus between algorithms is lower when looking at the weaker cyclones. Nonetheless, regardless of the tracking algorithm, there is robust agreement on the cyclones' climatological lifecycle: cyclogenesis primarily takes place in the mid-latitude Atlantic and Pacific sectors; the cyclones then follow a southeastward trajectory and undergo cyclolysis closer to the Antarctic continent (Keable, Simmonds and Keay, 2002; Simmonds, Keay and Lim, 2003; Yuan, Patoux and Li, 2009). The higher-latitude eastern Antarctic sectors are host to the highest cyclone density (Simmonds and Keay, 2000a, 2000b; Hoskins and Hodges, 2005; Yuan, Patoux and Li, 2009; Grieger et al., 2018; Hepworth et al., 2022).

Studies have linked large changes in sea-ice extent to sea-level pressure anomaly dipoles whose pressure gradient is perpendicular to the marginal ice zone (MIZ) edge (e.g., Vichi et al., 2019; Blanchard-Wrigglesworth et al., 2021b). This has helped build an understanding of the extreme effects a cyclone can have on the sea-ice edge. However, the relationship between episodes of high SIV and cyclones in the SO is still scarcely understood and yet to be quantified in the literature. Conventionally, SIV has been studied in the marginal ice zone (MIZ), defined as the region with 15 – 80% SIC (e.g., Stroeve et al., 2016). However, observations indicate that Antarctic sea-ice can be unconsolidated even when the ice-cover concentration exceeds 80% (e.g., Wadhams, et al., 1987; Alberello et al., 2019). More recent studies have re-evaluated the conventional definition of the MIZ (e.g., Vichi et al., 2019; Vichi, 2022). The threshold-based definition for the MIZ is an effective proxy in Arctic conditions but is less reliable for the Antarctic, where ice type is less linked to concentration values (Vichi, 2022). Therefore, the threshold-based definition for the MIZ might not always capture the effects cyclones have on SIV in the Antarctic. To define SIV, we build on the new indicator proposed by Vichi (2022), which is expressly designed for Antarctic conditions. We look at extreme SIV as an indicator for rapid synoptic-scale shifts in the location and/or extent of the MIZ. The term "extreme" is justified as the distribution of SIV is heavy-tailed (Vichi, 2022). We adapt the indicator to consider synoptic-scale variability using a three-day rolling standard deviation, reflecting the daily change in SIC. The sensitivity to the time window is further discussed in Section 4.4.1.

This study provides a systematic analysis of the extent to which extreme SIV may be caused by extratropical cyclones by assessing the co-occurrence of cyclones and extreme SIC changes in the various Antarctic regions. In Section 4.3, we present the data used in our study, while Section 4.4 details how the SIV indicator is calculated (Section 4.4.1) along with the methods used to assess the link between extreme SIV and extratropical cyclones (Sections 4.4.2 and 4.4.3). We consider the sensitivity of the link between SIV and cyclones to the distance of the sea-ice from cyclones as well as to the intensity of cyclones. A comprehensive characterization of the relationship between cyclones and extreme SIV is provided in Section 4.5. Concluding remarks are presented in Section 4.6.

4.3. Data

4.3.1. Atmospheric Data

We based our analysis on the European Centre for Medium-Range Weather Forecasts (ECMWF) ERA5 data set (Hersbach et al., 2020). ERA5 provides hourly data at a horizontal resolution of 0.25 degrees. However, the prescribed SIC data (Section 4.3.3) is updated only once per day at 00h00 UTC. Therefore, for consistency, daily data for both sea-ice and cyclone tracks were used throughout this study. We will use the term cyclone-days to indicate the total number of cyclones present in a given region at 00h00 UTC. This includes both multiple cyclones occurring on the same day and, if considering periods of multiple days, the total number of days the same cyclone was present at 00h00 UTC. The analysis is performed over the extended Austral winter season of May – September for the period 1979 – 2021, for a total of 6579 days.

As mentioned in Section 4.2, different regions of the SO show different spatial and seasonal SIC trends (Hobbs et al., 2016; Eayrs et al., 2020) as well as differences in density of cyclone tracks (Grieger et al., 2018). We, therefore, performed our analysis within separate SO sectors, following the sectors from Raphael and Hobbs (2014): (i) King Haakon VII, (ii) East Antarctic, (iii) Ross/Amundsen, (iv) Bellingshausen, and the (v) Weddell sectors.

4.3.2. Cyclone tracks

The SO extratropical cyclone tracks have been computed using the methodology of Hoskins and Hodges (2005). The method has been adapted for ERA5 hourly data at T63 filtering, and only retains cyclones with a lifespan greater than 1 day.

Following the methodology from Hepworth et al. (2022), only cyclone tracks over Antarctic sea-ice or 600 km north of the ice edge (defined as 15% SIC; see Section 4.2) were considered and each cyclone timestep was assigned a minimum mean sea level pressure (MSLP). Thereafter, the tracks identified at 00h00 UTC (see Section 4.3.1) were grouped into decile ranges, within each sector. These range from the 10% most intense cyclones (0 – 10 decile range) through to the 10% weakest cyclones (90 – 100 decile range).

4.3.3. ERA5 sea-ice concentration data

In ERA5, the prescribed SIC data are retrieved from two external products, namely the OSI SAF (409a) and the OSI SAF operational data sets. The former is used from 1979 August to September 2007, while the latter is used from September 2007 to present. These datasets are gap-filled, gridded reconstructions of SIC at a 25 km resolution, obtained from daily composites of the passive microwave radiometric signals from the ocean surface.

The OSI SAF sea-ice data are regridded onto the ERA5 model grid and, through outer-loop integrations, force the coupled domains of land surface, atmosphere, and ocean waves. Thereafter, a 4D-Variation inner-

loop is implemented from the forced atmosphere to the sea-ice, resulting in the final ERA5 sea-ice product (Hersbach et al., 2020).

4.4. Methods

4.4.1. Synoptic-scale SIC variability

The synoptic-scale SIV is quantified using a sea-ice variance indicator based on Vichi (2022) and modified to capture the time scales of the cyclones. The main difference is the drop of the background climatology for calculating anomalies. We initially reduced it from one month to a 7-days rolling climatology over the extended Austral winter season of May – September for the period 1979 – 2021, which led to a spurious detection of numerous extreme SIV events due to the large variability of the ice edge advance and retreat from year to year. If the 7-days edge is seasonally located more to the north or the south of the climatology, this difference is marked as an extreme independently of the presence of synoptic features. The chosen indicator that removed this alias was calculated from the 3-day rolling standard deviation. The sea-ice variance indicator quantifies the change in SIC relative to the day before and the day after, reflecting the daily change in SIC as well as the timescale of the typical lifespan of a cyclone between 50°S and 70°S. Simmonds and Keay (2000a) showed that the mean lifetime of cyclones (lasting more than 24 hours) is just over 3 days, while the cyclones which travel between 50° and 70°S, on average last 1 day longer than other systems. The use of a longer 5-day window does not qualitatively alter the SIV distribution presented in Figure 4.3b for the different sectors. Although this feature has not been studied in the Antarctic sea ice, the use of smoothed daily SIC fields interpolated onto the ERA5 grid is expected to reduce the day-to-day noise observed in satellite data in the Arctic (e.g., Comiso et al., 2017).

We created distributions of all the grid values of the sea-ice variance indicator separately for each sector (as listed in Section 4.3.1 and depicted in Figure 4.1), and calculated the 95th percentile. The values above each sector's percentile threshold were identified as regions of extreme SIV (refer to Figure 4.3b, which will be presected in Section 4.5.2). Figure 4.1 shows an example of the conventional location of the MIZ (between 15 – 80% SIC) and the sea-ice variance indicator for 04 July 2017 at 00h00 UTC (calculated from the 3-day rolling standard deviation from 03 – 05 July 2017). The explosive cyclone in the King Haakon VII sector (labelled "X" in Figure 4.1b) caused an extended region of extreme variability in the sea-ice (Vichi et al., 2019). Generally, the regions of extreme SIV overlap with the conventionally defined MIZ region, yet some local differences emerge. Indeed, there were large cyclones near or over sea ice in these two sectors on 04 July 2017 (Figure 4.1b). Additionally, the SIV indicator shows that, within the MIZ, there can be large spatial gradients in SIV: for example, at 0°, SIV ranged from 0.05 to 0.35 within 300 km (Figure 4.1d).

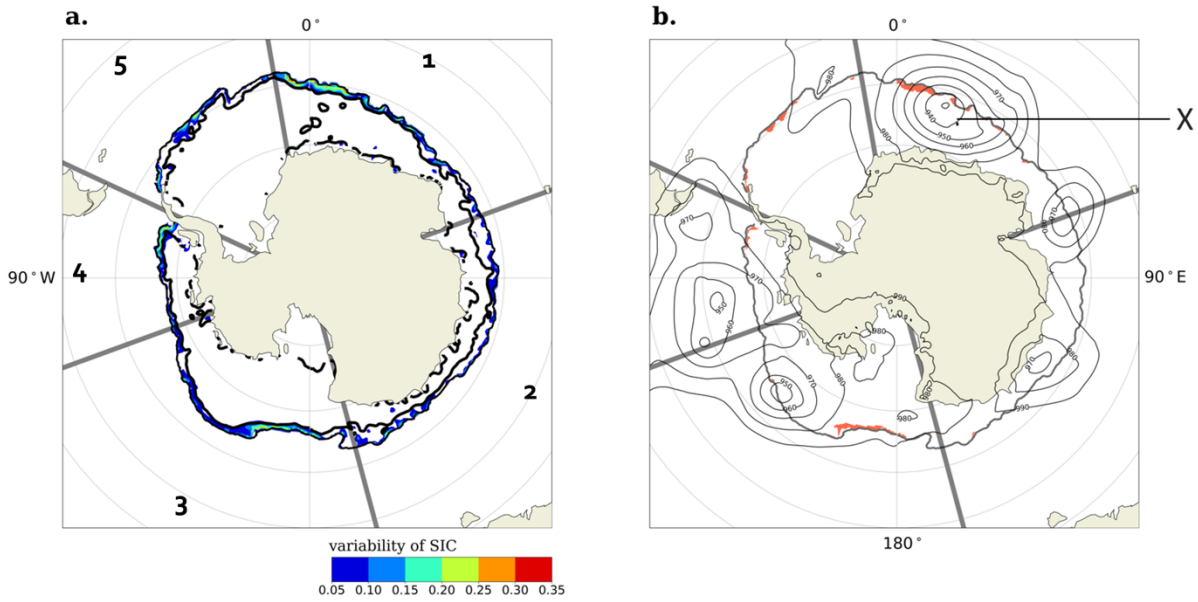

Figure 4.1: (a) SIV represented using the sea-ice variance indicator, and (b) regions of extreme SIV (orange). The thick grey radial lines mark the five sectors dividing the Southern Ocean: going clockwise from 10°W, the (1) King Haakon VII, (2) East Antarctica, (3) Ross/Amundsen, (4) Bellingshausen, and (5); Weddell sectors; as numbered in Panel a. The thin grey contour lines denote the sea-ice edge in both Panels. Panel a includes the 80% SIC contour (thick black contour), and Panel b includes the mean sea level pressure isolines (thin black contour lines every 10 hPa, starting from 930 hPa).

4.4.2. Search-Radius method

As an extratropical cyclone travels across the ocean surface, the cyclone contributes to altering its surrounding environment both dynamically (e.g., through near surface wind activity and by generating waves) and thermodynamically (e.g., through upper-ocean mixing and intensified heat fluxes; Hell et al., 2019). As a result, concurring as well as lagged effects on sea-ice can take place. Here, we focus on the concurring effects (i.e., the immediate impact) a cyclone has on extreme SIV within a given impact area defined through a search-radius.

For each SO sector, the location of each cyclone track centroid was extracted when over Antarctic sea-ice and 600 km north of the ice edge (see Section 4.3.1), and all grid cells defined as extreme SIV were identified as described in Section 4.4.1. A search-radius method was conducted: we computed the ratio between the number of grid cells with extreme SIV within a 600 km radius of a centroid and the total number of grid cells within the chosen sector defined as extreme SIV. This diagnostic is defined as a percentage of the total number of SIV points, hence it is related to the sea-ice area (SIA) in each sector. Indeed, for a given set of environmental conditions, the large differences in SIA observed in each sector would presumably affect the total number of extreme SIV points. An example of extreme SIV for 04 July 2017 at 00h00 UTC is shown in Figure 4.1b.

In our analysis, a cyclone is considered related to extreme SIV if at least one grid point with extreme SIV is within a 600 km radius of the cyclone's centroid. However, extratropical cyclones can have radii ranging from 500 to 2000 km (Hoskins and Hodges, 2005; Yuan et al., 2009; Uotila et al., 2011), depending on the phase of the cyclone's lifecycle (Simonds, 2000), and its geographical location (Lim and Simmonds, 2007). The more intense cyclones are typically comparatively small, ranging between 330 and 665 km (4 – 6° latitude; Uotila et al., 2011). To test the sensitivity of our results to the choice of search-radius, we additionally tested search radii of 400 km and 1000 km.

4.4.3. Statistical Significance Testing

To verify the link between extreme SIV and cyclones, a one-sided random-sampling test at the 5% significance level was executed. For each sector, we randomly drew the same number of grid cells as the number of cyclones-days per decile range (to test each class of intensity). The grid cells included in this random selection include the sea-ice region and 600 km north of the ice edge (i.e., the area of interest). This was repeated 1000 times for each sector and each decile range. The 95th percentile of the total number of randomly drawn grid cells that were within 600 km from extreme SIV, relative to the total number of extreme SIV grid cells, was calculated. Within each sector, these results provide an indicative upper confidence bound for a statistically significant link between synoptic-scale extreme SIV and cyclones of different intensities. If the results show that the SIV ratio is above the upper confidence bound of the random-sampling test (see the search-radius method in Section 4.4.2), we infer that there is a link between extreme SIV and cyclones.

We finally computed the cumulative percentage of extreme SIV caused by the cyclones over a given percentile range, and tested its significance by implementing the random-sampling test separately for each set of cyclone intensities (for example, implementing the random-sampling test for 0-10, 0-20, 0-30 percentiles, etc.). We refer to this number as the cumulative effect cyclones have on extreme sea-ice changes per sector.

4.5. Results

4.5.1. Case studies

To make an initial evaluation of the possible links between cyclones and extreme SIV, two case studies are presented in Figure 4.2.

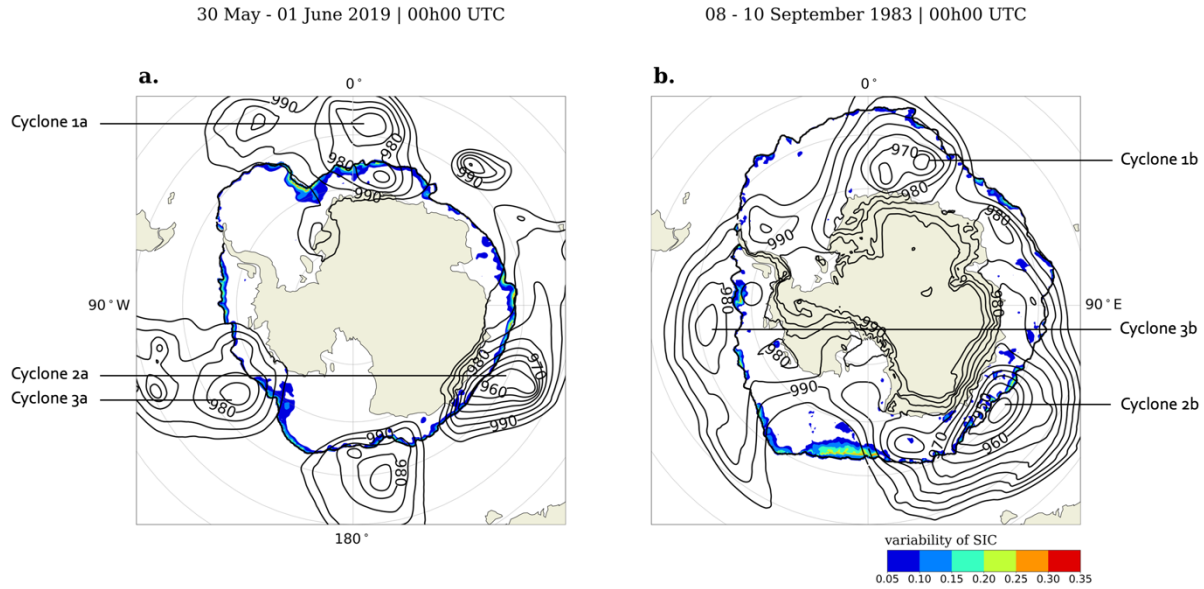

Figure 4.2: Variability of sea-ice concentration (SIC, colours) on (a) 30 May – 01 June 2019 at 00h00 UTC (case study 1), and (b) 18 – 20 September 1983 at 00h00 UTC (case study 2). Extreme SIV is denoted by the values greater than 0.20 (note that in later analysis, the threshold to define extreme SIV varies between sectors). The mean sea level pressure isolines are overlain (thin, black contour lines every 10 hPa, starting from 900 hPa), and the sea-ice edge is denoted by the thick, black contour lines. All data are from ERA5.

Cyclone 1a in case study 1 (30 May – 01 June at 00h00 UTC, Figure 4.2a) is one of the explosive cyclones identified by Jena et al. (2022). Extreme SIV is present along the MIZ edge from approximately 45°W to 45°E (within the King Haakon VII), 50°E to 110°E (East Antarctic sector), and 120°W to 175°W (within the Ross/Amundsen sector). An intense cyclone is identified in the East Antarctic sector, at 120°E (Cyclone 2a, 957 hPa), and other cyclones are identified in the King Haakon VII and Ross/Amundsen sectors: in the former sector at 0° - 15°E (Cyclone 1a; 969 hPa), and in the latter sector at 60° - 150°W (Cyclone 2a; 958 hPa). In case study 2 (18 – 20 September 1983 at 00h00 UTC, Figure 4.2b), there is extreme SIV close to the sea-ice edge in the Bellingshausen sector where a relatively weak cyclone is present (Cyclone 3b; 971 hPa). Like case study 1, case study 2 also shows a cyclone of similar strength around 0° - 15°E (Cyclone 4.1b; 963 hPa). However, Cyclone 1b displays lower SIV in its vicinity relative to cyclone 1a. Both case studies show extreme SIV in the Ross/Amundsen sector, with the presence of cyclones nearby (Cyclones 3a and 3b). Interestingly, case studies 1 and 2 display cyclones in the East Antarctic sector with SIV in its vicinity (Cyclones 2a and 2b, respectively), however the former is relatively weaker (958 hPa), with extreme

SIV on its trailing side, while the latter is stronger (942 hPa) with lower SIV on its trailing side. These case studies qualitatively suggest that cyclones may induce extreme SIV, but that this may only be partly dependent on the cyclones' intensity. We further hypothesise that the SIV located relatively further away from a cyclone may have been induced by lagging effects of a cyclone (e.g., Hell et al., 2019).

4.5.2. Distribution of cyclones and sea-ice concentration variability

Here, we analyse the full ERA5 data set to gain a more systematic understanding of the role SO cyclones play in driving SIV.

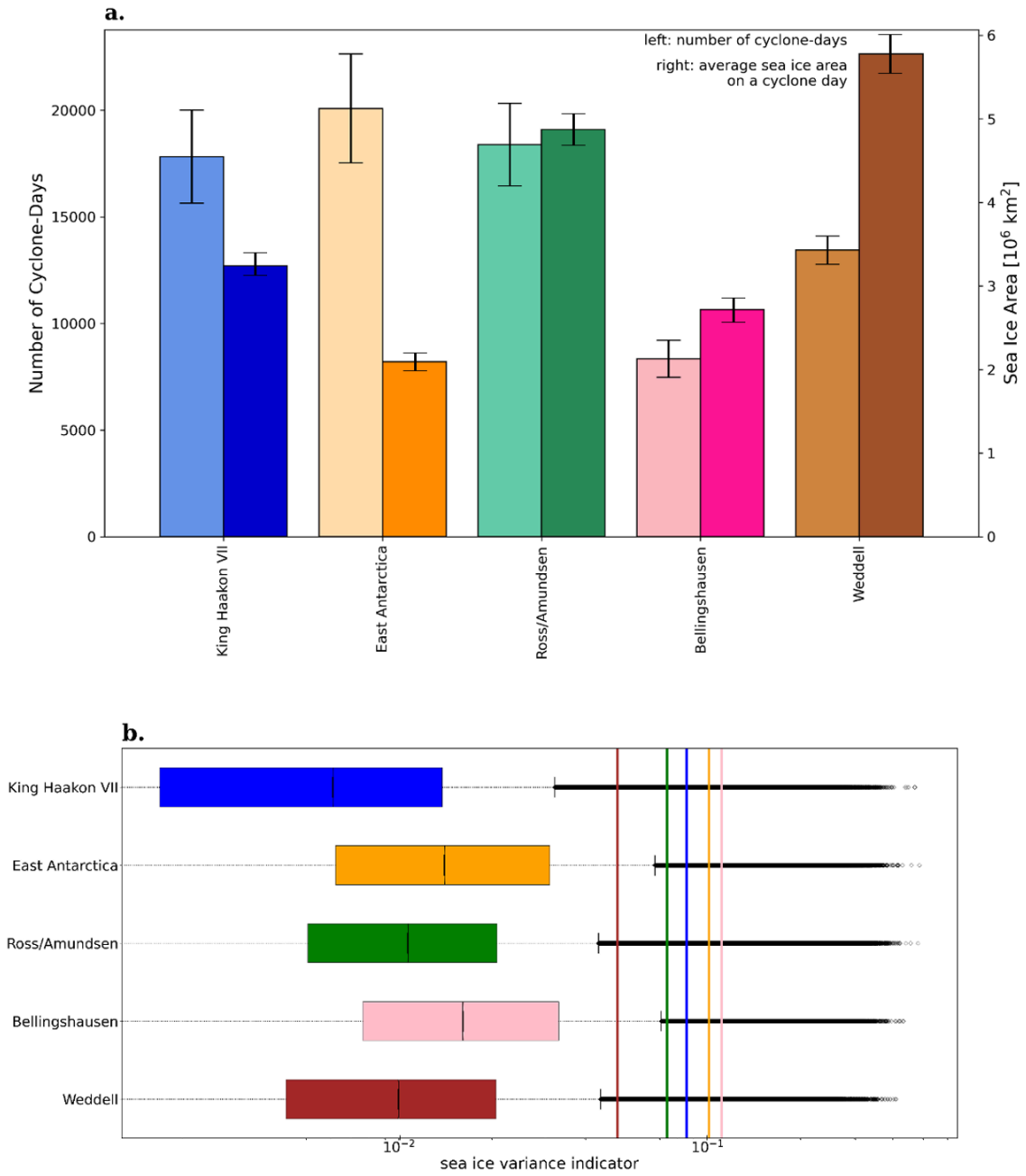

Figure 4.3: (a) Histogram of the total number of cyclone-days (left bars) and the total climatology sea ice area (right bars) for each Southern Ocean sector. The results for the number of cyclone-days using 400 km and 1000 km meridional distances from the sea-ice edge are denoted by the lower and upper limits of each range bar, respectively. (b) Box-and-whisker plot showing the distribution of the sea-ice variance indicator for each sector by presenting the 25^{th} and 75^{th} percentiles, and the median. The vertical colour-coded lines show the 95^{th} percentile for each sector, and the vertical black lines are made up of small, black circles representing outliers. Note the logarithmic scale on the X-axis. The calculations for both 11panels were performed over May – September from 1979 – 2021.

The term cyclone-days refers to the total number of cyclones present in a given SO sector, at 00h00 UTC (see Section 4.3.1). The highest number of cyclone-days is found within the East Antarctic sector with 20085 cyclone-days (Figure 4.3a), followed by the Ross Amundsen and King Haakon VII sectors with 18387 and 17816 cyclone-days, respectively. The large number of cyclone days found in the East Antarctic Sector can be partly explained by it being the sector with the widest longitudinal extent, but also because of the high density found in that sector in this work (Figure 4.5a) and in earlier studies with different reanalysis products (e.g., Hoskins and Hodges, 2005; Grieger et al., 2018). There are 13442 cyclone-days in the Weddell sector, while the Bellingshausen sector displays the lowest number of cyclone-days (8340). The bars on the right show the mean climatological SIA, per SO sector, computed over the extended Austral winter period (May – September) from 1979 – 2021. The Weddell sector presents the largest SIA (5.78 x 10^6 km^2), followed by the Ross/Amundsen (4.87 x 10^6 km^2) and King Haakon VII (3.24 x 10^6 km^2) sectors. The Bellingshausen and the East Antarctic sectors are regions with relatively lower SIA (2.71 x 10^6 km^2 and 2.10 x 10^6 km^2, respectively). We notice that East Antarctic has the largest number of cyclone-days over the smallest SIA.

Figure 4.3b shows the distribution of SIV and its 95^{th} percentile SIV per sector. In the three sectors displaying the relatively higher SIA (Ross/Amundsen, Weddell, and King Haakon VII; Figure 4.3a), the median SIV is lower (Figure 4.3b). Conversely, in the two sectors with the relatively lower SIA (East Antarctic and Bellingshausen; Figure 4.3a), the median SIV is higher (Figure 4.3b). The results of the 95^{th} percentile SIV show the Weddell sector as the least variable sector of SIC on a 3-day timescale (0.051), followed by the Ross/Amundsen (0.074), King Haakon VII (0.086), and East Antarctic (0.101), and finally the Bellingshausen (0.112) as the most variable sector (Figure 4.3b). The relatively lower 95^{th} percentile in the regions with higher SIA (the Weddell and Ross/Amundsen sectors) shows that these sectors are more likely to be comprised of larger portions of consolidated sea-ice, displaying smaller changes in SIC on synoptic timescales.

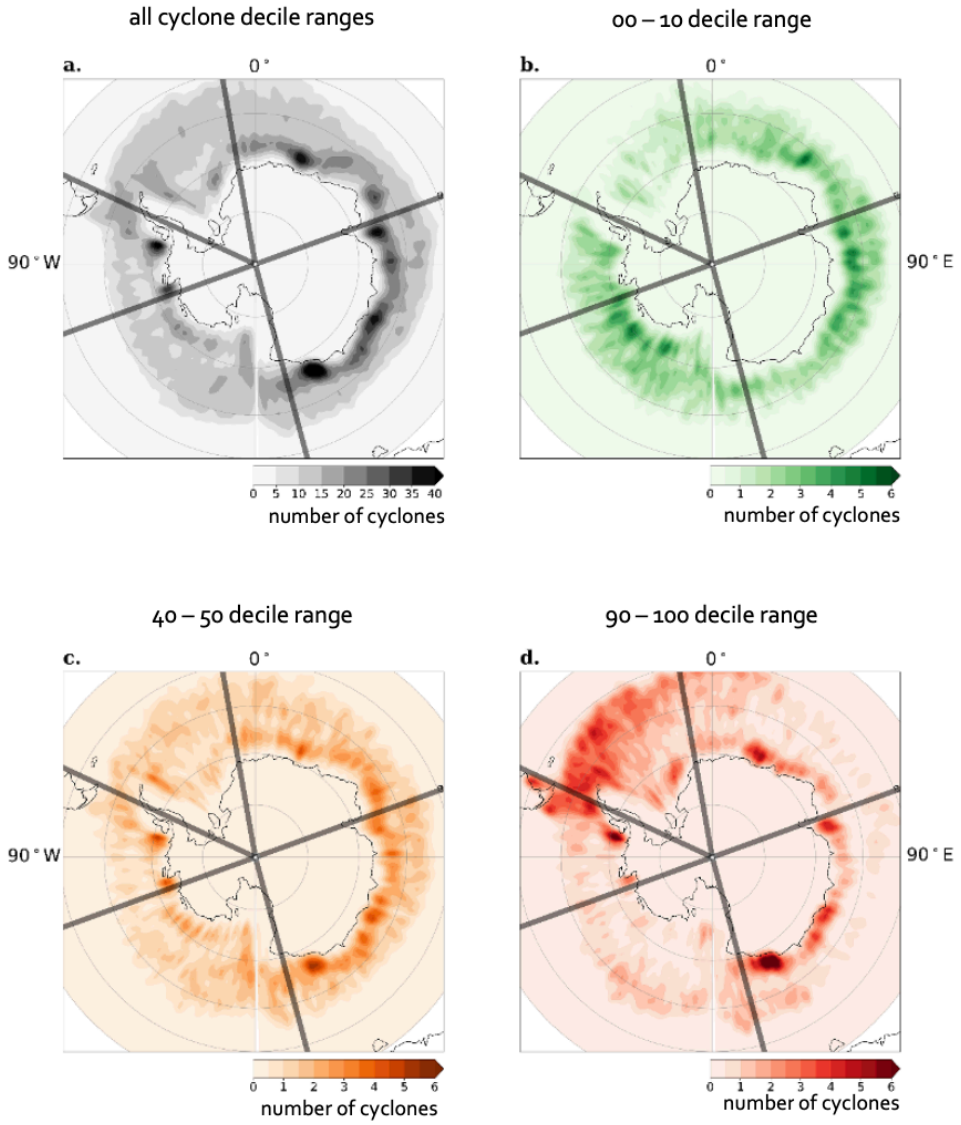
all cyclone decile ranges
a.
0 °
90 ° W
0 5 10 15 20 25 30 35 40
number of cyclones
00 – 10 decile range
b.
0 °
90 ° E
0 1 2 3 4 5 6
number of cyclones
40 – 50 decile range
c.
0 °
90 ° W
0 1 2 3 4 5 6
number of cyclones
90 – 100 decile range
d.
0 °
90 ° E
0 1 2 3 4 5 6
number of cyclones

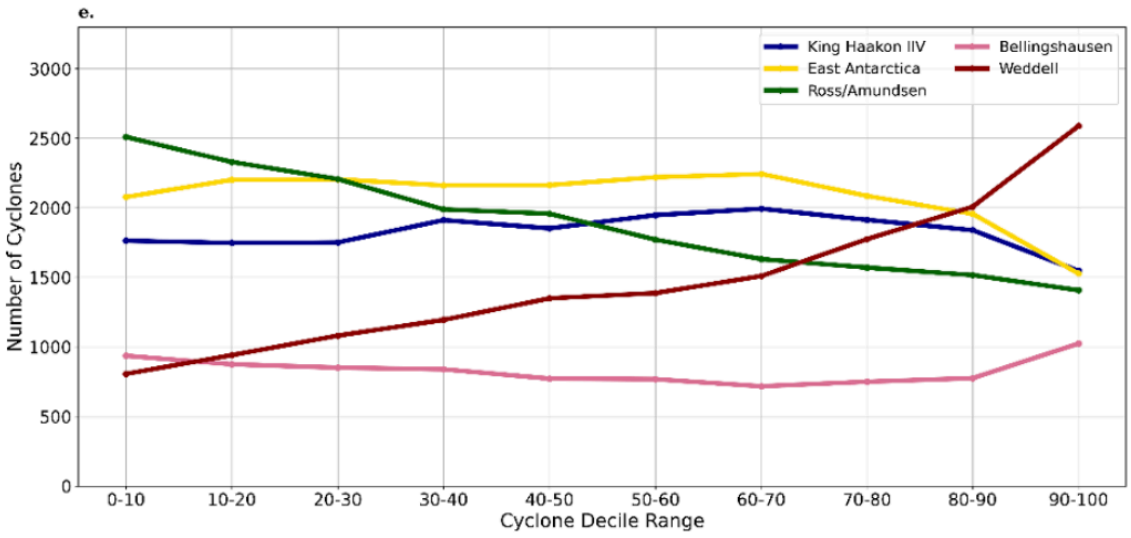
e.
King Haakon IIV
East Antarctica
Ross/Amundsen
Bellingshausen
Weddell
Number of Cyclones
3000
2500
2000
1500
1000
500
0
0-10
10-20
20-30
30-40
40-50
50-60
60-70
70-80
80-90
90-100
Cyclone Decile Range

Figure 4.4: Density of the number of cyclone-days, per grid point, smoothed using a Gaussian Filter (with σ=2) for (a) all cyclone-days, and within the decile range of (b) 0 – 10, (c) 40 – 50, and (d) 90 – 100. Panels a-d show the five Antarctic sectors depicted by the thick grey lines: going clockwise from 10°W, The King Haakon VII, East Antarctic, Ross/Amundsen, Bellingshausen, and Weddell sector. (e) Number of cyclone-days per Antarctic sector for each decile range. Each decile range represents cyclone intensity, where 0-10 decile range is the most intense cyclones and 90-100 decile range is the 10% weakest cyclones.

Thus far, our analysis has focused on all cyclones. To study the role of cyclone intensities, the cyclone tracks are grouped into decile ranges (see Section 4.3.2). Figure 4.4 shows the density of the intense cyclones (0 – 10 decile range; Figure 4.4a), intermediate cyclones (40 – 50 decile range; Figure 44.b), and the weak cyclones (90 – 100 decile range; Figure 4.4c), together with the total density (Figure 4.4a).

The cyclone distribution is similar to that documented by Simmonds and Keay, (2000a, 2000b), Hoskins and Hodges, (2005) Yuan, Patoux and Li, (2009), and Grieger et al., (2018) using earlier versions of atmospheric reanalyses. The highest number of cyclones are found close to the Antarctic continent in the King Haakon VII (a hotspot at 30°E) and eastern Antarctic regions (with hotspots at 70°E, 120°E, and 150°E). The intense cyclones are located relatively close to the Antarctic continent, and primarily distributed in the eastern Antarctic sector and from 70° - 150°W (Figure 4.4b). Similarly, cyclones of intermediate intensity are predominant in the East Antarctic sector and from 70° - 120°W. However, their distribution differs from that of the intense cyclones as they are more spread out over the sea-ice region and towards the edge (Figure 4.4c). The 10% weakest cyclones are mostly found in the Weddell sector, as well as near the Antarctic continent at 30° E, 120° E, and 150° E (Figure 4.4d). The overall distribution of the number of cyclone-days, per sector, and per decile range is presented in Figure 4.4e. The Ross/Amundsen sector shows a decrease in the number of cyclone-days as the cyclones become weaker. The Weddell sector shows the converse. The number of cyclone-days in the King Haakon VII, East Antarctic, and Bellingshausen sectors remain relatively similar throughout all decile ranges.

4.5.3. Link between cyclones and SIC extreme variability

The case studies in Figure 4.2 suggest that high SIV may be induced by cyclones, but it may be partly independent of the cyclones' intensity. Furthermore, Figure 4.4e shows that the distribution of cyclones of different intensities varies between the different SO sectors. This Section investigates to what extent extreme SIV is found in the neighbourhood of extratropical cyclones and its relationship with the cyclone intensity in a systematic way during the winter period.

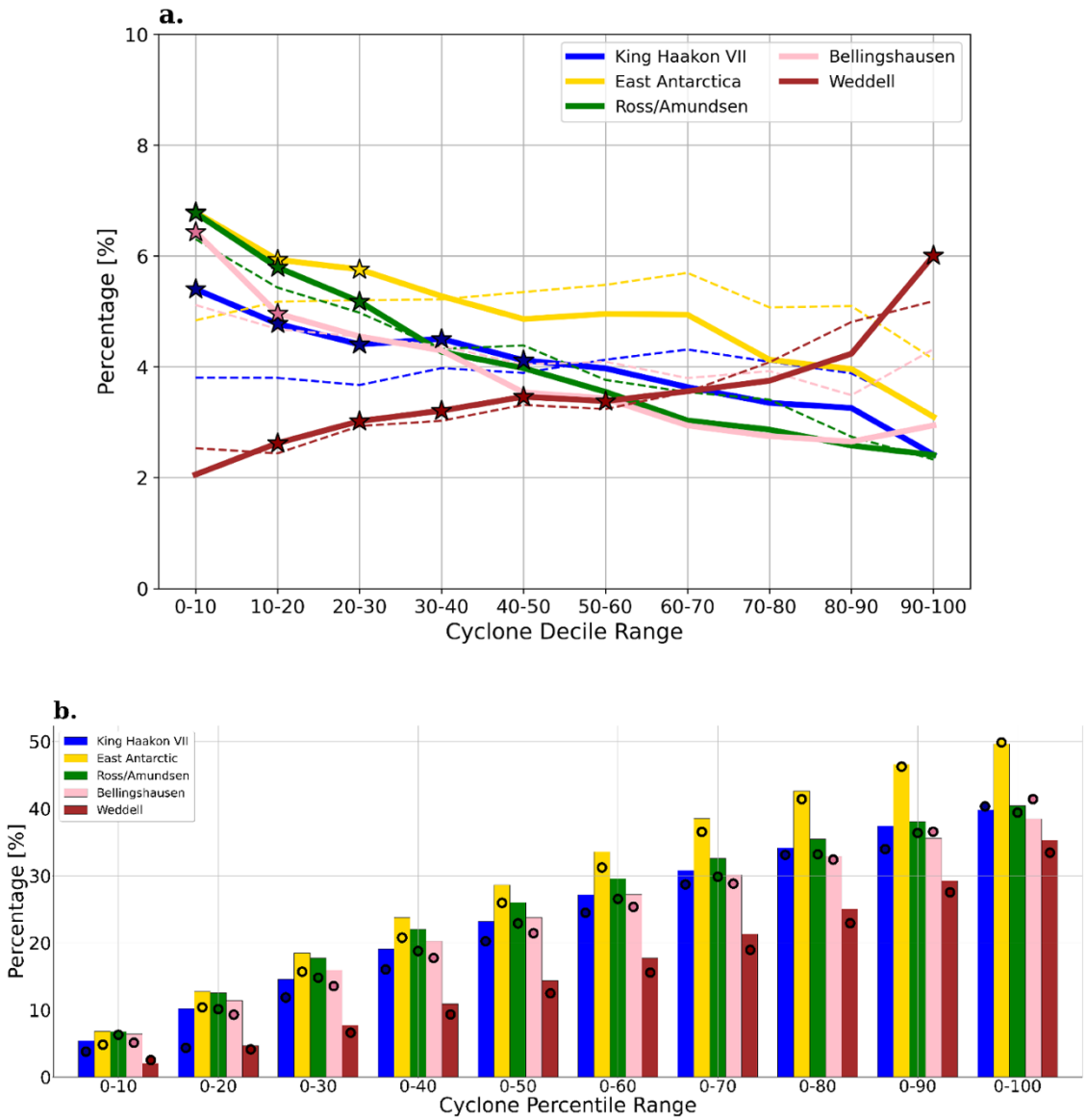

Figure 4.5: Percentage of (a) synoptic-scale extreme SIV in the vicinity of a cyclone for each sector (continuous lines) compared with the 95th percentile of the random-sampling test (dashed lines), and (b) the cumulative percentage of extreme SIV. The stars in Panel a indicate statistically significant percentile ranges, and the circles in Panel b indicate the 95th percentile cumulative significance bound (see Section 4.4.3).

Within all sectors apart from the Weddell sector, the highest percentage of extreme SIV is spatially associated with the top 10% intense cyclones (Figure 4.5a). As the cyclones become weaker (the decile range increases), the percentage of SIV within the vicinity of the cyclones gradually decreases. Interestingly, the opposite pattern is observed for the Weddell sector: the lowest percentage of extreme SIV is observed within the vicinity of the top 10% intense cyclones, and there is a gradual increase in extreme variability as the cyclones become less intense, with a sharp increase for the weakest cyclones.

If we consider each decile range separately (Figure 4.5a), there is only a significant link between extreme SIV and cyclones up until the 10 – 20 decile range in the Bellingshausen sector, the 20 – 30 decile range in

the East Antarctic and Ross/Amundsen sectors, and the 40 – 50 decile range in the King Haakon VII sector. Within the Weddell sector, there is a significant link from the 10 – 20 decile range until the 50 – 60 decile range. Interestingly, unlike the other sectors, there is also a significant link within the 90 – 100 decile range. The picture is different when we calculate the cumulative percentage of the cyclone decile ranges associated to extreme SIV (Figure 4.5b). The random-sampling test results (included in Figure 4.5a with the dashed lines and Figure 4.5b with the circles) provide the statistical significance of this spatial association between extreme SIV and cyclones (see Section 4.4.3). There is a significant link between cyclones and extreme SIV up until the 80th percentile of cyclone intensity in the Bellingshausen sector, and the 90th percentile within the King Haakon VII and East Antarctic sectors. However, within the Ross/Amundsen sector, there is a significant link within all percentage categories, and within the Weddell sector, there is not a significant link once the top 10% most intense cyclones are included.

4.6. Discussion and Conclusions

Sea-ice can influence climate in multiple ways, and understanding the processes that drive variability of Antarctic SIC is pivotal for projecting future regional climate change (Matear et al., 2015). Our focus was on the unexplored role of SO extratropical cyclones in engendering synoptic-scale extreme SIV. Studies have shown that, at the synoptic scale, there is a link between SIV and cyclones (e.g., Matear et al., 2015; Alberello et al., 2020; Vichi et al., 2019; de Jager and Vichi, 2022). However, before this study, a systematic investigation of the relationship between episodes of extreme SIV and cyclones had not been conducted. We leverage the methodology by Vichi (2022) to define synoptic-scale SIV using daily ERA5 SIC. We presented selected case studies that suggest that high SIV is associated with cyclones, but that the naïve picture of a direct relationship between cyclone intensity and SIV does not always hold. We then associated extreme SIV to specific cyclones per Antarctic sector following the search-radius method of Hepworth et al. (2022) and computed the link between extreme SIV and cyclones.

We highlight some caveats of our analysis. The way in which the SIC is assimilated in ERA5 (see Section 4.3.3) implies that the observed SIV is not necessarily dynamically coherent with the overlying atmospheric forcing, but rather acts as a boundary condition for the atmosphere. Our analysis further relies on the assumption that ERA5 provides a valid representation of high-latitude SO cyclones. Based on the analysis conducted by King et al. (2022), there was a relatively low correlation between near-surface temperatures and *in situ* observations. Given the influence of air-sea fluxes linking cyclones and sea ice, this factor might have a minor effect on the relationship between cyclones and sea ice. Furthermore, the SIV indicator we use is based on a 3-day variability window, and cyclones move over hundreds of kilometers of sea ice in this time frame. The extreme SIV may then happen as the result of mobilized sea ice, and hence could have been engendered at a larger distance from the cyclone core than the one used in our search radius. An additional caveat is that we use only one cyclone tracking algorithm. To investigate the robustness of our results to the choice of tracking algorithm, this analysis would need to be repeated using other cyclone

tracking methods. For example, recent studies have demonstrated that a change in cyclone tracking algorithm may cause the total number of SO cyclones to vary (e.g., Grieger et al., 2018; Messmer and Simmonds, 2021). After comparing results for several cyclone-tracking algorithms, Grieger et al. (2018) shows that there is a relatively large discrepancy between algorithms when focusing on weaker cyclones, while they produce similar results for stronger cyclones. The algorithm we selected is a middle-of-the-range cyclone-tracking algorithm: detecting a similar distribution of intense cyclones to other algorithms, and neither a relatively very high nor very low number of weak cyclones (Grieger et al., 2018). Finally, we only consider the concurring effect of cyclones on sea ice, and do not account for lagged effects. While lagged effects may indeed be important, considering them would make the task of connecting SIV to specific cyclones (which is needed in order to stratify the analysis by cyclone intensity) largely impossible.

Bearing in mind these constraints, our results demonstrated that the distribution of cyclones of varying intensity over sea ice and their link with extreme SIV in winter is different between each SO sector. Within the sectors with lower SIA (the King Haakon VII, East Antarctic, and the Bellingshausen sectors), there is a relatively even distribution of cyclones of all intensity categories (intense, intermediate, and weak cyclones). However, within the sectors with relatively higher SIA, intense cyclones are dominant in the Ross/Amundsen sector, while weaker cyclones are dominant in the Weddell sector. This may be attributed to the SO extratropical cyclones' lifecycle. In the Austral winter months (June – August), a net cyclogenesis takes place off the east coast of Argentina, and the new, weaker cyclones propagate westward, over the Weddell Sea. The Ross/Amundsen sector, however, experiences a net cyclolysis: As suggested by Simmonds and Keay (2000), the cyclones that are generated over New Zealand and Australia, travel south-westward toward the higher latitudes, and become more intense before contributing to the "cyclone graveyard" found over the Ross/Amundsen sector.

The SIV indicator shows that, within the MIZ, there can be large gradients of SIV on synoptic timescales. This is observed in Figure 4.1 where regions with high SIV mostly match the threshold-based definition of the MIZ (Figure 4.1a) but show local differences in the vicinity of cyclones (Figure 4.1b). Therefore, where the conventional MIZ definition does match a region of high SIV, it is likely that cyclones are not the primary drivers of short-term sea-ice features (such as the Ross Sea polynya). However, where high SIV extends beyond the threshold-defined MIZ, synoptic-scale drivers (e.g., cyclones) likely lead to extreme SIC changes in regions where sea-ice cover is outside the 15 – 80% SIC range (e.g., in the King Haakon VII sector and eastern Ross/Amundsen sector in Figure 4.1.a).

Interestingly, the median SIV presented in Figure 4.3b is generally very low, and the distributions per sector have several outliers: matching the heavy-tailed distribution presented by Vichi (2022). Extreme SIV is around 0.1, which is also a small variation around the typical SIC that is close to 1 in winter. This reduced variability is most likely a result of using the ERA5 SIC, which was done for consistency with the cyclone analysis. The variability is likely to be higher when directly analysing the satellite SIC (e.g. Vichi, 2022). The King Haakon VII sector has the lowest SIV median, followed by the Weddell and Ross/Amundsen sectors.

The 95th percentile SIV is also similar to that of the Ross/Amundsen sector. This shows that the regions with higher SIA are more likely to be composed of larger portions of consolidated sea ice which displays smaller changes in SIC on synoptic timescales. This is highlighted in the Weddell sector, where the SIA is relatively high, and where the 95th percentile SIV is the lowest amongst all sectors (Figure 4.3b). The King Haakon VII sector, however, differs from the Ross/Amundsen and Weddell sectors as it displays a relatively even distribution of cyclones of varying intensities (similar to the East Antarctic and Bellingshausen sectors, Figure 4.4e).

Within all sectors (apart from the Weddell sector), the intense cyclones (top 20%) are the major drivers in engendering extreme SIV. This, however, extends to the top 30% in the East Antarctic and Ross/Amundsen sectors, and the top 50% in the King Haakon VII sector. It is within the Weddell sector where relatively different results were observed: the 10% of weakest cyclones play a role in engendering extreme SIV (Figure 4.5a), which is attributed to the weaker cyclones being numerically dominant within this sector. After expanding our analysis to the cumulative effect cyclones have on extreme sea-ice changes, we found that, cumulatively, there is a significant link between extreme SIV and (1) cyclones up until the 0 – 80 percentile range within the Bellingshausen sector, (2) cyclones up until the 0 – 90 percentile range within the King Haakon VII and East Antarctic sectors, (3) all cyclones within the Ross/Amundsen sector, and (4) all cyclones beyond the 0 – 20 percentile range in the Weddell sector. Furthermore, Figure 4.5b shows that 30 – 40% of the total extreme SIV in each region is linked to cyclones within the 0 – 80 percentile range. The exception is the Weddell sector, where the link is stronger for the weaker cyclones, but the percentage of extreme SIV cumulatively explained by cyclones is less than 30% until the 90th percentile.

It is important to note that, in this study, we do not focus on the impact the increase in synoptic-scale SIV will have on the inter-annual sea-ice cover. Since divergence in the sea ice exposes the low-albedo open water, which may promote greater melt through increasing absorption of solar radiation (Lei et al., 2020), or - provided the atmosphere is sufficiently cold - areas for new ice growth (Kriegsmann and Brummer, 2014), we infer that there is opportunity for the total Antarctic sea-ice region to either expand or melt, depending on the conditions of the overlying atmosphere. This is in line with previous studies showing differences in regional inter-annual sea-ice extent trends (e.g., Turner et al., 2015; Maksym, 2019). We further infer that each SO sector may display relative differences in inter-annual sea-ice growth or melt trends.

Indeed, there is inherent uncertainties associated with SIV measurements which arise from the precision in retrieving sea-ice concentration through reanalyses. However, it is important to note that the uncertainties in SIC estimates in the high-latitude SO show minimal bias (Schneider and Reusch, 2016; Cerovečki et al., 2022), and do not diminish the significance of the results. Rather, they provide context within which these results should be interpreted. Our conclusions, therefore, remain robust. Based on our results, we interpret that cyclones do cause extreme SIV. However, not all cyclones have an impact: other processes play a part in engendering extreme SIV (e.g., near-surface katabatic winds, and mesoscale ocean currents). Conversely,

an extremely variable sea-ice environment may provide favourable conditions for cyclones surviving over sea-ice (e.g., Krinner et al., 2007). However, our methodology solely focuses on: (i) the concurrent role of cyclones and not on lagged effects or other atmospheric systems, and (ii) the cyclone-to-SIV link and not the converse. Lagged effects have been identified in the Arctic literature (e.g., Fang and Wallace, 1994; Wang et al., 2020). Antarctic sea ice is thinner and more mobile, and our study demonstrated that extreme SIV is located within the MIZ (cf. Figure 4.1). Lagged effects may partly explain the remainder of extreme variability not associated to the cyclones, which is more than 50% in our cumulative analysis. However, considering these effects would make the task of connecting SIV to specific cyclones (which was needed to stratify the analysis by cyclone intensity) largely impossible.

Under globally warming surface temperatures, there has been a shift in the number of cyclones and their intensity, as well as an increase in the baroclinicity at the poles (coupled with a decrease in baroclinicity at the midlatitudes), resulting in a poleward shift of cyclone tracks (Simmonds and Li, 2021). de Jager and Vichi (2022) recently found an increase in sea-ice rotational drift in the Weddell and King Haakon VII sectors, which may be linked to a change in atmospheric sea-ice features. Such a trend may also exist in other sectors. Our results suggest that a higher number of high-latitude SO cyclones, as well as more intense cyclones, may translate into more variability in SIC. We found a 30 – 40% association between cyclones and extreme SIV during the extended Austral winter period, and we anticipate this percentage to increase if, over time, the number and intensity of cyclones crossing Antarctic sea ice would increase as expected by the dominantly positive Antarctic Oscillation.

5 CHAPTER FIVE

The relationship between extratropical cyclones and Antarctic sea ice in the climate model CCAM

5.1. Chapter Overview

In the previous chapters, the atmospheric conditions driving the synoptic forcing on sea ice were obtained from reanalyses, while sea-ice variability was determined from the boundary conditions of the reanalyses. The coupling between sea ice and synoptic weather was thus indirectly inferred. This chapter investigates the third and final aim: to explore how a coupled climate model simulates the cyclones, the resultant synoptic-scale variability in sea-ice concentration, and, subsequently, their link (see Section 2.1.2). This was achieved by using a case study of the climate model CCAM (run in nudging mode with ERA-Interim reanalyses), and by comparing the results produced against those generated in Chapter 4.

5.2. Introduction: The value of climate models

Climate models are essential for projecting future climate change trends at global and regional scales (Engelbrecht et al., 2011), and since sea-ice cover has a direct impact on the regional and global climate (Section 1.1; Meier and Stroeve, 2008), using climate models to predict the state of the sea-ice environment provides opportunity for researchers to inform the public and to develop a necessary plan of action. For example, climate models provide essential information to the Intergovernmental Panel on Climate Change (IPCC) through the Climate Model Intercomparison Project (CMIP). The IPCC, comprising of international researchers, routinely produces regular assessment reports on the state of climate change, its impacts and, subsequently, proposes potential mitigation and adaptation measures (e.g., Mengel et al., 2018). In regard to sea ice, through using CMIP it has been predicted that, with every 1°C of global warming, the frequency of high temperature extremes, heavy precipitation, and cyclones subsequently increases (Ming et al., 2021). It is, therefore, plausible that the Antarctic sea-ice environment may be subject to changes due to the increase in frequency of these synoptic weather systems. Here, I design an experiment to observe the response of sea ice to atmospheric synoptic-scale conditions using a case study climate model, CCAM. This experiment has not undergone testing with CCAM before.

5.3. Data and Methodology

5.3.1. CCAM: a case study climate model

There is currently low confidence in climate model projections for Antarctic sea ice (Roach et al., 2020). Due to the high-energy nature of the Southern Ocean, the atmosphere-ice dynamics are relatively different in comparison to that of the Arctic (Section 1.1). One complicated characteristic of Antarctic sea ice that makes it challenging to simulate using climate models is its non-linear physics (Carriers et al., 2017; Luo et al., 2023): the sea ice is continuously impacted by external forcing such as force from near-surface wind (e.g., Godfred-Spenning and Simmonds, 1996), ocean currents (e.g., Armitage et al., 2018), or rafting ice floes driven by wave motion (e.g. Hopkins and Shen, 2001).

For this study, the climate model, CCAM, was used (see Section 2.2.2) at a 6-hourly model output and re-gridded to a 1° x 1° resolution from 1979 – 2017. The simulation was initialised in 1979, and was employed using a semi-implicit, semi-Lagrangian method to solve the hydrostatic primitive equations. A major difference between CCAM and other atmospheric models is that, due to its variable resolution, it can be integrated with high resolution over a specific domain, making it suitable for regional climate modelling (Mcgregor and Dix, 2008).

The hypothesis of this thesis is that cyclones play a key role in engendering variability in Antarctic sea-ice concentration at the synoptic-scale. Therefore, here I focus on evaluating CCAM's ability to simulate Southern Ocean cyclone-ice interactions. This constitutes as an experimental design aimed at evaluating the

response of sea ice to synoptic forcing, with subsequent evaluation of the results against those derived from reanalysis (as presented in Chapter 4). Notably, this is a first experiment of its kind.

Simulated SIC variability was obtained using the same method described in Section 4.3.1, which computes a the sea-ice variance (SIV) indicator. In summary, the sea-ice variance indicator was calculated from the 3-day rolling standard deviation, quantifying the change in SIC relative to the day before and the day after. Extreme variability in SIC was then identified using the values above the 95th percentile of the sea-ice variance indicator, per SO sector. Overall, for this analysis, the variables simulated using CCAM were mean sea level pressure (MSLP) and sea-ice concentration (dynamically driven by the model atmosphere), stored at a 6-hourly frequency.

5.3.2. Southern Ocean cyclone tracks

The SO extratropical cyclone tracks have been computed using the methodology of Hoskins and Hodges (2005). This method is adapted for CCAM 6-hourly data at T63 filtering and only extracts cyclones with a lifespan greater than 1 day. However, one major difference was that, in this chapter, only MSLP was used to identify cyclones, and not MSLP and vorticity (Table 2.2). This was because, at the time of analysis, wind velocity fields used to calculate vorticity were not available at the same output frequency.

The CCAM analysis performed in this chapter is over the extended Austral winter season of May – September for the period 1979 – 2017, and within the separate SO sectors used in Chapter 4: (i) King Haakon VII, (ii) East Antarctic, (iii) Ross/Amundsen, (iv) Bellingshausen, and the (v) Weddell sectors. Following the same methodology as in Chapter 4, only cyclone tracks over Antarctic sea ice or 600 km north of the ice edge (defined as 15% SIC; see Section 1) were considered and each cyclone timestep was assigned a minimum MSLP. Thereafter, the tracks were grouped into decile ranges: the 10% most intense cyclones (0 – 10 decile range) through to the 10% weakest cyclones (90 – 100 decile range).

5.3.2. Cyclone's area of impact: the search-radius method

The results presented in Sections 3.3 and 4.4, show that the relationship between cyclones and a variable of interest is partly dependent on the cyclone's intensity. Moreover, Figure 5.2 shows that the distribution of cyclones of different intensities (using ERA5 or CCAM) varies between the different SO sectors. Therefore, the search-radius method used in this section identifies the relationship between cyclones and the extreme variability in sea-ice concentration, using CCAM, (i) for each cyclone decile range, and (ii) within each Southern Ocean sector.

A detailed description of how the search-radius was implemented to analyse the relationship between extratropical SO cyclones and the synoptic-scale variability in Antarctic SIC is provided in Section 4.3.2. In summary, for each SO sector, the ratio was calculated between (i) the number of grid cells with extreme sea-ice variability within a 600 km radius of a cyclone's centroid and (ii) the total number of grid cells within the chosen sector defined as extreme sea-ice variability. A cyclone is considered to engender extreme sea-

ice variability if at least one grid point with extreme variability is within a 600 km search radius of the cyclone's centroid. Additionally, a one-sided random-sampling test at the 5% significance level was conducted. The same method applied using ERA5 (see Section 4.4.3) was executed using the results from CCAM.

5.4. Results

Figure 5.1a shows the total number of cyclones-days, per sector, and per decile range using CCAM, while Figure 5.1b – f shows the total number of cyclone-days per decile range, normalised by the average number of cyclones for both CCAM and ERA5.

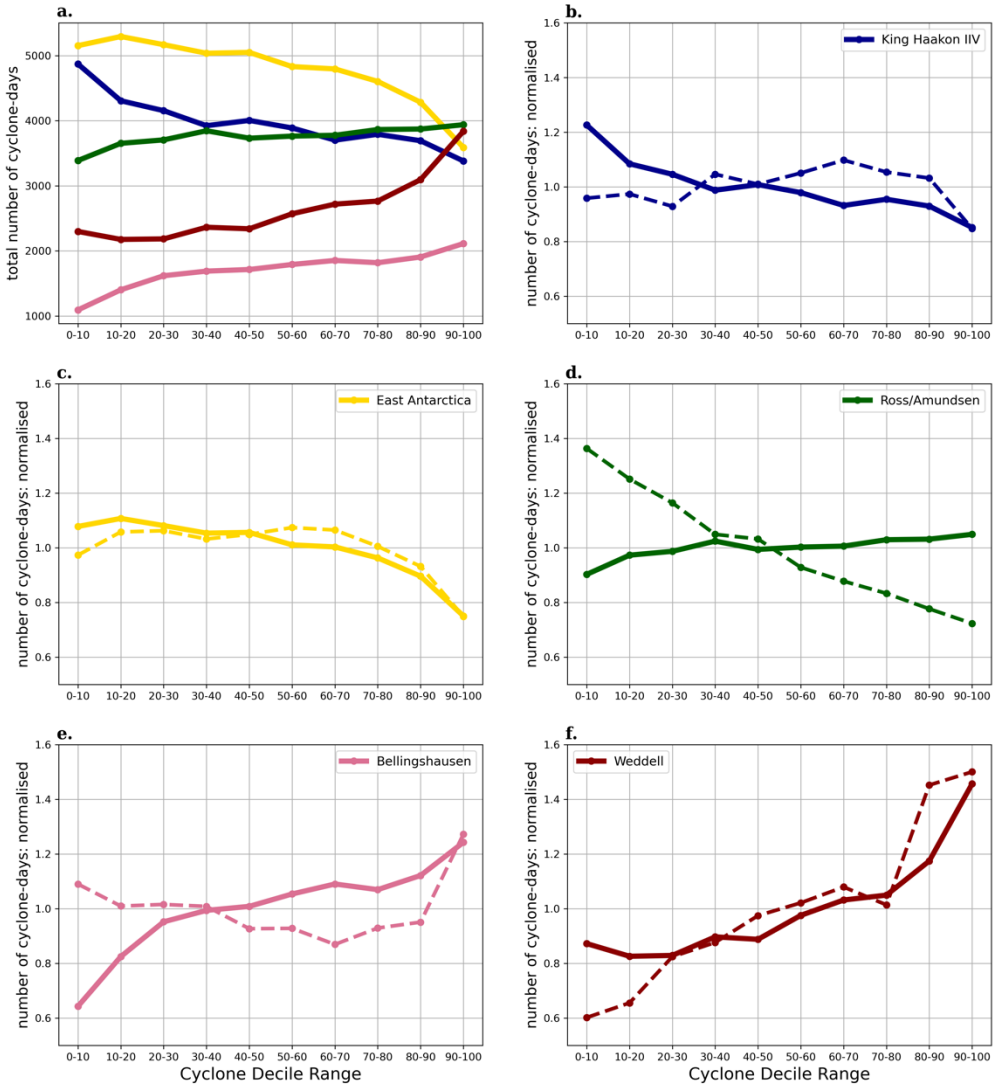

Figure 5.1: (a) Total number of cyclones-days for each Southern Ocean sector and decile range using CCAM, and the total number of cyclone-days normalised by the average number of cyclones for the (b) King Haakon VII, (c) East Antarctic, (d) Ross/Amundsen, (e) Bellingshausen, and (f) Weddell sectors, for CCAM (solid lines) and ERA5 (dashed lines).

The total number of SO cyclones calculated within a given area varies depending on the cyclone-tracking algorithm used (e.g. Grieger et al., 2018; Messmer and Simmonds, 2021) and the variables used to detect a cyclone (Pinto et al., 2005; Hoskins and Hodges, 2005). The total number of cyclone-days using CCAM (Figure 5.1a) is larger than those presented in Figure 4.4e using ERA5, but is, nonetheless, within the uncertainty range presented by Grieger et al. (2018) (which was based on a three-month analysis (June –

August), while this analysis is based on the extended Austral winter period of five months (May – September)).

By normalising the number of cyclones by the average number of cyclones within the respective SO sector (Figures 5.1b – f), I can compare the relative number of cyclone-days, per decile range, between CCAM and ERA5. One key characteristic of the Weddell sector which was observed in Chapter 4 with ERA5 was that the weaker cyclones were more abundant. This is also observed when using CCAM (Figure 5.1f), which, considering that the nudging only constraints the large-scale synoptic weather, it indicates that the model naturally develops relatively more weaker cyclones in this region. Interestingly, in CCAM, weaker cyclones are also more abundant in the Bellingshausen sector, displaying a continuous increase in number, while in ERA5 an overall slight decrease and then sharp increase in number of cyclones was shown (Figure 5.1e).

The sector displaying the most similar distribution of cyclones for both CCAM and ERA5 is the East Antarctic sector: where, overall, intense cyclones are more abundant, and then the number of cyclones decrease slightly until the 70 – 80 decile range, and then display a sharp decrease until the 90 – 100 decile range (Figure 5.1c). Similarly, the King Haakon VII sector is more abundant in intense cyclones, following a linear decrease in the relative number of weaker cyclones. This is, however, slightly different to the results produced using ERA5 which showed a relatively uniform number of cyclones throughout the decile ranges (Figure 5.1b). Finally, when compared to all sectors, the Ross/Amundsen sector displays a distinctive contrast between the two products: the number of cyclones using CCAM remains relatively uniform throughout the decile ranges, while ERA5 shows a large proportion of intense cyclones with a linear decrease in the relative number of weaker cyclones (Figure 5.1d).

Figure 5.2 illustrates the spatial density distribution per sector. Additionally, Table 5.1 provides a summary of the number of cyclones and average sea-ice area per sector using ERA5 and CCAM.

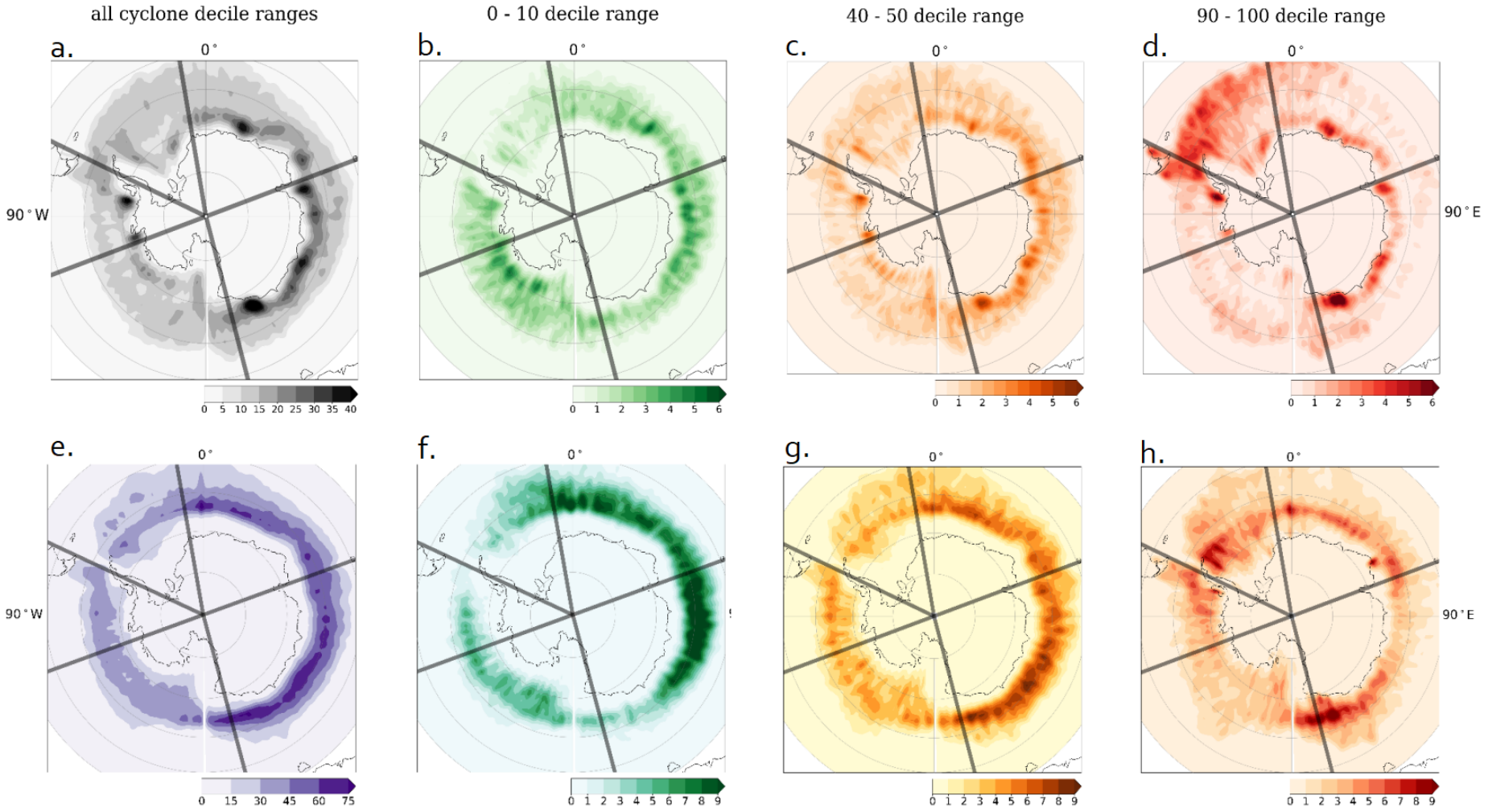

Figure 5.2: Density of the number of cyclones, per grid point, (a,e) for all cyclone-days, and within the decile range of (b,f) 0 – 10, (c,g) 40 – 50, and (d,h) 90 – 100. Cyclones were identified using ERA5 (top row; a – d, reproduced for convenience from Chapter 4) and CCAM (bottom row; e – h). The five Antarctic sectors depicted by the thick grey lines: going clockwise from 10°W, The King Haakon VII, East Antarctic, Ross/Amundsen, Bellingshausen, and Weddell sector.

Two main differences are that intense to intermediate cyclones are located further away from the Antarctic continent in CCAM, and the weaker cyclones appear to be located relatively close to the continent. However, despite the higher abundance highlighted in Figure 5.1, the density of cyclones per sector is similar when using both ERA5 and CCAM: specifically, the highest number of cyclones are found in the King Haakon VII and eastern Antarctic sectors (Figures 5.2a,e) – this includes intense cyclones (0 – 10 decile range Figures 5.2b,f) and cyclones of intermediate intensity (40 – 50 decile range; Figure 5.2c,g). Moreover, the 10% weakest cyclones are predominantly found in the Weddell sector, with additional hotspots closer to the continent at around 165°E and within the King Haakon VII sector (Figure 5.2 d,h).

Since this study selects cyclones over the Antarctic sea ice and 600 km north of the ice-edge, there is a possibility that the relatively higher number of cyclones simulated by CCAM is a result from a relatively higher Antarctic sea-ice area. This is because the area considered was over the sea ice and 600 km north of the ice edge. Therefore, if there is more sea ice, there is more area considered, and, therefore, potential for a higher number of cyclones. The total number of ERA5 cyclone-days and the total sea-ice area, per sector, was presented in Figure 4.3a, and this analysis was repeated using CCAM (Figure 5.3).

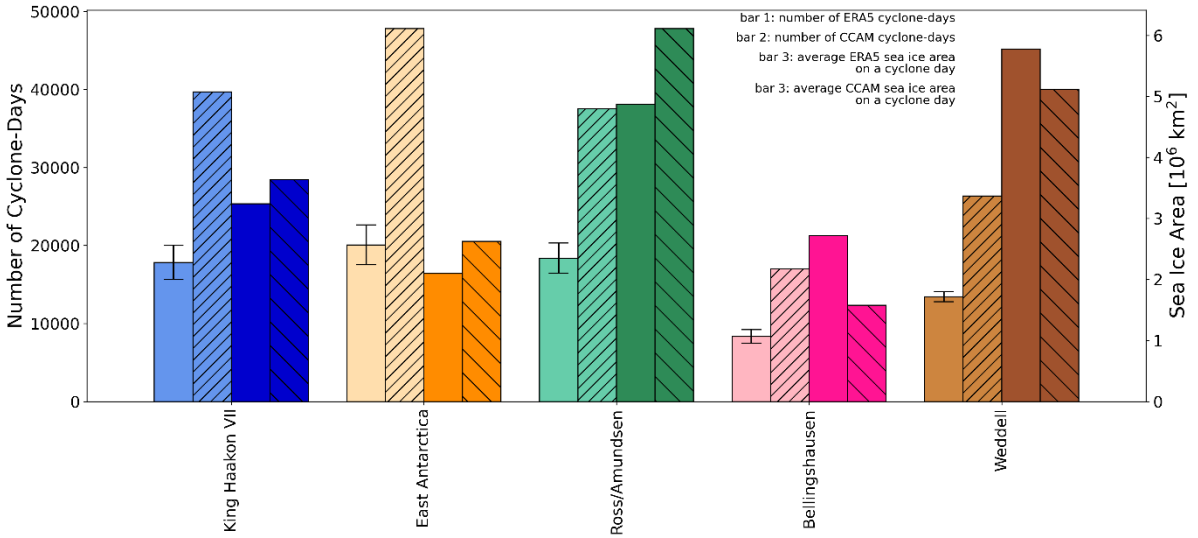

Figure 5.3: Histogram of the total number of ERA5 and CCAM cyclones (first and second bars, respectively), and the total sea-ice area calculated using ERA5 (third bars) and CCAM (fourth bars) for each Southern Ocean sector. The results presented using CCAM are denoted using hatchings.

The sea-ice area calculated from CCAM's sea-ice simulations is slightly different to that calculated using ERA5. There is more average sea ice over the extended Austral winter period in the Ross/Amundsen sector, King Haakon VII, and East Antarctic sectors, while the Bellingshausen and Weddell sectors hold a lower area of sea ice.

Table 5.1: The total number of cyclones and average sea-ice area, per Southern Ocean sector, using ERA5 and CCAM. Calculations are over the extended Austral winter period, May – September, from 1979 – 2017.

Sector	ERA5 number of cyclones	CCAM number of cyclones	ERA5 sea-ice area (10^6 km^2)	CCAM sea-ice area (10^6 km^2)
King Haakon VII	18385	39710	3.24	3.36
East Antarctica	20085	47800	2.10	2.62
Ross/Amundsen	17816	37533	4.87	6.11
Bellingshausen	8340	16996	2.71	1.57
Weddell	13442	26344	5.78	5.11

5.4.1. Simulated variability in Antarctic sea-ice concentration

To gain a better understanding of the variability of SIC simulated using CCAM, the distribution of the sea-ice variance indicator done for ERA5 in Figure 4.3b was repeated using CCAM (Figure 5.4). This compares the distribution of SIC data assimilated into the reanalyses with sea ice dynamically simulated by the nudged atmosphere in CCAM.

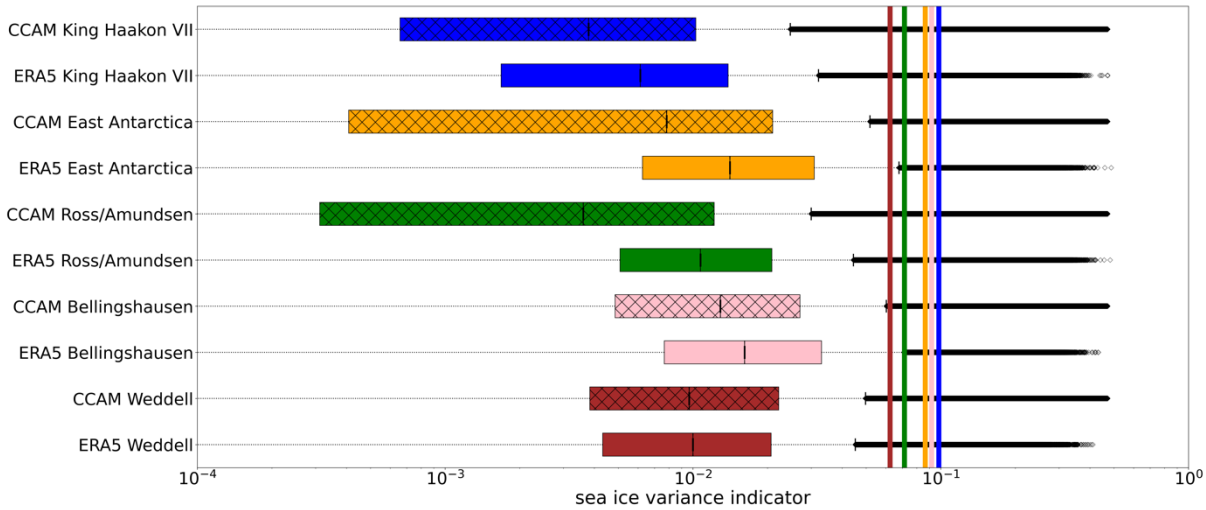

Figure 5.4: Colour-coded box-and-whisker plot showing the distribution of the sea-ice variance indicator for each sector (by presenting the 25th and 75th percentiles, and the median) from CCAM (bars with hatchings) and compared with ERA5 (Figure 4.3b; plain bars). The colour-coded vertical lines show the 95th percentile for CCAM in each sector.

The 25th percentile of the sea-ice variance indicator calculated using CCAM is lower that ERA5 for the East Antarctic and Ross/Amundsen sectors. The median is also generally lower than ERA5 in all sectors especially in the Ross/Amundsen sector where the median is much lower and below the 25th percentile from ERA5. This shows that, overall, the average synoptic variability of SIC simulated using CCAM is lower, apart for the Weddell sector that is the region with more persistent consolidated sea-ice conditions.

The thresholds for the extremes are, in contrast, more similar. The analysis of the 95th percentile presented in Section 4.5.2 showed the Weddell sector as the region with lower SIC extremes on a 3-day timescale, followed by the Ross/Amundsen, King Haakon VII, and East Antarctic, and finally the Bellingshausen as the sector with the highest extremes (Figure 4.3b). The 95th percentile results using CCAM also show the Weddell sector as the region with lower SIC extremes, followed by the Ross/Amundsen sector. Thereafter, the results slightly differ from that of ERA5 as the East Antarctic and Bellingshausen sectors follow as the second and third sectors with more SIC extremes, respectively, with the King Haakon VII sector is the region with the most extremes.

5.4.2. Link between extreme sea-ice variability and extratropical cyclones

It was shown in Chapter 4 (using ERA5) that, within all sectors apart from the Weddell sector, the highest percentage of extreme variability in SIC was spatially associated with the top 10% intense cyclones (00 – 10 decile range) and the association decreased with the weaker cyclones (Figure 4.5). These results are reported in Figure 5.5b for convenience, and compared with CCAM using the same search-radius method (Figure 5.5a).

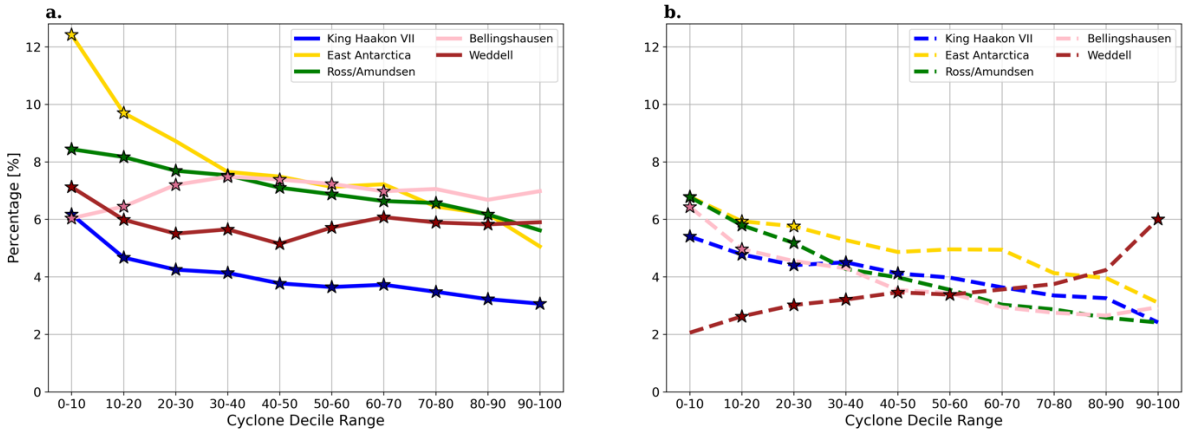

Figure 5.5: The percentage of the synoptic-scale extreme variability of Antarctic sea-ice concentration in the vicinity of a cyclone for each sector, calculated using (a) CCAM and (b) ERA5. The star symbol indicates the intensity range where the link between cyclones and extreme SIC variability is significant.

With respect to the results shown in Chapter 4, the association between cyclones and extreme variability in SIC is stronger, especially in the East Antarctic sector (Figure 5.5a). In the Bellingshausen sector, the spatial association continues to become stronger until the 20 – 30 decile range, following a plateau. Furthermore, the Weddell sector shows a rather constant association around 6% (Figure 5.5a), which is in contrast with the results of ERA5 that showed the peculiar increase with the weakest cyclones (Figure 5.5b). In addition, the associations are significant for most of the deciles in many sectors, while with the ERA5 data it was significant only for the most intense cyclones. An exception is the East Antarctic sector, which is significant for the first two most intense cyclone decile ranges (figure 5.5a).

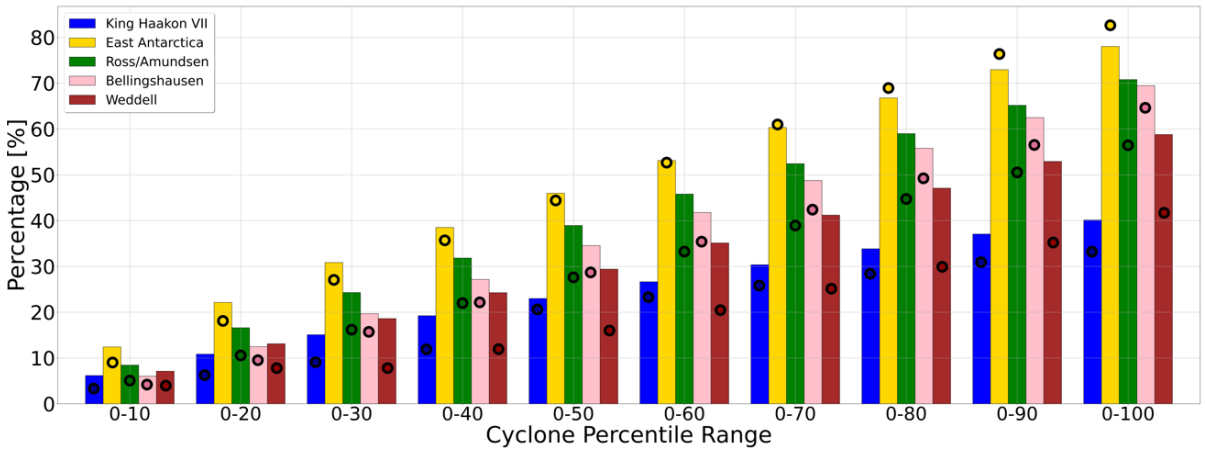

Figure 5.6: The cumulative percentage of extreme variability in sea-ice concentration for each Southern Ocean sector using CCAM. The circles indicate the 95th percentile cumulative significance bound.

CCAM has a more significant and a more direct association between cyclones and extreme SIC changes than found in ERA5, as presented in Figure 5.6. The cumulative percentage of the cyclone decile ranges associated to extreme variability in SIC increases more than in Figure 4.5 where the cumulative maximum was 50%.

Within all sectors, apart from the East Antarctic sector, when the weakest categories are added, there is a significant link between cyclones and extreme variability in SIC throughout all cyclone percentage categories. In the model, 50 – 60% of the total extreme variability in SIC is linked to cyclones within all sectors. The King Haakon VII sector is strikingly different from ERA5 because it shows the lowest percentage of association, while, with the reanalyses, it was more similar to the other sectors (see Figure 4.5).

5.5. Discussion and Conclusions

Here, the third and final aim of this thesis was explored: to analyse how the coupled atmospheric model, CCAM, simulates the relationship between cyclones and synoptic-scale extreme variability in SIC. This was achieved by comparing the results against those generated using the reanalysis product, ERA5. Currently, there is low confidence in climate model projections for Antarctic sea ice (Roach et al., 2020). Since much of our understanding of Antarctic sea ice and its variability is developed by using models (King et al., 2022), comparing them to reanalysis outputs builds understanding of the model's performance as well as insight into the accuracy of predictions made. The simulations used in this study, with the spectral nudging towards reanalyses data, allow us to take maximum advantage of this comparison exercise.

Studies have shown that the total number of cyclones may vary depending on the cyclone tracking algorithm used (e.g., Grieger et al., 2018; Messmer and Simmonds, 2021). Although this chapter used the same tracking algorithm as the study presented in Chapter 4 (Hoskins and Hodges (2005) algorithm) there was a

large difference in the number of cyclone's identified per region (Figures 5.2 and 5.3). A factor influencing this noticeable difference was the variables used to identify a cyclone (Table 2.2): the extratropical cyclone tracks in Chapter 4 were identified using ERA5 vorticity and MSLP, while those in this chapter were identified using only MSLP simulated by CCAM due to a technical issue in the storage procedure. Therefore, the number of cyclones using CCAM were greater because more "non-significant systems" can be eliminated using vorticity (Pinto et al., 2005). Moreover, although the MSLP simulated was nudged towards reanalyses, this took place on a coarser grid (1° x 1° relative to 0.25° x 0.25°) and at a lower frequency (6-hourly relative to 1-hourly). Nonetheless, the relative distribution of cyclones between each SO sector were similar when using both ERA5 and CCAM: (i) the Bellingshausen and Weddell sectors hold the lowest and second lowest number of cyclones, respectively, (ii) the King Haakon VII and East Antarctic sectors display a similar number of cyclones to one another, and (iii) the East Antarctic sector display the highest number of cyclones. This is in line with the literature which shows that maximum cyclone density is found in the higher-latitude eastern Antarctic region (Simmonds and Keay, 2000a; Simmonds and Keay, 2000b; Grieger et al., 2018; Hoskins and Hodges, 2005; Yuan et al., 2009). Furthermore, within the Southern Ocean, new, weaker cyclones which have developed off the east coast of Argentina commonly travel over the Weddell sector. This feature is evident in ERA5 (Figure 5.1d; as discussed in Chapter 4) as well as in CCAM (Figure 5.1h).

There are three hotspots of intense cyclones found in the King Haakon VII, East Antarctic, and Ross/Amundsen sectors when using ERA5 cyclone tracks (Figure 5.2b). However, using CCAM, the hotspot in the Ross/Amundsen sector is not as evident (Figure 5.2f). Moreover, even though the number of cyclone tracks identified using CCAM MSLP is relatively higher in all SO sectors, the number is lower than expected in the Ross/Amundsen sector (when comparing it to the number of cyclones in King Haakon VII and East Antarctic sectors, Figure 5.1f). Therefore, the "cyclone graveyard" of stronger cyclones typically observed in the Ross/Amundsen sector is not prominent in the simulated climate despite the nudging. This discrepancy may be due to not using vorticity to identify the cyclone tracks and/or the coarser resolution of CCAM, which could also be responsible for the most intense cyclones being situated relatively further away from the continent despite the nudging.

The Ross/Amundsen sector stood out again when comparing the results of the distribution of the sea-ice variance indicator between sectors (see Figure 5.4), Overall, a good representation of the sea-ice field is simulated using the sea-ice component of CCAM in all sectors apart from the Ross/Amundsen sector. This was observed through the median of the sea-ice variance indicator which shows the average variability of the sea-ice field (over a 3-day time window). The results show that relative to ERA5 (which assimilates satellite data), (i) the median variability of SIC in the Bellingshausen and Weddell sectors is similar, (ii) the median in the King Haakon VII and East Antarctic sectors are only slightly lower, whereas (iii) the median in the Ross/Amundsen sector is much lower. Nevertheless, the simulated SIC is less variable than in ERA5, which was, in turn, characterized by reduced variability in Section 4.6. Furthermore, the 95th percentile of

the sea-ice variance indicator shows the threshold for extreme variability in SIC. Interestingly, although in CCAM the sea-ice variance values for the 25th percentile and the median were relatively lower than for the ERA5 values, the 95th percentile thresholds were slightly higher (Figure 5.4) than those presented in Section 4 (Figure 4.3b). However, since these results were only slightly higher, it shows that CCAM is, nonetheless, capable of capturing the magnitude of extreme variability in SIC.

Lastly, how the coupled climate model CCAM simulates the link between cyclones and the resulting synoptic-scale variability in sea-ice concentration was explored. The results showing the extent to which the synoptic-scale variability in SIC was engendered by cyclones (per SO sector) were markedly interesting (Figure 5.5): the Weddell sector was the only sector in Section 4 which showed a significant link between extreme sea-ice variability and the 10% weakest cyclones (Figure 5.5b). However, using CCAM, there is a significant link with cyclones of all decile ranges apart from the 10% weakest cyclones. This shows that, even though the weakest cyclones are most abundant in this sector (Figure 5.1a,f), the sea-ice variability does not readily respond to atmospheric forcing with the weakest cyclones. This also holds true for the Bellingshausen and Ross/Amundsen sectors, where there is a significant link is not with the weakest cyclones but rather with the cyclones up until the 60 – 70 and 80 – 90 cyclone decile ranges, respectively. Overall, CCAM simulates a tighter sea ice/cyclone relationship within all sectors apart from the East Antarctic sector. This is evidenced by the cumulative percentage results shown in Figure 5.8b, which reaches values of 50 – 60% in most sectors (the Ross/Amundsen, Bellingshausen, and Weddell sectors across all cyclones ranges), and approximately 40% in the King Haakon VII sector (across all cyclone decile ranges) and the East Antarctic sector (until the cyclones in the 0 – 50 percentile range). With CCAM simulating a higher number of cyclones in each SO sector, and since these cumulative results using CCAM are higher than those calculated using ERA5 (approximately 30 – 40% of extreme variability in SIC; Figure 4.5b), these results support the statement made in Chapter 4: that if, over time, the number of cyclones were to increase, this will result in more variability in SIC.

With the exception of the major difference in the number of cyclones between ERA5 and CCAM, overall, the differences between the products were relatively minor. The cyclones from atmospheric forcing had a relatively larger influence on the variability of the sea-ice compared to the results produced using ERA5. This may be attributed to the CCAM sea-ice field responding freely to atmospheric forcing.

6 CHAPTER SIX

Synthesis

The interannual variability in mean Antarctic sea-ice coverage recorded using satellites from 1979 has shown a pattern of increase and decrease, with an overall average increase at the circumpolar scale (Figure 1.2a; Simmonds and Li, 2021). This average increase has, however, masked large regional variations (Hobbs et al., 2016). For example, there has been an overall increase in sea-ice cover in the Weddell and Ross seas but a corresponding decrease in the Amundsen and Bellingshausen sectors (Figure 1.2b; Stammerjohn et al., 2008; Eayrs et al., 2020). Due to the cooling characteristics of sea ice, it is recognized as an important feature in the global climate (Figure 1.1). Future projections, using climate models, have investigated the implications of global warming on sea-ice coverage. For example, rising atmospheric temperatures are predicted to cause an increase in the frequency of high temperature extremes, heavy precipitation, and cyclones (Ming et al., 2021), which may contribute to a changing Antarctic sea-ice field, both dynamically (e.g., through near surface wind activity) and thermodynamically (e.g., Hell et al., 2019). However, climate models fail to reproduce the observed trends of these regional variations (e.g., Sun and Eisenman, 2021).

Irrespective of the expansion in Antarctic sea-ice extent from 1979 – 2015, climate models typically simulate a decline in sea-ice cover in response to increasing greenhouse forcing (e.g., Maksym, 2012, 2019; Sun and Eisenman, 2021). Indeed, sea-ice cover would decrease if an increase in atmospheric and oceanic temperatures were the only factor involved in influencing sea-ice dynamics. However, unlike the Arctic, the Antarctic continent is unbounded by land, promoting a high-energy circumpolar SO and, in turn, a sea-ice environment that is continuously impacted by concurrent atmospheric and oceanic processes: Thus, leading to an ever-changing sea-ice cover (increasing and decreasing) at an interannual and synoptic scale. As an example, SO extratropical cyclones may induce divergence in the sea-ice field, which, through increasing absorption of solar radiation, promotes sea-ice melt (Lei et al., 2020). Conversely, if the overlying atmosphere is sufficiently cold, divergence may promote areas for new ice growth (Kriegsmann and Brummer, 2014). In general, predicting future Antarctic sea ice conditions with confidence proves to be difficult due to the limited understanding of the processes impacting Antarctic sea ice and its interactions with the atmosphere and ocean (Kennicutt et al., 2015).

Keeping in mind that there are a host of atmospheric phenomena impacting the Antarctic sea-ice environment, this work solely focussed on studying the impact cyclones have on engendering extreme atmospheric temperate and moisture anomalies, and, ultimately, extreme variability in sea-ice concentration.

Southern Ocean extratropical cyclones have been found to engender synoptic-scale variability in sea-ice concentration and drift (e.g., Vichi et al., 2019; Jena et al., 2021; de Jager and Vichi, 2022; Womack et al., 2022), however, the *extreme* variability at the synoptic scale had not yet been studied. Consequently, this thesis was formulated about three main aims (listed in Section 1.2.1). Before this study, a systematic investigation of these aims had not yet been conducted. Thus, here, a contribution to the body of knowledge subject on the Antarctic sea-ice region, its overlying atmosphere, and their relationship have been presented, including an investigation of this relationship obtained from a climate model experiment.

6.1. Summary of Findings and Conclusions

In this section, the main findings of this thesis are summarised in relation to each aim presented in section 1.2.1.

i. Association between cyclones and atmospheric rivers and extreme warm, moist airmasses over ice-covered regions.

The fact that atmospheric phenomena and Antarctic sea ice are closely linked is a core theme of this thesis. The Earth's system gains energy in the low-latitudes, and the excess energy is transported and deposited to the high-latitudes which, in turn, has a continuous effect on the sea-ice environment. Chapter 3 focussed on key drivers that transport heat and moisture to the South Pole, namely, cyclones and atmospheric rivers, which may result in extreme weather conditions over the Antarctic sea ice. Unlike Chapters 4 and 5, this chapter did not adopt a sector-specific approach, as the primary focus was not on the impact of sea ice. It will be interesting to explore this aspect by repeating the analysis across the Southern Ocean sectors in order to unravel any potential sea-ice-related insights.

The distributions of extreme temperature anomalies from the ERA-Interim reanalyses are located closer to the Antarctic continent, while extreme moisture anomalies and atmospheric rivers are distributed closer to the sea-ice edge. The link between intense cyclones and extreme temperature anomalies is evident, while moisture anomalies are associated with atmospheric rivers. Approximately a quarter of the intense cyclones are associated with extreme temperature anomalies while half of the atmospheric rivers are linked to extreme moisture events. Indeed, cyclones are considered to be a primary transport mechanism of heat and moisture into the polar regions (particularly in winter; Grieger et al., 2018), however, this analysis (albeit based on one cyclone-tracking algorithm) demonstrated that the relationship between SO extratropical cyclones and temperature and moisture extremes over Antarctic sea ice proves more nuanced than expected. Furthermore, although warmer air tends to have a higher capacity of holding moisture, an extreme temperature anomaly was rarely identified within the vicinity of the same cyclone as an extreme moisture anomaly. This implies that atmospheric rivers and extratropical cyclones in the Antarctic region are not always associated, and the impact on the sea ice is variable and difficult to predict. The following points have been systematically determined in this thesis, and can be used to drive further research:

- Extreme atmospheric anomalies over sea ice can also occur in the absence of cyclones or atmospheric rivers;
- Intense cyclones have a stronger association with extreme temperature anomalies than atmospheric rivers;
- Approximately half of the atmospheric rivers are in the vicinity of extreme moisture anomalies, while the link between cyclones and extreme moisture events is weak;
- Atmospheric rivers are more likely to present concurrent extreme temperature and extreme moisture anomalies.

ii. Extreme variability of Antarctic sea-ice concentration and links to extratropical cyclones.

Since Southern Ocean extratropical cyclones play a role in the weather circulations over the sea-ice environment (Chapter 3), and recent observations have hinted toward cyclones impacting the variability of Antarctic sea ice (e.g., Vichi et al., 2019; Jena et al., 2021), it was hypothesized that SO extratropical cyclones are a key driver of extreme variability in Antarctic SIC at the synoptic scale. The sector-based approach allows for a better understanding and interpretation of the complex and regionally variable trends in Antarctic sea ice, which are different from region to region. The distribution of cyclones is also dependent on the sector, due to the different areas of cyclogenesis and cyclolysis. While this study does not address the physical link between cyclones and sea-ice variability, observational studies presented in the introduction to Chapter 4 have previously evidenced a plausible association in terms of time and space. Consequently, this work aimed to statistically confirm the existence of this association in the various sectors.

The sectors with the higher sea-ice area (the Ross/Amundsen and Weddell sectors) displayed the lowest median sea-ice variance indicator. This shows that these regions are relatively more likely to be comprised of larger portions of consolidated sea ice, presenting smaller changes in sea-ice concentration at the synoptic scale. Conversely, the regions with relatively lower sea-ice area (the King Haakon VII, East Antarctic, and Bellingshausen sectors) had higher median sea-ice variance indicator, revealing that these regions may be comprised of floes that are relatively more responsive to synoptic variability as well as to how this variability is affected by climate.

In Chapter 3, I showed that intense cyclones displayed a higher link to extreme temperature anomalies (relative to moisture anomalies or atmospheric rivers). In Chapter 4, the emphasis was also on intense cyclones as they displayed a significant link to extreme variability in SIC. From these results, it is evident that stronger, more powerful cyclones have the ability to engender extreme variability in SIC relative to weaker cyclones. This is in line with a case study presented by Vichi et al. (2019) who presented an explosive cyclone in the King Haakon VII sector that caused an extended region of extreme synoptic-scale variability close to the sea-ice edge (see Figure 1.6). Interestingly, however, within the Weddell

sector, there is a significant link between extreme sea-ice variability and the 10% weakest cyclones. It was within this sector where weak cyclones were most frequent (likely as a result of the new, weaker cyclones propagate westward from the coast of Argentina, and over the Weddell Sea; Simmonds and Keay, 2000). Therefore, my results additionally show that the number of cyclones play a role in engendering extreme variability in sea-ice cover. This shows that, indeed, intense cyclones engender extreme variability, but if the cyclones continuously persist over the sea-ice environment, irrespective of their strength, extreme changes in sea-ice cover may be induced. Therefore, if, over time, there is a poleward shift of cyclone tracks (due to the decrease in baroclinicity at the mid-latitudes, coupled with an increase in baroclinicity at the higher Antarctic latitudes; Simmonds and Li, 2021), this may translate into more variability in Antarctic sea-ice concentration.

Overall, cumulatively, a total of 30 – 40% extreme variability in SIC was engendered by cyclones. This is true for all sectors apart from the Weddell sector where there is not a significant link once the top 10% most intense cyclones are included. Since the cumulative total is less than half, my findings suggest that other atmospheric phenomena play a role in the extreme variability in SIC at a synoptic scale, for example, near-surface winds (e.g., Godfred-Spenning and Simmonds, 1996; Turner et al., 2015; Holland and Kwok, 2012; Kwok et al., 2016; Blanchard-Wrigglesworth et al., 2020), and sea surface temperature (e.g., Raphael, 2007; Stammerjohn et al., 2011).

iii. Relationship between cyclones and synoptic-scale variability in sea-ice concentration in a climate model.

In Chapter 4, extreme variability in SIC and the extent to which it is engendered by cyclones was explored using reanalysis products that assimilate satellite SIC. Hence, there is no direct dynamical link between the atmosphere and the underlying sea-ice cover, and the link is only inferred through the optimization process via the boundary conditions. This analysis was repeated in Chapter 5 using the climate model CCAM developed in South Africa, from a simulation that was nudged to the reanalyses. This allowed the evaluation of the performance of CCAM in capturing this link, while maintaining a similar synoptic variability, with a sea-ice model that is free to evolve according to the atmospheric forcing.

Overall, there was a relatively larger number of cyclone tracks calculated from CCAM compared to ERA5. This may be due to the fact that the former used only MSLP to identify cyclones owing to a storage issue, while the latter used MSLP and vorticity. However, despite this discrepancy in the absolute number of cyclones, the relative density and regional distribution were in agreement with that using ERA5 and with the literature (e.g., Grieger et al., 2018).

In all sectors, intense to intermediate cyclones were located further away from the Antarctic continent than found in ERA5, while the weaker cyclones were appropriately identified relatively closer to the continent (Figure 5.2). The information closer to the continent regarding intense and intermediate

cyclones might have been missed due to not using vorticity to identify the cyclone tracks and to the coarser resolution of CCAM. When focusing on the Ross/Amundsen sector, the discrepancy in the number of cyclones could have been due to the absence of the hotspot of intense cyclones I identified as the "cyclone graveyard" in Chapters 4 and 5 (which is characteristically located close to the Antarctic continent in this region; Simmonds and Keay, 2000; Figures 3.6b, 4.4b, and 5.2b). This is supported by Figure 5.1d, where, in the Ross/Amundsen sector, the average number of intense cyclones using CCAM is much lower than when using ERA5. Additionally, I believe that the relatively large gap of information missing between the continent and the sea ice may have resulted in a skewed analysis of the sea-ice field simulated in the Ross/Amundsen sector: Relative to using ERA5, the median variability of SIC using CCAM was much lower in the Ross/Amundsen sector (while remaining relatively similar in the other sectors; Figure 5.4). The discrepancy in the total number of cyclones in this sector may have led to the discrepancy in its sea-ice field. In other words, since the sea-ice variability was dynamically driven by the model atmosphere, and since the hotspot of intense cyclones was absent in the Ross/Amundsen sector, the median ice variability engendered by cyclones in this sector will be much lower relative to the results using ERA5.

In ERA5, I found that the association between extreme variability in SIC and cyclones was explained by the cyclones' intensity, while, with CCAM, I observed that a similar intensity distribution was obtained for the Weddell sector but a different association with extreme sea-ice variability. This may imply that the modelled sea ice responds less to the weaker storms. Overall, when investigating the significant link between synoptic-scale variability in SIC and cyclones (per SO sector), using ERA5, there was an emphasis on intense cyclones engendering extreme variability (Figure 5.5b). However, using CCAM, extreme variability in SIC only depended on cyclone intensity in the East Antarctic sector. In the other sectors, on average, cyclones of all intensities (apart from the 10% weakest ones) had a significant link to extreme variability in SIC at a synoptic scale (Figure 5.5a). This shows that the association between extreme SIC and cyclones is stronger and more significant in CCAM simulations. This may be due to a combination of the relatively higher number of cyclones and the direct coupling between the atmosphere and sea ice.

6.2. Caveats and Future Research

Each analysis presented in Chapters 3 – 5 used one cyclone-tracking algorithm. To investigate the robustness of the results presented in this thesis to the choice of tracking algorithm, the analyses would need to be repeated using other cyclone tracking methods. A similar requirement is needed for the atmospheric model used in Chapter 5, CCAM. The sea-ice variability was dynamically driven by the model atmosphere, and it will be interesting to repeat this analysis on an ensemble of climate models (where sea ice evolves freely) to compare outputs. Nevertheless, since the sea ice model used in this study is relatively new to CCAM, there is a shortage of information regarding its output capabilities (e.g., Thatcher et al.,

2016). This study, therefore, extends on this model by providing insight into how it responds to atmospheric forcing. Furthermore, owing to a storage issue, only CCAM MSLP was used to identify cyclones (in Chapter 5), which resulted in a higher number of cyclones relative to those identified using MSLP and vorticity from ERA5. Indeed, this enabled the investigation of the implications an increase in cyclone-tracks may have on the variability of SIC. However, this does leave the open question of how the results might have been different if CCAM MSLP and vorticity were used. Thus, posing an opportunity for future research to produce this direct comparison. Additionally, the influence of atmospheric rivers on extreme sea-ice variability should be explored.

As an extratropical cyclone travels within the vicinity of the sea-ice region, lagged effects can take place: such as swells penetrating the ice (e.g., Squire, 2018), and sea-ice break-up promoting air-sea interactions which subsequently regulate sea-ice growth and melt (Kousal et al., 2022). However, in this thesis, I focussed solely on the concurrent effects a cyclone may have on sea ice within a maximum radius of 1000 km (see Section 2.4). Therefore, if future studies were to consider lagged effects, the percentage of extreme variability in SIC engendered by cyclones will likely be higher. Finally, it is important to note that the methodology focussed on an atmosphere-to-ice relationship, and not the converse. However, it has been found that extremely variable sea ice conditions can promote cyclones surviving over the sea ice (e.g., Krinner et al., 2007). Therefore, this research can be complemented with future research which investigates the ice-to-cyclone relationship.

In closing, due to the limited understanding of the processes impacting Antarctic sea ice and its interactions with the atmosphere, it has traditionally been difficult to predict future Antarctic sea ice conditions (Kennicutt et al., 2015). My work presented here contributes towards understanding the atmosphere-ice interactions over the extended Austral winter period, with a strong focus on extreme variability in SIC engendered by cyclones. Therefore, since, under globally warming surface temperatures, there has been a poleward shift of cyclone tracks (Simmonds and Li, 2021), this thesis will aid future studies in investigating the implications that a rise in cyclone frequency may have on the Antarctic sea-ice field within each Southern Ocean sector.

List of References

Alberello, A. Bennetts, L., Heil, P., Eayrs, C., Vichi, M., MacHutchon, K., Onorato., M., and Troffoli, A. (2019) 'Drift of Pancake Ice Floes in the Winter Antarctic Marginal Ice Zone During Polar Cyclones', *Journal of Geophysical Research: Oceans*, pp. 1–35.

Armitage, T.W.K., Kwok, R., Thompson, A.F., and Cunningham, G. (2018). 'Dynamic Topography and Sea Level Anomalies of the Southern Ocean: Variability and Teleconnections', *Journal of Geophysical Research: Oceans,* 123(1): 613 – 630. doi: 10.1002/2017JC0113534.

Aue , L., Röntgen, L., Dorn, W., Uotila, P., Vihma, T., Spreen, G., and Rinker, A. (2023). 'Impact of three intense winter cyclones on the sea ice cover in the Barents Sea: A case study with a coupled regional climate model'. *Frontiers in Earth Science*, 11:1112567. doi: 10.3389/feart.2023.1112467.

Barthélemy, A., Goosse, H., Fichefet, T., and Lecomte, O. (2018). 'On the sensitivity of Antarctic sea ice model biases to atmospheric forcing uncertainties'. *Climate Dynamics*, 51(4): 1585–1603.

Batrak, Y., and Müller, M. (2019). 'On the warm bias in atmospheric reanalyses induced by the missing snow over Arctic sea-ice', 10:4170. doi: 10.1038/s41467-019-11975-3.

Blanchard-Wrigglesworth, E., Roach, L.A., Donohoe, A., and Ding, Q. (2021a) 'Impact of Winds and Southern Ocean SSTs on Antarctic Sea Ice Trends and Variability', *Journal of Climate*, 34(3), pp. 949–965. doi: 10.1175/JCLI-D-20-0386.1.

Blanchard-Wrigglesworth, E., Donohoe, A., Roach, L. A., DuVivier, A., and Bitz, C. M. (2021b). 'High-Frequency Sea Ice Variability in Observations and Models', *Geophysical Research Letters*, 48(14), e2020GL092356.

Bromwich, D.H., Werner, K., Casati, B., Powers, J.G., Gorodetskaya, I. V., Massonnet, F., Vitale, V., et al. (2020). 'The year of polar prediction in the southern hemisphere (YOPP-SH)', *Bulletin of the American Meteorological Society*, 101(10): E1653–E1676.

Campbell, E.C., Wilson, E.A., Moore, G.W.K., Riser, S.C., Brayton, C.E., Mazloff, M.R., and Talley, L.D. (2019). 'Antarctic offshore polynyas linked to Southern Hemisphere climate anomalies', *Nature*, 570(7761): 319–325.

Carriers, T., Buehner, M., Lemieux, J.F., and Toudal Pedersen, L. (2017). 'Sea ice analysis and forecasting: Towards an increased reliance on automated prediction systems', Cambridge University Press. doi: 10.1017/9781108277600

Cassano, J.J., Uotila, P., and Lynch, A. (2006). 'Changes in synoptic weather patterns in the polar regions in the twentieth and twenty-first centuries, Part 1: Arctic', *International Journal of Climatology*, 26(8): 1027–1049.

Catto, J.L., Madonna, E., Joos, H., Rudeva, I., and Simmonds, I. (2015). 'Global relationship between fronts and warm conveyor belts and the impact on extreme precipitation', *Journal of Climate*, 28(21): 8411–8429.

Cerovečki, I., Sun, R., Bromwich, D.H., Zou, X., Mazzlof, M.R., and Wang, S. (2022). 'Impact of downward longwave radiative deficits on Antarctic sea-ice extent predictability during the sea ice growth period', *Environmental Research Letters,* 17. doi: 10.1088/1748-9326/ac7d66.

Clancy, R., Bitz, C.M., Blanchard-Wriggleworth, E., McGraw, M.C. (2022). 'A cyclone-centered perspective on the drivers of asymmetric patterns in the atmosphere and sea ice during Arctic cyclones', *Journal of Climate: American Meteorological Society*, 1 – 47. doi: 10.1175/JCLI-D-21-0093.1.

Dee, D.P., Uppala, S.M., Simmons, A.J., Berrisford, P., Poli, P., Kobayashi, S., Andrae, U., et al. (2011). 'The ERA-Interim reanalysis : configuration and performance of the data assimilation system', *Q. J. R. Meteorol,. Soc.,* 137: 553–597. doi: 10.1002/qj.828.

Eayrs, C., Holland, D., Francis, D., Wagner, T., Kumar, R., and Li, X. (2019). 'Understanding the Seasonal Cycle of Antarctic Sea Ice Extent in the Context of Longer-Term Variability', *Reviews of Geophysics*, 57(3), pp. 1037–1064. doi: 10.1029/2018RG000631.

Elvidge, A.D., Renfrew, I.A., Brooks, I.M., Srivastava, P., Yelland, M.J., and Prytherch, J. (2021). 'Surface Heat and Moisture Exchange in the Marginal Ice Zone: Observations and a New Parameterization Scheme for Weather and Climate Models', *Journal of Geophysical Research: Atmospheres*, 126(17).

Engelbrecht, F.A., Landman, W.A., Engelbrecht, C.J., Landman, S., Bopape, M.M., Roux, B., McGregor, J.L., and Thatcher, M. (2011).' Multi-scale climate modelling over Southern Africa using a variable-resolution global model', *Water SA*, 37(5): 647–658.

Engelbrecht, F.A., McGregor, J.L., and Engelbrecht, C.J. (2009). 'Dynamics of the conformal-cubic atmospheric model projected climate-change signal over southern Africa', *International Journal of Climatology*. 1013–1033.

Eyring, V., Gleckler, P.J., Heinze, C., Stouffer, R.J., Taylor, K.E., Balaji, V., Guilyardi, E., et al. (2016). 'Towards improved and more routine Earth system model evaluation in CMIP', *Earth System Dynamics*, 7(4): 813–830.

Finlon, J.A., Rauber, R.M., Wu, W., Zaremba, T.J., McFarquhar, G.M., Nesbitt, S.W., Schnaiter, M., et al. (2020). 'Structure of an Atmospheric River Over Australia and the Southern Ocean: II. Microphysical Evolution', *Journal of Geophysical Research: Atmospheres*, 125(18).

Francis, D., Mattingly, K., Lhermitte, S., Temimi, M., and Heil, P. (2020). 'Atmospheric extremes triggered the biggest calving event in more than 50 years at the Amery Ice shelf in September 2019', *The Cryosphere Discussions*, 28(September 2019): 1–30.

Francis, D., Mattingly, K.S., Temimi, M., Massom, R., and Heil, P. (2020). 'On the crucial role of atmospheric rivers in the two major Weddell Polynya events in 1973 and 2017 in Antarctica', *Science Advances*, 6(46): 1–14.

Genthon, C., Krinner, G., and Sacchettini, M. (2003). 'Interannual Antarctic tropospheric circulation and precipitation variability', *Climate Dynamics*, 21(3–4): 289–307. doi: 10.1007/s00382-003-0329-1.

Gettelman, A., and Rood, R.B. (2016). 'Essence of a Climate Model', pp 37–58. doi: 10.1007/978-3-662-48959-8_4

Godfred-spenning, C.R., and Simmonds, I.A.N. (1996). 'An analysis of Antarctic sea-ice and extratropical cyclone associations', *International Journal of Climatology,* 16, 1315-1332.

Gorodetskaya, I.V., Tsukernik, M., Claes, K., Ralph, M.F., Neff, W.D.M., and Van Lipzif, N.P.M. (2014). 'The role of atmospheric rivers in anomalous snow accumulation in East Antarctica', *Geophysical Research Letters*, 41(17), pp. 6199–6206. doi: 10.1002/2014GL060881.

Grieger, J., Leckebusch, G.C., Donat, M.G., Schuster, M., and Ulbrich, U. (2014). 'Southern Hemisphere winter cyclone activity under recent and future climate conditions in multi-model AOGCM simulations', *International Journal of Climatology*, 34(12): 3400–3416. doi: 10.1002/joc.3917.

Grieger, J., Leckebusch, G.C., Raible, C.C., Rudeva, I., and Simmonds, I. (2018). 'Subantarctic cyclones identified by 14 tracking methods, and their role for moisture transports into the continent', *Tellus, Series A: Dynamic Meteorology and Oceanography*, 70(1): 1–18. doi: 10.1080/16000870.2018.1454808.

Guan, B., and Waliser, D. E. (2015). 'Detection of atmospheric rivers: Evaluation and application of an algorithm for global studies', *Journal of geophysical research: Atmospheres,* 175(4449), p. 238. doi: 10.1038/175238c0.

Hell, M.C., Cornelle, B.D., Gille, S.T., Miller, A.J., and Bromirski, P.D. (2019). 'Identifying ocean swell generation events from ross ice shelf seismic data', *Journal of Atmospheric and Oceanic Technology*, 36(11): 2171–2189.

Hepworth, E., Messori, G. and Vichi, M. (2022) 'Association Between Extreme Atmospheric Anomalies Over Antarctic Sea Ice, Southern Ocean Polar Cyclones and Atmospheric Rivers', *Journal of Geophysical Research: Atmospheres*, 127(7), pp. 1–15. doi: 10.1029/2021JD036121.

Hersbach, H., Bell, B., Berrisford, P., Hirahara, S., Horanyi, A., Munoz-Sabater, J., Nicolas, J., et al. (2020). 'The ERA5 global reanalysis', *Quarterly Journal of the Royal Meteorological Society*, 146(730), pp. 1999–2049. doi: 10.1002/qj.3803.

Hobbs, W. R., Massom, R., Stammerjohn, S., Reid, P., Williams, G., and Meier, W. (2016) 'A review of recent changes in Southern Ocean sea ice , their drivers and forcings', *Global and Planetary Change*, 143, pp. 228–250. doi: 10.1016/j.gloplacha.2016.06.008.

Hodges, K.I. (1994). 'A General Method for Tracking Analysis and its Application to Meteorological Data', *American Meteorolocal Sociatey,* 122: 2573–2586.

Holland, M.M., and Hunke, E.C. (2022). A review of the Arctic sea ice climate predictability in large-scale Earth system models', *Special issue on the New Arctic Ocean,* 35(4): 20–27.

Holland, P. R., and Kwok, R. (2012). 'Wind-driven trends in Antarctic sea-ice drift', *Nature Geoscience*, 5(12), pp. 872–875. doi: 10.1038/ngeo1627.

Hopkins, M.A., and Shen, H.H. (2001). 'Simulation of pancake-ice dynamics in a wave field', *Annals of Glaciology*, 33: 355–360.

Hoskins, B.J., and Hodges, K.I. (2005). 'A new perspective on Southern Hemisphere storm tracks', *Journal of Climate*, 18(20): 4108–4129. doi: 10.1175/JCLI3570.1.

Iovino, D., Selivanova, J., Masina, S., and Cipollone, A. (2022). 'The Antarctic Marginal Ice Zone and Pack Ice Area in CMEMS GREP Ensemble Reanalysis Product', *Frontiers in Earth Science*, 10(February): 1–16. doi: 10.3389/feart.2022.745274.

de Jager, W. and Vichi, M. (2022). 'Rotational drift in Antarctic sea ice: Pronounced cyclonic features and differences between data products', *Cryosphere*, 16(3), pp. 925–940. doi: 10.5194/tc-16-925-2022.

Jena, B., Bajish, C.C., Turner, J., Ravichandran, M., Anilkumar, N., and Kshitija, S. (2022). 'Record low sea ice extent in the Weddell Sea, Antarctica in April/May 2019 driven by intense and explosive polar cyclones', *Climate and Atmospheric Science*, 5(1). d oi:10.1038/s41612-022-00243-9.

Katzfey, J. (2015). 'Climate Scenarios for the Philippine Climate Change Adaptation Project (PhilCCAP)', *CSIRO, Australia,* 1 – 43.

Keable, M., Simmonds, I., and Keay, K. (2002). 'Distribution and temporal variability of 500 hPa cyclone characteristics in the Southern Hemisphere', *International Journal of Climatology*, 22(2): 131–150. doi: 10.1002/joc.728.

Kennicutt II, M.C., Chown, S.L, Cassano, J.J., Liggett, D., Peck, L.S., Massom, R., Rintoul, S.R., Storey, J., et l. (2015). 'A roadmap for Antarctic and Southern Ocean science for the next two decades and beyond', *Antarctic Science*, 27(1): 3 – 18. doi: 10.1017/S0954102014000674.

King, J.C., Marshall, G.J., Colwell, S., Arndt, S., Allen-Sader, C., and Phillips, T. (2022). 'The Performance of the ERA-Interim and ERA5 Atmospheric Reanalyses Over Weddell Sea Pack Ice', *Journal of Geophysical Research: Oceans*, 127(9).

Kohout, A.L., Williams, M.J.M., Dean, S.M., and Meylan, M.H. (2014). 'Storm-induced sea-ice breakup and the implications for ice extent', *Nature*, 509(7502): 604–607. doi: 10.1038/nature13262.

KÖnig, W., Sausen, R., and Sielmann, F. (1993). Objective Identification of cyclones in GCM Simulations', *J. Climate,* 6, 2217–2231.

Kousal, J., Voermans, J.J., Liu, Q., Heil, P., and Babanin, A. V. (2022). 'A Two-Part Model for Wave-Sea Ice Interaction: Attenuation and Break-Up', *Journal of Geophysical Research: Oceans*, 127(5).

Krinner, G., Magand, O., Simmonds, I., Genthon, C., and Dufresne, J.L. (2007). 'Simulated Antarctic precipitation and surface mass balance at the end of the twentieth and twenty-first centuries', *Climate Dynamics*, 28(2–3): 215–230.

Kriegsmann, A. and Brümmer, B. (2014). 'Cyclone impact on sea ice in the central Arctic Ocean: A statistical study', *Cryosphere*, 8(1), pp. 303–317. doi: 10.5194/tc-8-303-2014.

Kwok, R., Pang, S.S., and Kacimi, S. (2017). 'Sea ice drift in the Southern Ocean: Regional patterns, variability, and trends', *Elementa*, 5. doi: 10.1525/elementa.226.

Lambert, S. J. (1988), 'A Cyclone Climatology of the Canadian Climate Centre General Circulation Model', *J. Climate,* 1, 109–115.

Lecomte, O., Goosse, H., Fichefet, T., Holland, P.R., Uotila, P., Zunz, V., and Kimura, N. (2016). 'Impact of surface wind biases on the Antarctic sea ice concentration budget in climate models', *Ocean Modelling*, 105: 60–70. doi: 10.1016/j.ocemod.2016.08.001.

Lim, E.P., and Simmonds, I. (2007). 'Southern hemisphere winter extratropical cyclone characteristics and vertical organization observed with the ERA-40 data in 1979-2001', *Journal of Climate*, 20(11): 2675–2690.

Lei, R., Gui, D., Heil, P., Hutchings, J., and Ding, M. (2020). 'Comparisons of sea ice motion and deformation, and their responses to ice conditions and cyclonic activity in the western Arctic Ocean between two summers', *Cold Regions Science and Technology*, 170(November 2018), p. 102925. doi: 10.1016/j.coldregions.2019.102925.

Liang, K., Wang, J., and Yang, Q. (2023). 'The Role of Atmospheric Rivers in Antarctic Sea Ice Variations', *Geophysical Research Letters*, 50: 1 – 10. doi: 10.1029/2022GL102588.

Lin, J., Qian, T., Bechtold, P., Grell, G., Zhang, G.J., Zhu, P., Freitas, S.R., Barnes, H., and Han, J. (2022). 'Atmospheric Convection', *Atmosphere - Ocean*, 60(3–4): 422–476. doi: 10.1080/07055900.2022.2082915

Lim, E. P., and Simmonds, I. (2007). 'Southern hemisphere winter extratropical cyclone characteristics and vertical organization observed with the ERA-40 data in 1979-2001', *Journal of Climate*, 20(11), pp. 2675–2690. doi: 10.1175/JCLI4135.1.

Luo, H., Yang, Q., Mazloff, M., and Chen, D. (2023). 'A Balanced Atmospheric Ensemble Forcing for Sea Ice Modeling in Southern Ocean', *Geophysical Research Letters*, 50(5).

Lynch, A., Uotila, P., and Cassano, J.J. (2006). 'Changes in synoptic weather patterns in the polar regions in the twentieth and twenty-first centuries part 2: Antarctic', *International Journal of Climatology*, 26(9): 1181–1199. doi: 10.1002/joc.1305.

Mai, V., Ming Ha, T., and Nam Pham, Q. (2018). 'Study on sensitivity of CCAM model to the sea surface temperature boundary conditions', *Environmental Sciences: Climatology,* 6:83 – 89.

Massonnet, F., Fichefet, T., Goosse, H., Vancoppenolle, M., Mathiot, P., and König Beatty, C. (2011). 'On the influence of model physics on simulations of Arctic and Antarctic sea ice', *Cryosphere*, 5(3): 687–699. doi: 10.5194/tc-5-687-2011.

Matear, R.J., O'Kane, T.J., Risbey, J.S., and Chamberlain, M. (2015). 'Sources of heterogeneous variability and trends in Antarctic sea-ice', *Nature Communications*, 6, 8656. doi: 10.1038/ncomms9656.

Maksym, T., Stammerjohn, S.E., Ackley, S., and Masson, R. (2012). 'Antarctic sea ice – A polar opposite?'. *Oceanography,* 25(3): 140 – 151. doi: 10.5670/oceanog.2012.88.

Maksym, T. (2019). 'Arctic and Antarctic Sea Ice Change: Contrasts, Commonalities, and Causes', *A Review of Marine Science*, 11:187 – 213. doi: 10.1146/annurev-marine-010816-060610.

McDonald, A.J., and Cairns, L.H. (2020). 'A New Method to Evaluate Reanalyses Using Synoptic Patterns: An Example Application in the Ross Sea/Ross Ice Shelf Region', *Earth and Space Science*, 7(1). doi: 10.1029/2019EA000794.

McGregor, J.L., and Dix, M.R. (2008). 'An Updated Description of the Conformal-Cubic Atmospheric Model', In: Hamilton, K., Ohfuchi, W. (eds) High Resolution Numerical Modelling of the Atmosphere and Ocean. *Springer, New York, NY*. doi: 10.1007/978-0-387-49791-4_4.

Meier, W.N., and Stroeve, J. (2008). 'Comparison of sea-ice extent and ice-edge location estimates from passive microwave and enhanced-resolution scatterometer data', *Annals of Glaviology,* 42, pp. 65–70. doi: 10.3189/172756408784700743.

Mengel, M., Nauels, A., Rogelj, J., and Schleussner, C.F. (2018). 'Committed sea-level rise under the Paris Agreement and the legacy of delayed mitigation action', *Nature Communications*, 9(1).

Messmer, M., and Simmonds, I. (2021). 'Global analysis of cyclone-induced compound precipitation and wind extreme events', *Weather and Climate Extremes*, 32: 100324. doi: 10.1016/j.wace.2021.100324.

Ming, A., Rowell, I., Lewin, S., Rouse, R., Aubry, T., and Boland, E. (2021). 'Key messages from the IPCC AR6 Climate Science Report', *Cambridge Centre for Climate Science*. doi: 10.33774/coe-2021-fj53b.

Monaghan, A.J., Bromwich, D.H., Chapman, W., and Comiso, J.C. (2008). 'Recent variability and trends of Antarctic near-surface temperature', *Journal of Geophysical Research Atmospheres*, 113(4).

Morello, L. (2013). 'Summer storms bolster Arctic ice', *Nature*. 500(7464), pp. 512. doi: 10.1038/500512a.

Nash, D., Waliser, D., Guan, B., Ye, H., and Ralph, F.M. (2018). 'The Role of Atmospheric Rivers in Extratropical and Polar Hydroclimate', *Journal of Geophysical Research: Atmospheres*, 123(13): 6804–6821. doi: 10.1029/2017JD028130.

Neu, U., Akperov, M.G., Bellenbaum, N., Benestad, R., Bleder, R., Caballero, R., Cocozza, A., Dacre H.F. et al. (2013), 'IMILAST: A community effort to intercompare extratropical cyclone detection and tracking algorithms', *Bull. Amer. Meteor. Soc.*, 94, 529-547. doi: 10.1175/BAMS-D-11-00154.1

Nilsson, E.D., Rannik, Ü., and Håkansson, M. (2001). 'Surface energy budget over the central Arctic Ocean during late summer and early freeze-up', *Journal of Geophysical Research,* 106: 32,187 – 32,205.

Olson, R., An, S. Il, Kim, S.K., and Fan, Y. (2021). 'A novel approach for discovering stochastic models behind data applied to El Niño–Southern Oscillation', *Scientific Reports*, 11(1).

Oort, A.H., and Piexoto J,P. (1983). 'Global Angular Momentum and Energy Balance Requirements from Observations', *Advances in Geology,* 25, pp. 355 – 490. doi: 10.1016/S0065-2687(08)60177-6

Papritz, L., Pfahl, S., Rudeva, I., Simmonds, I., Sodemann, H., and Wernli, H. (2014). 'The role of extratropical cyclones and fronts for Southern Ocean freshwater fluxes', *Journal of Climate*, 27(16): 6205–6224. doi: 10.1175/JCLI-D-13-00409.1.

Park, R. (2010). 'Development of the new Conformal-Cubic Atmospheric Model (CCAM) in capturing the past season's major rain events', *CSIR 3rd Biennial Conference 2010. Science Real and Relevant.* CSIR International Convention Centre, Pretoria, South Africa, 30 August – 01 September 2010, pp 1.

Parkinson, C.L., and Cavalieri, D.J. (2012). 'Antarctic sea ice variability and trends, 1979-2010', *Cryosphere*, 6(4): 871–880.

Patoux, J., Yuan, X., and Li, C. (2009). 'Satellite-based midlatitude cyclone statistics over the Southern Ocean: 1. Scatterometer-derived pressure fields and storm tracking', *Journal of Geophysical Research Atmospheres*, 114. D04105, doi:10.1029/2008JD010873

Perovich, D., Smith, M., Light, B., and Webster, M. (2021). 'Freshwater Sources and Sinks for Arctic Sea Ice in Summer', *The Cryosphre,* pp. 1 – 16. doi: 10.5194/tc-2021-114. https://doi.org/10.5194/tc-2021-114.

Persson, P.O.G., Shupe, M.D., Perovich, D., and Solomon, A. (2017). 'Linking atmospheric synoptic transport, cloud phase, surface energy fluxes, and sea-ice growth: observations of midwinter SHEBA conditions', *Climate Dynamics*, 49(4), pp. 1341–1364. doi: 10.1007/s00382-016-3383-1.

Pinto, J.G., Spangehl, T., Ulbrich, U., and Speth, P. (2005). 'Sensitivities of a cyclone detection and tracking algorithm: Individual tracks and climatology', *Meteorologische Zeitschrift*, 14(6): 823–838. doi: 10.1127/0941-2948/2005/0068.

Pirazzini, R. (2004). 'Surface albedo measurements over Antarctic sites in summer', *Journal of Geophysical Research D: Atmospheres*, 109(20).

Raphael, M.N. (2007). 'The influence of atmospheric zonal wave three on Antarctic sea ice variability', *Journal of Geophysical Research Atmospheres*, 112(12): 1–9. doi: 10.1029/2006JD007852.

Raphael, M. N. Hobbs, W. (2014). 'Advance and retreat', *Rhodes Cook Letter*, 11(4), pp. 3–6. doi: 10.2202/1558-4291.1063.

Roach, L.A., Dörr, J., Holmes, C.R., Massonnet, F., Blockley, E.W., Notz, D., Rackow, T., et al. (2020). 'Antarctic Sea Ice Area in CMIP6', *Geophysical Research Letters*, 47(9).

Schmidt, F. (1977). 'Variable fine mesh in spectral global models', *Beitr, Phys. Atmos.*, 50, pp. 211 – 217.

Schneider, D.P., and Reusch, D.B. (2016). 'Antarctic and Southern Ocean Surface Temperature in CMIP5 Models in the Context of Surface Energy Budget', *American Meteorological Society,* 29: 1689 – 1716.

Schreiber, E. A. P. and Serreze, M. C. (2020). 'Impacts of synoptic-scale cyclones on Arctic sea-ice concentration: A systematic analysis', *Annals of Glaciology*, 61(82), pp. 139–153. doi: 10.1017/aog.2020.23.

Simmonds, I. (2000). 'Size changes over the life of sea level cyclones in the NCEP reanalysis', *Monthly Weather Review*, 128(12): 4118–4125. doi: 10.1175/1520-0493(2000)129<4118:SCOTLO>2.0.CO;2.

Simmonds, I. (2003). 'Modes of atmospheric variability over the Southern Ocean', *Journal of Geophysical Research: Oceans*, 108(4). doi: 10.1029/2000jc000542.

Simmonds, I. (2015). 'Comparing and contrasting the behaviour of Arctic and Antarctic sea ice over the 35 year period 1979-2013', *Annals of Glaciology*, 56(69): 18–28. doi: 10.3189/2015AoG69A909.

Simmonds, I., and Keay, K. (2000a). 'Mean southern hemisphere extratropical cyclone behavior in the 40-year NCEP-NCAR reanalysis', *Journal of Climate*, 13(5): 873–885. doi: 10.1175/1520-0442(2000)013<0873:MSHECB>2.0.CO;2.

Simmonds, I., and Keay, K. (2000b). 'Variability of Southern Hemisphere extratropical cyclone behavior, 1958-97', *Journal of Climate*, 13(3): 550–561. doi: 10.1175/1520-0442(2000)013<0550:VOSHEC>2.0.CO;2.

Simmonds, I., Keay, K., and Bye, J. A. T. (2012), 'Identification and climatology of Southern Hemisphere mobile fronts in a modern reanalysis', *Journal of Climate*, 25(6), pp. 1945–1962. doi: 10.1175/JCLI-D-11-00100.1.

Simmonds, I., Keay, K., and Lim, E.P. (2003). 'Synoptic activity in the seas around Antarctica', *Monthly Weather Review*, 131(2): 272–288. doi: 10.1175/1520-0493(2003)131<0272:SAITSA>2.0.CO;2.

Simmonds, I. and Li, M. (2021). 'Trends and variability in polar sea ice, global atmospheric circulations, and baroclinicity', *Annals of the New York Academy of Sciences*, 1504(1), pp. 167–186. doi: 10.1111/nyas.14673.

Simmonds, I., and Wu, X. (1993). 'Cyclone behaviour responses to changes in winter southern hemisphere sea-ice concentration', *Q. J. R. Meteorological. Society.,* pp. 119, 1121–1148.

Sinclair, V.A., and Dacre, H.F. (2019). 'Which Extratropical Cyclones Contribute Most to the Transport of Moisture in the Southern Hemisphere?', *Journal of Geophysical Research: Atmospheres*, 124(5): 2525–2545. doi: 10.1029/2018JD028766.

Smith, G.C., Allard, R., Babin, M., Bertino, L., Chevallier, M., Corlett, G., et al. (2019). 'Polar ocean observations: A critical gap in the observing system and its effect on environmental predictions from hours to a season', *Frontiers in Marine Science*, 6, 429. doi: 10.3389/fmars.2019.00429.

Squire, V.A. (2018). 'A fresh look at how ocean waves and sea ice interact', *Philosophical Transactions of the Royal Society A: Mathematical, Physical and Engineering Sciences*, 376(2129).

Stammerjohn, S.E., Martinson, D.G., Smith, R.C., Yuan, X., and Rind, D. (2008). 'Trends in Antarctic annual sea ice retreat and advance and their relation to El Niño-Southern Oscillation and Southern Annular Mode variability', *Journal of Geophysical Research: Oceans*, 113(3).

Stammerjohn, S., Maksym, T., Heil, P., Massom, R., Vancoppenolle, M., and Leonard, K. (2011). 'The influence of winds, sea-surface temperature and precipitation anomalies on Antarctic regional sea-ice conditions during IPY 2007', *Deep-Sea Research Part II: Topical Studies in Oceanography*, 58(9–10), pp. 999–1018. doi: 10.1016/j.dsr2.2010.10.026.

Stewart, K.D., Hogg, A.M.C., England, M.H., and Waugh, D.W. (2020). 'Response of the Southern Ocean Overturning Circulation to Extreme Southern Annular Mode Conditions', *Geophysical Research Letters*, 47(22).

Stopa, J.E., Sutherland, P., and Ardhuin, F. (2018). 'Strong and highly variable push of ocean waves on Southern Ocean sea ice', *Proceedings of the National Academy of Sciences of the United States of America*, 115(23): 5861–5865.

Stroeve, J. C., Jenouvrier, S., Campbell, G.G., Barbraus, C., and Delord, K. (2016). 'Mapping and assessing variability in the Antarctic marginal ice zone, pack ice and coastal polynyas in two sea ice algorithms

with implications on breeding success of snow petrels', *Cryosphere*, 10(4), pp. 1823–1843. doi: 10.5194/tc-10-1823-2016.

Sun, S., and Eisenman, I. (2021). 'Observed Antarctic sea ice expansion reproduced in a climate model after correcting biases in sea ice drift velocity', *nature communications*, 12:1060. doi: 10.1038/s41467-021-21412-z

Thatcher, M., and McGregor, J.L. (2009). 'Using a scale-selective filter for dynamical downscaling with the conformal cubic atmospheric model', *Monthly Weather Review*, 137(6): 1742–1752.

Thatcher, M., McGregor, J., Dix, M., and Katzfey, J. (2016). 'A new Approach for Coupled Regional Climate Modelling Using More than 10,000 Cores', *HAL Open Science: 11th International Symposium on Environmental Software Systems (ISESS), Mar 2015, Melbourne, Australia*. Pp. 599 – 607. doi:10.1007/978-3-319-15994- 2_6

Thompson, D.W.J., and Wallace, J.M. (2000). 'Annular modes in the extratropical circulation. Part II: Trends', *Journal of Climate*, 13(5): 1018–1036. doi: 10.1175/1520-0442(2000)013<1018:AMITEC>2.0.CO;2.

Turner, J., Hosking, J., Marshall, T., and Phillips, T. (2015). 'Recent changes in Antarctic Subject Areas', *Philosophical Transaction of The Royal Society A*, 373(2045), pp. 1–12.

Turner, J., Holmes, C., Caton Harrison, T., Phillips, T., Jena, B., Reeves-Francois, T., Fogt, R., et al. (2022). 'Record Low Antarctic Sea Ice Cover in February 2022', *Geophysical Research Letters*, 49(12).

Ulbrich, U., Leckebusch, G.C., and Pinto, J.G. (2009). 'Extra-tropical cyclones in the present and future climate: A review', In: *Theoretical and Applied Climatology*. Springer Wien: 117–131.

Uotila, P., Vihma, T., Pezza, A.B., Simmonds, I., Keay, K., and Lynch, A.H. (2011). 'Relationships between Antarctic cyclones and surface conditions as derived from high-resolution numerical weather prediction data', *Journal of Geophysical Research Atmospheres*, 116(7), pp. 1–14. doi: 10.1029/2010JD015358.

Uotila, P., Holland, P.R., Vihma, T., Marsland, S.J., and Kimura, N. (2014). 'Is realistic Antarctic sea-ice extent in climate models the result of excessive ice drift?', *Ocean Modelling*, 79: 33–42. doi: 10.1016/j.ocemod.2014.04.004.

Vichi, M., Eayrs, C., Alberello, A., Bekker, A., Bennetts, L., Holland, D., de Jong, E., et al. (2019). 'Effects of an Explosive Polar Cyclone Crossing the Antarctic Marginal Ice Zone', *Geophysical Research Letters*, 46(11): 5948–5958. doi: 10.1029/2019GL082457.

Vichi, M. (2022). 'A statistical definition of the Antarctic marginal ice zone', *The Cryosphere*, 2021(October), pp. 1–23. doi: 10.5194/tc-2021-307.

Wadhams, P., Lange, M. A. and Ackley, S. F. (1987). 'The ice thickness distribution across the atlantic sector of the Antarctic ocean in midwinter', *Journal of Geophysical Research: Oceans*, 92(C13), pp. 14535–14552. doi: 10.1029/JC092iC13p14535.

Walker, E., Mitchell, D., and Seviour, W. (2020). 'The numerous approaches to tracking extratropical cyclones and the challenges they present', *Weather*, 75(11): 336–341.

Weeks, W.F., and Ackley, S.F. (1986). 'The Growth, Structure, and Properties of Sea Ice', *The Geophysics of Sea Ice,* pp 9 – 164. doi: 10.1007/978-1-4899-5352-0_2

Wille, J.D., Favier, V., Dufour, A., Gorodetskaya, I. V., Turner, J., Agosta, C., and Codron, F. (2019). 'West Antarctic surface melt triggered by atmospheric rivers', *Nature Geoscience*, 12(11): 911–916. doi: 10.1038/s41561-019-0460-1.

Womack, A., Vichi, M., Alberello, A., and Toffoli, A. (2022). 'Atmospheric drivers of a winter-to-spring Lagrangian sea-ice drift in the Eastern Antarctic marginal ice zone', *Journal of Glaciology*, 68(271): 999–1013.

Xu, G., Ma, X., Chang, P. and Wang, L. (2020). 'Image-processing-based atmosphric river tracking method version 1 (IPART-1)', *Geosci. Model Dev.,* 13, 4639-4662. doi:10.5194/gmd-13-4639-2020.

Yuan, X. (2004). 'ENSO-related impacts on Antarctic sea ice: A synthesis of phenomenon and mechanisms', *Antarctic Science*, 16(4): 415–425.

Yuan, X., Patoux, J., and Li, C. (2009). 'Satellite-based midlatitude cyclone statistics over the Southern Ocean: 2. Tracks and surface fluxes', *Journal of Geophysical Research Atmospheres*, 114(4): 1–18. doi: 10.1029/2008JD010874.

Zhang, Z., Ralph, F. M., and Zheng, M. (2019). 'The Relationship Between Extratropical Cyclone Strength and Atmospheric River Intensity and Position', *Geophysical Research Letters*, 46(3), pp. 1814–1823. doi: 10.1029/2018GL079071.

Zhu, Y., and Newell, R.E. (1998). 'A proposed algorithm for moisture fluxes from atmospheric rivers', *Monthly Weather Review*, 126(3): 725–735. doi: 10.1175/1520-0493(1998)126<0725:APAFMF>2.0.CO;2.